AD-A040 937 ROME AIR DEVELOPMENT CENTER GRIFFISS AFB N Y F/G 7/5
STUDIES OF ELECTRON INTERACTIONS WITH COMMUNICATIONS MATERIALS.(U)
FEB 77 J C ASHLEY, M W WILLIAMS
UNCLASSIFIED RADC-TR-77-74 NL

1 OF 2
ADA040937



AD A040937

RADC-TR-77-74
Final Technical Report
February 1977

(10)

STUDIES OF ELECTRON INTERACTIONS WITH COMMUNICATIONS MATERIALS

Oak Ridge National Laboratory

COPY AVAILABLE TO DDC DOES NOT
PERMIT FULLY LEGIBLE PRODUCTION

Approved for public release; distribution unlimited

This research was sponsored by the Defense Nuclear Agency under Subtask Z99QAXTA040, Work Unit 61, entitled "Secondary Electron Transport Phenomenology and in part by the Energy Research and Development Administration under contract with Union Carbide Corp.

DDC
RECEIVED
JUN 27 1977
D

ROME AIR DEVELOPMENT CENTER
AIR FORCE SYSTEMS COMMAND
GRIFFISS AIR FORCE BASE, NEW YORK 13441

AD No.
DDC FILE COPY

This report has been reviewed by the RADC Information Office (OI) and is releasable to the National Technical Information Service including foreign nations.

This technical report has been reviewed and is approved.

John N Bradford

JOHN N. BRADFORD
Contract Monitor

REPORT DOCUMENTATION PAGE

1. REPORT NUMBER: RADC-TR-77-74	2. GOVT ACCESSION NO.
4. TITLE (and Subtitle): STUDIES OF ELECTRON INTERACTIONS WITH COMMUNICATIONS MATERIALS.	5. TYPE OF REPORT & PERIOD COVERED: Final Rept. July 1970 - September 1976
7. AUTHOR(s): J. C. Ashley, M. W. Williams	8. CONTRACT OR GRANT NUMBER(s): Y76-886
9. PERFORMING ORGANIZATION NAME AND ADDRESS: Oak Ridge National Laboratory, Health Physics Division, Oak Ridge, Tennessee 37830	10. PROGRAM ELEMENT, PROJECT, TASK AREA & WORK UNIT NUMBERS: 62704H, CDNA0008
11. CONTROLLING OFFICE NAME AND ADDRESS: Hq Defense Nuclear Agency, Washington DC 20305	12. REPORT DATE: February 1977; 13. NUMBER OF PAGES: 115
14. MONITORING AGENCY NAME & ADDRESS (if different from Controlling Office): Deputy for Electronic Technology (RADC), Hanscom AFB, Massachusetts 01731, Monitor: John N. Bradford/ETSR (617)861-4892	15. SECURITY CLASS. (of this report): Unclassified; 15a. DECLASSIFICATION DOWNGRADING SCHEDULE

16. DISTRIBUTION STATEMENT (of this Report)

APPROVED FOR PUBLIC RELEASE; DISTRIBUTION UNLIMITED.

(12) 110p.

17. DISTRIBUTION STATEMENT (of the abstract entered in Block 20, if different from Report)

18. SUPPLEMENTARY NOTES: This research was sponsored by the Defense Nuclear Agency under Subtask Z99QAXTA040, Work Unit 61, entitled "Secondary Electron Transport Phenomenology and in part by the Energy Research and Development Administration under contract with Union Carbide Corp. This report is a summary of work performed under AF Project Order Nos. Y70-837, Y71-912, Y72-923, Y73-938, Y74-866, Y75-886.

19. KEY WORDS (Continue on reverse side if necessary and identify by block number)
Electron, Energy Loss, Theory, Mean Free Path
Transport

20. ABSTRACT (Continue on reverse side if necessary and identify by block number)

This report summarizes various theoretical and experimental studies designed to yield information on electron interactions with various communications materials. Experimental electron slowing-down spectra have been obtained for Si and for Al_2O_3 and various theoretical models proposed to account for these spectra. Attempts to measure electron attenuation lengths for photo-excited electrons in carbon, polystyrene, and gold over a range of photon energies from 20 to 64 eV, are described. A critique of photoelectric yield

→ next page

DD FORM 1 JAN 73 1473 EDITION OF 1 NOV 65 IS OBSOLETE

UNCLASSIFIED

SECURITY CLASSIFICATION OF THIS PAGE (When Data Entered)

309050

methods for measuring electron attenuation lengths stresses the difficulty of obtaining small values (≲10 Å) of this quantity to an accuracy of even ±10%. Theoretical models combined with experimental data have resulted in tabulations of mean free path, energy loss, energy straggling, range, and range straggling for electrons in Al, Al_2O_3, Si, SiO_2, Ni, Cu, Ag, Au, Ge, and GaAs.

ACCESSION for
NTIS White Section
DDC Buff Section
UNANNOUNCED
JUSTIFICATION
BY
DISTRIBUTION/AVAILABILITY CODES
Dist. AVAIL. and/or SPECIAL
A 23

DDC
RECEIVED
JUN 27 1973
D

PREFACE

The material described in this report is the result of collaborations, over different periods of time, of several scientists. Except as noted, all are members of the Health Physics Division of the Oak Ridge National Laboratory.

Over the course of this project, the following have taken leading roles in guiding and performing this work:

E. T. Arakawa

R. D. Birkhoff

R. H. Ritchie

Others making substantial contributions to this project:

V. E. Anderson (Computer Sciences Division, ORNL)

J. C. Ashley

A. J. Braundmeier (Consultant from Southern Illinois University)

T. A. Callcott (Consultant from The University of Tennessee)

L. C. Emerson (now Metals and Ceramics Division, ORNL)

R. N. Hamm

T. Inagaki (now Osaka Kyoiku University, Japan)

C. J. Tung (Postdoctoral Fellow from The University of Tennessee)

M. W. Williams

We point out that the Ph.D. research of Dr. C. J. Tung (Ph.D., The University of Tennessee, 1975) was largely concerned with problems arising in the course of this project.

The continuing advice and assistance of E. A. Burke, J. C. Garth, and J. N. Bradford of the Rome Air Development Center is gratefully acknowledged.

TABLE OF CONTENTS

ABSTRACT..... 1

PREFACE..... 3

I. PROGRAM OBJECTIVE 6

II. REVIEW OF PROGRAM..... 7

A. Electron Slowing-Down Spectra

B. Electron Attenuation Lengths from Photoelectric Yield Measurements

C. Tabulations of Electron Interaction Parameters in Solids

III. IMPLICATIONS FOR FUTURE WORK..... 19

IV. REFERENCES..... 22

A. Publications and Reports Resulting from Work Done Under this Contract

B. Other References

V. APPENDICES..... 25

A. Classical Binary Collision Cross Sections of Atomic Systems

B. Electron Slowing-Down Studies in Al_2O_3

C. Theory of the Linear Response Function of a Model Insulator

D. Electron Slowing-Down Spectra in Al_2O_3

E. Electron Attenuation Lengths in Carbon Films

F. Optical Properties of Polystyrene from the Near Infrared to the X-Ray Region and Convergence of Optical Sum Rules

G. Electron Attenuation Lengths in the Vacuum Ultraviolet and Soft X-Ray Regions

H. Calculations of Mean Free Paths and Stopping Powers of Low Energy Electrons ($\leq$ 10 keV) in Solids using a Statistical Model

I. PROGRAM OBJECTIVE

The objective of this program was to gain better understanding of the basic interactions of ionizing radiations with materials of importance as electronic components of communications or guidance systems. The knowledge gained should lead to a better design of components and an appreciation of their response to abnormal situations such as could exist during the passage of an extremely high energy cosmic ray or might occur in the high radiation environment associated with a nuclear explosion.

Our approach has been both theoretical and experimental. The energy spectrum of electrons generated by ionizing radiations and the attenuation length or range of electrons as a function of electron energy have been studied. A spherical, electrostatic electron spectrometer, the "Keplertron", specifically designed to measure slowing-down spectra in solids, was used to obtain the electron energy spectra. These spectra were then analyzed in terms of existing theories and in terms of new models developed for this project. Attempts have been made to obtain values for electron attenuation lengths from photoelectric yield observations. This has proved to be particularly difficult for small electron attenuation lengths of $\lesssim$ 10 Å: a conclusion supported by theoretical studies of photoemission.

In line with our overall objective, theoretical models and subsequent calculations based on experimental results have resulted in tabulations of mean free path, energy loss, energy straggling, range, and range straggling for electrons in various metals, semiconductors, and insulators.

II. REVIEW OF PROGRAM

A. ELECTRON SLOWING-DOWN SPECTRA

When a medium is irradiated by ionizing radiations, a flux of electrons is generated. The primary flux may consist of high energy Compton or photoelectrons from X-ray irradiation or beta rays from radioactive decay processes. As these high energy electrons slow down in the medium, they excite other electrons. The more energetic of these are called *delta rays*, while those with a few Rydbergs or less of energy are usually referred to as *secondaries*. If the medium is very large, homogeneous, and isotropic, attention may be focused on the generation and slowing-down of these electrons without regard for the spatial variation of the flux.

The purpose of this research was to determine the spectrum of electrons which are generated by ionizing radiations in materials of importance in electronics applications. Such materials include metals, semiconductors, and insulators. The electron spectra of interest have been designated[18] as *slowing-down spectra* or *degradation spectra* by theorists, Spencer and Fano in the first case, and Platzman in the second. Our study has utilized an experimental facility at the Oak Ridge National Laboratory called the "Keplertron", which is a spherical, electrostatic, electron spectrometer[19] and sources made radioactive in the Oak Ridge Research Reactor or the High Flux Isotope Reactor. A companion theoretical effort has involved numerical solutions of the Boltzmann transport equation and comparisons with the experimental results.

The materials studied in this portion of the contract were the semiconductor Si and the insulator Al_2O_3. Investigations of these materials formed a natural extension of earlier, comprehensive studies carried out in our group on several metallic media. Electron slowing-down studies on metals

Contract" (page 22) will be written based on work done under the contract.

have been reviewed in a publication of the National Academy of Sciences[20] and elsewhere.[1]

For the semiconductor Si, the electron slowing-down flux spectrum has been measured over the energy range from a few eV to 30 keV using neutron-activated samples.[2] The spectrum is found to be similar to slowing-down spectra generated in metals by beta particles. Absolute agreement with predictions of the Spencer-Fano theory[18] is found for energies above 10 keV. Experimental fluxes are found to be somewhat larger than these predictions for lower energies. A companion theoretical calculation has been carried out based on valence electron cross sections obtained from an electron gas model and on inner-shell cross sections obtained from sum-rule-corrected binary encounter theory.* These cross sections describe the effects of plasmon creation and electron-hole pair production in the valence band and excitation of electrons from the K- and L-levels. Monte Carlo calculations of the slowing-down spectrum were made using these cross sections. This theory, as well as an empirically shell-corrected Spencer-Attix theory,[21] gives a spectrum with magnitudes which are smaller than experimental values by a factor of $\sim$ 4 in the 10 to 100 eV range. A detailed account of this work has been published in The Physical Review.[3]

Since insulators are frequently used in components of electronic devices, it is important to know their response to radiation. Aluminum oxide was chosen as a representative material for this study partly because of its use in MOS devices where it replaces silicon dioxide in those cases where

---

*A description of our theoretical work on classical binary collision cross sections of atomic systems, which has been prepared for publication, is included in this report as Appendix A.

IV. REFERENCES

radiation hardening is important. Details of sample preparation and procedures for the experimental measurements are described in Appendices B-1 and B-2 along with the observed electron slowing-down spectrum for ^{164}Dy beta rays in Al_2O_3. The measured spectrum exhibits an overall shape which is similar to that for the semiconductor Si and the metals measured previously. The electron flux is generally higher than that seen for a typical metal.

Two theoretical calculations have been carried out to compare with the measured fluxes. One calculation, analogous to that performed for silicon,[3] used Monte Carlo techniques employing inelastic cross sections obtained from a sum-rule-constrained, classical binary collision model. The resulting spectrum, shown in Appendix B-2, has been described previously.[4,5] Above 10 keV the calculated spectrum shows approximately the same energy dependence as the data but is $\sim$ 40% lower. At lower energies the theory falls somewhat below the experimental data but tends to converge with it at $\sim$ 10 eV. The overall agreement was encouraging considering the uncertainties involved in using the approximate inner-shell cross sections over such a broad range of energies.

In hopes of resolving the rather large discrepancy between theory and experiment in the energy range from around 40 eV to 2000 eV, a second theoretical calculation was done. A theoretical model for the response function of an insulator was developed (see Appendix C) to describe the behavior of the valence band electrons and then applied to Al_2O_3. Cross sections for excitation of inner-shell electrons from the Al and O ion cores based on detailed, theoretical calculations of atomic generalized oscillator strengths, combined with a tight binding-OPW model description of valence band electrons, were used in a Boltzmann-type integral equation to obtain the electron slowing-down flux. These results are described briefly in Reference 6. Later this

[3] T. Arakawa, M. W. Williams, R. N. Hamm, R. D. Birkhoff, and

calculation was further improved by including Auger cascade transitions. This more detailed calculation, summarized in Appendix D, gave essentially the same result for the electron slowing-down spectrum in Al_2O_3 as the earlier Monte Carlo calculation and thus did not resolve the discrepancy noted above between theory and experiment.

A recent review paper on electron slowing-down spectra[5] gives an overview of the studies on Si and Al_2O_3 described above as well as the studies of metallic media. A detailed account of the theoretical work involved in the electron slowing-down flux calculations has been published as an ORNL report.[7]

B. ELECTRON ATTENUATION LENGTHS FROM PHOTOELECTRIC YIELD MEASUREMENTS

A knowledge of the range of electrons as a function of their energy in each of the materials involved in a communications system is necessary in order to estimate the effects of ionizing radiations on that system. Since the range and mean free path of electrons in a medium are related to the attenuation length associated with electrons emitted from the surface of the medium, measurements of electron attenuation lengths can yield the desired values of the range. Conventionally these quantities have been determined from electron transmission measurements through thin films. However, for electrons with energies of only a few electron volts above the Fermi level up to $\sim$ 1000 eV, it is known that electron attenuation is very strong and the associated lengths are therefore very short; in fact $\lesssim$ 10 Å. It is thus impossible at present to prepare homogeneous films which are sufficiently thin for these measurements.

We had previously proposed[25] a method of obtaining short electron attenuation lengths from measurements of photoelectric yield with an analysis based on a theory by Pepper.[22] Under this contract we used our proposed method to obtain values of electron attenuation lengths of photoexcited electrons in thick films of carbon[8] (see also Appendix E-1),

16. C. L. Ivey, J. C. Ashley, R. H. Ritchie, and V. E. Anderson,

of aluminum,[9] and of polystyrene from measurements of total photoelectric yield as a function of photon angle of incidence, over the range of photon energies from 20 to 64 eV. For a given photon energy the yield, $Y(\theta)$, for a photon angle of incidence θ, relative to the yield $Y(0)$ for normal incidence, shows a single maximum when plotted vs θ if the film is infinitely thick and if its refractive index, n, is less than unity. The position of this maximum in $G(\theta)$, where $G(\theta) = Y(\theta)/Y(0)$, is in the vicinity of θ_c where $\theta_c = \sin^{-1} n$, when n is close to unity. The magnitude of $G(\theta_c)$ should be sensitive to both the extinction coefficient, k, and the electron attenuation length, L. Initially, a three parameter least-squares fit of the photoelectric yield to the theory[25] was attempted. However, it was soon apparent that we could not obtain meaningful values of both k and L from a least-squares fit of an experimental curve of $G(\theta)$ vs θ. Values of k were thus obtained independently and a two parameter least-squares fit of $G(\theta)$ vs θ employed to yield values of n and L. For carbon, thin self-supporting films could not be prepared for transmission measurements and k values were obtained from observations of reflectance as a function of angle of incidence using thick evaporated carbon films similar to those used for the photoelectric yield measurements. The uncertainties in the k values obtained by this technique were quite large over the range of photon energies from 20 to 64 eV. However, the reflectance vs photon angle of incidence measurements yield both n and k values and it was felt, at that time, that a consistency check could be made by comparing the values of n obtained at a given photon energy from the reflectance and from the photoelectric yield measurements. We later found that the consistency we obtained in n for carbon from the two experimental techniques was not a sufficient condition for reliability of the L values obtained. For polystyrene, thin films suitable for optical transmission measurements over the whole energy range could be fabricated. The values of

k obtained have formed the basis for a detailed study and analysis of the optical properties of polystyrene[10] (see Appendix F). These optical properties are required in the calculations involved in producing a tabulation of electron energy loss, energy straggling, range, and range straggling for electrons in polystyrene (compare Part II-C and Part III). Despite the consistency of the n values obtained from reflectance and from photoelectric yield data, the magnitude of some of the L values obtained for carbon were considered questionable, and a detailed sensitivity analysis was thus undertaken. Three techniques had been used to obtain k values for carbon: transmission through thin carbon films on a thin Al substrate, reflectance as a function of photon angle of incidence using thick carbon films, and the three parameter least-squares fit to the $G(\theta)$ vs θ curves. The values used in the calculations[8] of L were those obtained from the reflectance measurements. These were thought to be the most accurate and were in fact the average of all the results. Uncertainties in k of $\sim$ 50% were estimated from the range of k values obtained by the three methods. On the other hand $G(\theta)$ was found to be reproducible to $\sim$ 1%. These uncertainties in k and $G(\theta)$ were found to lead to large uncertainties $\Delta L(k)$ and $\Delta L(G)$, respectively, in the values calculated for L from the experimental $G(\theta)$ vs θ data. For example at 22.3 eV, L = (113 $\pm$ 91) Å where $\Delta L(k)$ = 81 Å and $\Delta L(G)$ = 10 Å, at 40.8 eV, L = (19 $\pm$ 30) Å where $\Delta L(k)$ = 29 Å and $\Delta L(G)$ = 1 Å, and at 59.2 eV, L = (10 $\pm$ 45) Å where $\Delta L(k)$ = 44 Å and $\Delta L(G)$ = 1 Å. Appropriate error bars should be added to the L values graphed for carbon in Reference 8. If L is small ($\lesssim$ 10 Å), as is generally thought over the whole of the energy range studied here for carbon, it can be shown that, in general, to obtain L to $\pm$1 Å (i.e., to at best $\sim$ $\pm$10%), not only $G(\theta)$ but also k must be known to better than $\pm$1%. There may be other inaccuracies in the values of L calculated by this technique due to the sample not being homogeneous and/or

the sample surface not being perfectly clean, smooth, and planar. In addition the model used in the derivation of the theoretical variation of $G(\theta)$ with θ in terms of the definition of L may be inadequate. In fact photoelectric yield continues to be the subject of theoretical and experimental investigations designed to elucidate the processes involved and the significance of the measured electron attenuation length.

Since analysis of $G(\theta)$ vs θ yielded questionably high values of L ($\sim$ 150 Å to 50 Å) for carbon in the photon energy region from 20 to 30 eV, we turned to a second technique[11] (see Appendices E-2 and G) based on photoelectric yield measurements. A wedge-shaped carbon film was deposited on a glass substrate and the thickness, t, as a function of position along the wedge obtained from a combination of transmittance and independent interferometric measurements. The total yield $Y(t)$ normalized to the yield $Y(\infty)$ for a thick sample, was obtained as a function of t over the same energy range of 20 to 64 eV. These data indicated that the values of L for photoexcited electrons in carbon are much smaller in the region of 20 to 40 eV than those obtained from observations of $G(\theta)$ vs θ. All electron attenuation lengths in solid media are thought to be small ($\lesssim$ 10 Å) in the region of $\sim$ 15 to $\sim$ 1000 eV. The values inferred by inspection of $Y(t)/Y(\infty)$ vs t were in fact in this range for carbon. However, a detailed interpretation of these data for evaporated carbon films was subject to several theoretical and experimental uncertainties. Gold is simpler to work with and the optical properties of gold are better documented in the literature than those of carbon. Hence, it was thought that measurements of $Y(t)/Y(\infty)$ vs t for gold films would provide a check on the carbon data and its interpretation. Data was thus obtained on gold films and an analysis in terms of the theory proposed by Pepper[22] was attempted. The range of film thickness required for an accurate determination of attenuation length depends on the optical properties of the film

and the value of L of the emitted electrons. For a strongly absorbing film and small L the thickness available should range from $t < L$ to $t = \infty$. For weakly absorbing films, one does not need to have films with $t < L$, but small enough thicknesses should be used that the first, and strongest, structure in $Y(t)/Y(\infty)$ vs t is accurately specified. Furthermore, these films need to be homogeneous and continuous and to have smooth interfaces with the substrate and with vacuum in order for $Y(t)/Y(\infty)$ vs t to yield meaningful L values. A literature survey has now shown that using currently available techniques for making thin films, all films are discontinuous for t less than about 50 to 300 Å, the thickness at which continuity occurs depending on the method of preparation. In many cases, values of L calculated from observations on ultrathin films would be more dependent on the method of film preparation, and hence film structure, than on the basic electronic properties of the material of the film. Thus this method is generally unsuitable for the determination of L values in the UV and soft X-ray region. In view of this conclusion, some L values obtained by this method and published in the literature turn out to be meaningless, except insofar as they set upper bounds on the actual values of L. This was the case for our $Y(t)/Y(\infty)$ vs t data for both carbon and gold.

Examination of variations of these two methods, such as $G(\theta)$ vs θ for thin films of known thickness, or the ratio of photoelectric yields for a thin film illuminated from the front and from the back through the substrate, as a function of film thickness, reveals that all methods for determining L which involve photoelectric yield measurements appear subject to the same limitations when L is small and the material is moderately to strongly absorbing.

To summarize our attempts to get electron attenuation lengths from photoelectric yield measurements; when the medium is strongly absorbing,

techniques involving thick films must be used to determine L values. However, to obtain L to ±1 Å when L is less than about 10 Å requires that k be known to within ±1%. For strongly absorbing materials in the energy range of interest, k cannot presently be measured to this accuracy. Thus L cannot be obtained with any meaningful degree of accuracy. When the medium is weakly absorbing and L is short, both thick- and thin-film techniques can be used, but data should be interpreted with great care. Films should not be employed that are so thin that they are not continuous. Effective L values calculated from observations on such films are dependent on film structure and hence are not characteristic of the bulk material. When effective L values can be obtained by a method employing thin films that are thick enough to be continuous and homogeneous, they should be corrected for size effects so that the electron attenuation lengths obtained correspond to those for electrons escaping across a planar interface between the semi-infinite medium and vacuum. Using currently developed experimental techniques L values can be obtained for weakly absorbing materials, but it is extremely difficult to get values accurate to even ±10% by any known photoemission technique. Finally, especially for short attenuation lengths, the theories of photoemission employed in their derivation need to be refined.

Although, as already described, observations of $G(\theta)$ vs θ from a thick sample cannot be analyzed for electron attenuation lengths when the sample is strongly absorbing, the relative yields for a given photon energy are found to be characteristic of the material. Generally, $G(\theta)$ vs θ is reproducible to ±1% and is relatively insensitive to surface conditions. These data, currently unavailable in the open literature, are of practical interest in the development of improved photoemitters in the vacuum ultraviolet and soft X-ray regions. Our accumulated $G(\theta)$ vs θ data on a variety of metals, semiconductors, and insulators[11] are currently being prepared for publication

without attempting to obtain the associated L values. In some cases, where the material is strongly absorbing, analysis of $G(\theta)$ vs θ assuming a range of small L values may be the easiest and most accurate way of obtaining the optical properties n and k. This possibility is presently being investigated.

C. TABULATIONS OF ELECTRON INTERACTION PARAMETERS IN SOLIDS

A quantitative description of the interaction of electrons with matter over a large range of energies is a subject of basic importance in a wide variety of theoretical and applied areas. From the theoretical standpoint, calculations, by other groups, of energy loss and range of electrons in many different materials had previously formed the basis of at least two extensive tabulations.[23,24] Both of these works were restricted to electron energies $\geq$10 keV and were based on the Bethe theory of stopping power including various modifications and corrections (e.g., density-effect corrections). We felt that calculations of mean free paths, energy loss, etc., for electrons of energy $\leq$10 keV, based on the best currently available theoretical models, would provide useful guides for interpretation of experimental data as well as input for calculations in applied areas. Theoretical models developed and tested in our group and elsewhere over many years have formed the basis for our calculational efforts in this part of the program. Our attention has focused on inelastic interactions in which electron excitations play a major role. Thus we consider incident electron energies from a few eV to 10 keV. Inelastic processes in the "subexcitation" region of energies (a few eV or less), for example phonon generation, must be treated using different theoretical techniques. For the electron energy range studied in this work, the principal mechanisms determining the interaction parameters are excitation of electrons from the conduction or valence bands and from the inner shells of the ion cores of the solid into continuum energy levels.

Four reports have resulted from work performed under this part of the contract. These reports provide tabulations of inverse mean free paths, stopping power, ranges calculated in the continuous-slowing-down approximation (CSDA), and straggling in ten solids for electrons of energies from a few eV through 10 keV. Also included in these reports is a complete description of the theoretical models and techniques employed in the calculations. The solids studied, the report number, and a brief description of the material contained in each report are listed below. The references indicated give complete information on report title, number, and date of publication.

1. Al and Al_2O_3; AFCRL-TR-75-0583; Reference 12

The interaction of electrons with the solids Al and Al_2O_3 is described based on the electron gas model for the conduction band electrons in Al, a model insulator theory for the valence electrons in Al_2O_3, and inner shell ionization derived from atomic, generalized oscillator strengths. Contributions to the inverse mean free path and stopping power from the various interaction processes are tabulated for electron energies from 0.5 eV to 10 keV for Al and from 10 eV to 10 keV for Al_2O_3. Electron range in the continuous-slowing-down approximation and straggling are tabulated for electron energies from 10 eV to 10 keV for both materials.

2. Si and SiO_2; RADC-TR-76-125; Reference 13

The interaction of electrons with the solids Si and SiO_2 is described based on a "modified electron gas model" for the valence band electrons in Si, a model semiconductor theory for the valence band electrons in SiO_2, and inner shell ionization derived from atomic, generalized oscillator strengths. Contributions to the inverse mean free path and stopping power from the various interaction processes are tabulated for electron energies from threshold ($\sim$ 4 eV above the Fermi level) to 10 keV for Si and from 10 eV to

10 keV for SiO_2. Electron range in the continuous-slowing-down approximation and straggling are tabulated for electron energies from 10 eV to 10 keV for both materials.

3. Ni, Cu, Ag, and Au; RADC-TR-76-220; Reference 14

A statistical model is described and employed to calculate inverse mean free path, stopping power, and mean square energy loss for electrons of energy from 0.5 eV to 10 keV above the Fermi level in several solids. From these calculations, electron range in the continuous-slowing-down approximation and straggling are evaluated for electron energies from 10 eV to 10 keV. Tables of these quantities are presented for the solids Ni, Cu, Ag, and Au. Graphical displays of the inverse mean free path and stopping power for these four solids are also included.

A brief description of the use of this statistical model in calculations of electron inelastic mean free paths and energy loss is found in Reference 15. This paper is also included in this report as Appendix H.

4. Ge and GaAs; RADC-TR-76-350; Reference 16

The interaction of electrons with the solids Ge and GaAs is described based on a model semiconductor theory for the valence band electrons and inner-shell ionization derived from classical-binary-collision cross sections. Contributions to the inverse mean free path and stopping power from the various interaction processes are tabulated for electron energies from threshold ($\sim$ 2 eV for Ge and $\sim$ 2.5 eV for GaAs) to 10 keV. Electron range in the continuous-slowing-down approximation and straggling are tabulated for electron energies from 10 eV to 10 keV for both materials.

III. IMPLICATIONS FOR FUTURE WORK

The work performed under this contract has provided a wealth of new and useful information concerning electron interactions with communications materials. However, the studies reported here also raise many new questions and suggest several areas requiring additional study.

One logical result of our theoretical and experimental studies is tabulations of mean free path, energy loss, energy straggling, range, and range straggling for electrons in materials of relevance to communications or guidance systems, whether they be metals, semiconductors, or insulators. The models developed for the tabulations outlined in this report are for isotropic, homogeneous media. These models may require modification before they can be employed in the calculations necessary to produce the tabulations for organic polymers. In addition, the existing tabulations need to be extended to lower energies. In order to do this it is necessary to examine, in more detail than is presently available, low-energy electron scattering processes. Such a study should consider electron elastic scattering, which, though not involved in energy degradation, must certainly affect transmission in a significant manner. Effects due to the presence of long- or short-range crystalline order in the solid, and inelastic (or quasi-elastic) scattering processes such as phonon excitation in the "subexcitation" region of energies should be investigated. The effect of plasmon damping on low-energy electron mean free paths also needs to be considered.[17]

The theoretical models involved in the analysis of photoelectric yield measurements to obtain electron attenuation lengths require further study. In particular the shorter the values of the attenuation lengths, the more important it is to take into account the properties of the region in the vicinity of the surface. In the models employed in the present study planar

interfaces and homogeneous media have been assumed. In the UV and soft X-ray regions such models have yielded electron attenuation lengths comparable with, or less than, the rms surface roughness height. Even assuming no other uncertainties, it is difficult to know the significance of such values in terms of the model assumed and the known imperfections of the surface region. Finally, the theoretical relationship between range, electron attenuation length, and mean free path still needs to be elucidated.

Experimentally, the problems encountered in this study indicate two clear-cut directions for further investigations: (a) to develop ways by which the extinction coefficient of moderately to strongly absorbing materials might be obtained to a greater accuracy than is presently possible and (b) to investigate ways of measuring electron attenuation lengths which do not depend for their validity on the homogeniety of thin films used in the measurements.

Specific projects which need to be undertaken and which would follow naturally from the work performed under this contract and its extensions suggested above are:

(i) Tabulation of mean free path, etc., for polystyrene,

(ii) Measurement of optical properties of other organic materials, such as polyethylene, and their use in tabulations of mean free path, etc.,

(iii) Spatial distribution of Auger electron-hole cascades generated by ionizing radiations,

(iv) Structure of heavy ion tracks,

and

(v) Slowing-down spectrum in Al metal.

Finally, it should be mentioned that several additional publications not listed under "Publications and Reports Resulting from Work Done Under this

Contract" (page 22) will be written based on work done under the contract. These papers will report on the slowing-down spectrum in Al_2O_3, the experimental photoelectric yield data as a function of photon angle of incidence, and possibly give critiques on obtaining optical properties and/or electron attenuation lengths from these data.

IV. REFERENCES

A. Publications and Reports Resulting from Work Done Under this Contract

1. R. H. Ritchie and V. E. Anderson, IEEE Trans. Nucl. Sci. NS-18, 141 (1971).
2. L. C. Emerson and R. D. Birkhoff, "Electron Spectrum in Irradiated Silicon," Proceedings of IEEE Annual Conference on Nuclear and Space Radiation Effects, Durham, New Hampshire, July 20-23, 1971.
3. L. C. Emerson, R. D. Birkhoff, V. E. Anderson, and R. H. Ritchie, Phys. Rev. B 7, 1798 (1973).
4. L. C. Emerson, R. D. Birkhoff, V. E. Anderson, J. C. Ashley, Dayashankar, and R. H. Ritchie, "Electron Slowing-Down Spectrum in Al_2O_3," Proceedings of IEEE Annual Conference on Nuclear and Space Radiation Effects, Fort Collins, Colorado, July 15-18, 1974, pp. 163-164.
5. R. H. Ritchie, C. J. Tung, V. E. Anderson, and J. C. Ashley, Rad. Res. 64, 181 (1975).
6. J. C. Ashley, C. J. Tung, and R. H. Ritchie, IEEE Trans. Nucl. Sci. NS-22, 2533 (1975).
7. C. J. Tung, R. H. Ritchie, J. C. Ashley, and V. E. Anderson, "Inelastic Interactions of Swift Electrons in Solids," ORNL-TM-5188 (January 1976).
8. E. T. Arakawa, A. J. Braundmeier, M. W. Williams, R. N. Hamm, and R. D. Birkhoff, "Electron Attenuation Lengths in Carbon Films," Proceedings of IEEE Annual Conference on Nuclear and Space Radiation Effects, Fort Collins, Colorado, July 15-18, 1974, pp. 159-162;

E. T. Arakawa, M. W. Williams, R. N. Hamm, R. D. Birkhoff, and A. J. Braundmeier, "Electron Attenuation Lengths in Carbon Films," Proceedings of IV International Conference on Vacuum UV Radiation Physics, Hamburg 1974 (Pergamon-Vieweg), pp. 580-581 (Appendix E-1).

9. T. A. Callcott and E. T. Arakawa, Phys. Rev. B 11, 2750 (1975).

10. T. Inagaki, R. N. Hamm, M. W. Williams, and E. T. Arakawa, "Optical Properties of Polystyrene from the Near Infrared to the X-Ray Region and Convergence of Optical Sum Rules." Submitted to The Physical Review (see also Appendix F).

11. "Electron Attenuation Lengths in the Vacuum Ultraviolet and Soft X-Ray Regions," in Health Physics Division Annual Progress Report, June 30, 1976, ORNL-5171, pp. 160-162, and previous reports in this series (see also Appendix G).

12. J. C. Ashley, C. J. Tung, V. E. Anderson, and R. H. Ritchie, "Inverse Mean Free Path, Stopping Power, CSDA Range, and Straggling in Aluminum and Aluminum Oxide for Electrons of Energy $\leq$ 10 keV," AFCRL-TR-75-0583 (December 1975).

13. C. J. Tung, J. C. Ashley, V. E. Anderson, and R. H. Ritchie, "Inverse Mean Free Path, Stopping Power, CSDA Range, and Straggling in Silicon and Silicon Dioxide for Electrons of Energy $\leq$ 10 keV," RADC-TR-76-125 (April 1976).

14. J. C. Ashley, C. J. Tung, R. H. Ritchie, and V. E. Anderson, "Inverse Mean Free Path, Stopping Power, CSDA Range, and Straggling in Ni, Cu, Ag, and Au for Electrons of Energy $\leq$ 10 keV Calculated from a Statistical Model," RADC-TR-76-220 (June 1976).

15. J. C. Ashley, C. J. Tung, R. H. Ritchie, and V. E. Anderson, IEEE Trans. Nucl. Sci. (to be published, 1976) (see also Appendix H).

16. C. J. Tung, J. C. Ashley, R. H. Ritchie, and V. E. Anderson, "Inverse Mean Free Path, Stopping Power, CSDA Range, and Straggling in Ge and GaAs for Electrons of Energy $\leq$ 10 keV," RADC-TR-76-350 (1976).

17. J. C. Ashley and R. H. Ritchie, Phys. Status Solidi B 62, 253 (1974).

B. Other References

18. L. V. Spencer and U. Fano, Phys. Rev. 93, 1172 (1954); R. L. Platzman, Intern. J. Appl. Rad. Isotopes 10, 116 (1961).

19. H. H. Hubbell, Jr., W. J. McConnell, and R. D. Birkhoff, Nucl. Instr. and Meth. 31, 18 (1964).

20. R. D. Birkhoff, in Penetration of Charged Particles in Matter: A Symposium (National Academy of Sciences, Washington, DC, 1970) pp. 1-15.

21. L. V. Spencer and F. H. Attix, Rad. Res. 3, 239 (1955).

22. S. V. Pepper, J. Opt. Soc. Am. 60, 805 (1970).

23. M. J. Berger and S. M. Seltzer in "Studies in Penetration of Charged Particles in Matter" (National Academy of Sciences-National Research Council, Washington, DC, 1964, Publ. No. 1133) pp. 205-268.

24. L. Pages et al, Atomic Data 4, 1-127 (1972).

25. E. T. Arakawa, R. N. Hamm, and M. W. Williams, J. Opt. Soc. Am. 63, 1131 (1973).

APPENDIX A

Classical Binary Collision Cross Sections of Atomic Systems

R. H. Ritchie and J. C. Ashley

Health Physics Division, Oak Ridge National Laboratory

Oak Ridge, Tennessee 37830

and

Dayashankar

Directorate of Radiation Protection

Bhaba Atomic Research Centre, Bombay 11, India

ABSTRACT

We have considered the generalized oscillator strength (GOS) corresponding to various distributions of speed of a target electron in an atomic system upon which a fast electron is incident. The classical binary collision (CBC) model is employed. We have evaluated the integral over all energy transfer of the GOS for each of the distributions and find that for large momentum transfer all of those considered satisfy the Bethe sum rule. At small momentum transfer all fail to satisfy this rule due to the fact that large impact parameter collisions are not described properly in the CBC model. Procedures for supplementing the GOS such that experimental mean excitation energies, polarizabilities, etc., for a given atomic system are reproduced will be discussed in a succeeding paper.

---

*Research sponsored in part by the U. S. Atomic Energy Commission under contract with Union Carbide Corporation. Supported in part by Defense Nuclear Agency through Air Force Cambridge Research Laboratories, Office of Aerospace Research, under Contract No. Y71-912, but does not necessarily reflect endorsement by the sponsor.

I. Introduction

Much progress has been made in recent years toward construction of theoretical cross sections for excitation and ionization of electrons from stationary states in atomic systems.[1] However, many such approaches involve detailed numerical solutions of the Schrödinger or Dirac equations in an assumed potential (usually self-consistent in some sense) and require separate studies for each shell in an atom.

At a more empirical level, studies of the classical binary collision (CBC) model have become popular following the demonstration by Gryzinski[2] that this model has much physical content and is capable of giving quite reasonable predictions of ionization cross sections for atomic and molecular systems which may be exceedingly cumbersome to treat on a more fundamental basis.

The CBC model has been applied[2, 3] to the problem of obtaining estimates of quantities such as stopping power for atomic systems for charged particles with low enough energy that the asymptotic Bethe-Bloch formula is not accurate. These efforts suffer from the defect that the CBC formulas used are based on the Gryzinski velocity distribution which is employed to characterize the ground state electrons; a number of workers[4] have objected to this velocity distribution because of its unphysical, ad hoc character.

The authors have been concerned for some time with the study of electron slowing-down distributions in condensed matter at electron kinetic energies comparable with ionization energies in the atoms making up the material.[5] In

order to construct inelastic differential cross sections for such materials we have studied the CBC model in some detail. We have evolved certain simple procedures for fitting CBC model cross sections in the large momentum transfer region, where they are most reliable, with information on cross sections in the region of small momentum transfer. Although in essence semi-empirical, our procedures result in simple analytic differential cross sections which are constrained to be accurate in the average in certain respects described below. They may be employed to estimate charged particle inelastic cross sections, stopping power, mean angular deflections, etc., for complicated many-electron systems which should be useful at arbitrary energy.

Our approach is based on sum-rule considerations, but experimental data on average excitation energies, polarizabilities, etc. may also be used in this connection.

II. Classical Binary Collision Model

Binary-encounter classical collision theory has enjoyed much attention following its application by Gryzinski[2] to a number of physical processes which until then had been treated mainly by quantum-theoretic methods. Thomson,[6] Thomas[7] and Williams[8] earlier developed the theory in some detail; however, Gryzinski's work was apparently done without knowledge of the efforts of these authors. Subsequently a number of mathematical corrections and discussions of Gryzinski's results took place.[9] It now appears that when such theory is correctly applied rather good agreement with experiment and with Born-approximation

quantum theoretical results may be obtained. It is particularly valuable in that it leads to very convenient scaling laws.[10] Also it may be applied to systems which are quite cumbersome to treat using quantum methods.

A. Differential Cross Section

The basic doubly-differential cross section on the binary collision model is given by[6, 7, 8]

$$\frac{\partial^2\sigma}{\partial q\,\partial\varepsilon} = \frac{2\pi m e^4}{E_1 v_2 q^2}\,\theta(\varepsilon-\varepsilon_i) \tag{1}$$

where E_1 = energy of incident electron

v_2 = speed of struck electron = $\sqrt{2E_2/m}$

$\vec{q}$ = momentum transfer in collision

ε = energy transfer in collision

ε_i = "ionization energy" of struck electron ,

for spherically symmetric distributions of velocities of the atomic electron. The law of conservation of momentum yields

$$q_{\substack{\max\\\min}} = \sqrt{2m}\cdot\left\{\begin{array}{l}(\varepsilon+E_2)^{1/2} \pm E_2^{1/2}\\ E_1^{1/2} \pm (E_1-\varepsilon)^{1/2}\end{array}\right\}\qquad\begin{array}{l}E_1 \geq \varepsilon + E_2\\ E_1 \leq \varepsilon + E_2\end{array} \tag{2}$$

The quantity $\theta(x)$ is the unit step function. Note that this cross section refers to one struck electron bombarded by a fast electron and excited into a continuum state.

B. Generalized Oscillator Strength

The first Born approximation in quantum mechanics yields the following expression for the differential cross section for excitation of the n^{th} excited state in a system of electrons bombarded by a fast electron possessing incident energy E_1:

$$\frac{d^2\sigma_n}{dq\,d\varepsilon} = \frac{4\pi m e^4}{E_1 q^3} \left| F_n(q,\varepsilon) \right|^2 \tag{3}$$

for axially symmetric systems. This expression is valid in the non-relativistic limit and does not include exchange effects. Here

$$F_n(q,\varepsilon) = \langle n | \sum_i \exp(i\vec{q}\cdot\vec{r}_i) | 0 \rangle \tag{4}$$

is the matrix element of the density operator evaluated for transitions between the ground state with eigenvector $|0\rangle$ and an excited state with eigenvector $|n\rangle$, corresponding to the energy difference $\varepsilon = E_n - E_0$.

The well-known general sum rule[11] may be written

$$S\,\varepsilon \left| F_n(q,\varepsilon) \right|^2 = Z_2 q^2/2m \tag{5}$$

where Z_2 is the number of electrons in the system and where S indicates a sum over discrete final states and an integral over continuum final states.

The differential oscillator strength for transitions into the continuum may be defined as

$$\frac{df}{d\varepsilon} = \frac{2m\varepsilon}{Z_2 q^2} \left| F_n(q,\varepsilon) \right|^2 . \tag{6}$$

In terms of this quantity

$$\frac{d^2\sigma}{dq\,d\varepsilon} = \frac{2\pi e^4 Z_2}{E_1 \varepsilon q} \frac{df}{d\varepsilon} \tag{7}$$

is the doubly differential cross section for excitation into continuum final states. Vriens and Bonsen[12] have studied the differential GOS for ionization into continuum final states.

C. Classical Differential Cross Sections for Various Speed Distributions of the Struck Electron

1. The Virial Distribution - In this case the excitation energy is taken equal to $\frac{1}{2}mv_2^2 = E_2$. The generalized oscillator strength corresponding to the resulting differential cross section may be written

$$\frac{df}{d\varepsilon} = \frac{E_1 q\varepsilon}{2\pi e^4} \frac{d^2\sigma}{dq\,d\varepsilon} = \frac{m\varepsilon}{v_2 q^3} \theta(\varepsilon - E_2) \tag{8}$$

from Eqs. (7) and (1). In the last form of Eq. (8) Z_2 has been set equal to one. Conservation of momentum leads to

$$q_{(\substack{max\\min})} = \sqrt{2m}\left[(E_2+\varepsilon)^{1/2} \pm E_2^{1/2} \right] \tag{9}$$

where it is sufficient to consider $E_1 >> (E_2, \mathcal{E})$ in evaluating the generalized oscillator strength on this model. If we compute the integral of the GOS from Eq. (8) subject to the restriction given in Eq. (9) we find that

$$f_v(\eta) \equiv \int_{\bar{E}_2}^{\infty} d\mathcal{E}\, \frac{df}{d\mathcal{E}} = \begin{cases} 1, & (\eta > 1+\sqrt{2}) \\ [\eta^2(\eta+2)^2 - 1]/8\eta^3, & (\sqrt{2}-1 < \eta < \sqrt{2}+1) \\ 0, & (\eta < \sqrt{2}-1) \end{cases} \tag{10}$$

where $\eta = q/\sqrt{2mE_2}$. In Fig. (1) $f_v(\eta)$ is plotted as a function of η. For large enough momentum transfer the oscillator strength defined according to quantum mechanics in the Born approximation sums to exactly unity, as it should. For smaller q the summed oscillator strength falls below this value and becomes identically zero for q small. Thus one expects the virial distribution on the classical binary collision model to fail badly for small momentum transfers according to these considerations. Others[4, 9] have noted that the classical binary collision model is inadequate there because resonant energy transfers in distant collisions are not included at all in this model.

It may be noted that if Eq. (1) is integrated over the values of q allowed in Eq. (2) a cross section differential in energy is obtained:

$$\frac{d\sigma}{d\varepsilon} = \frac{\pi e^4}{E_1 \varepsilon^2}\left(1 + \frac{4}{3}\frac{E_2}{\varepsilon}\right)\theta(\varepsilon - E_2), \qquad (E_2 < E_1 - \varepsilon)$$

$$= \frac{\pi e^4}{3E_1\varepsilon^3}\left(\frac{E_1-\varepsilon}{E_2}\right)^{1/2}(4E_1 - \varepsilon)\,\theta(\varepsilon - E_2), \qquad (E_2 > E_1 - \varepsilon) \tag{11}$$

which agrees with that obtained by others.[10]

2. Gryzinski Speed Distribution - The normalized distribution assumed by Gryzinski[2] in his early work on the CBC model is

$$f(v_2) = \frac{v_0^2}{v_2^3}\, e^{-v_0/v_2} \tag{12}$$

where v_0 is the mean speed. Averaging the CBC cross section over this distribution, we find

$$\frac{d^2\sigma}{dq\,d\varepsilon} = \frac{4\pi m e^4}{E_1 v_0 q^4} F(v_0/v_{2m})\,\theta(\varepsilon - \varepsilon_i) \tag{13}$$

where $F(x) = 1 - (1 + x + x^2/2)e^{-x}$, $\xi = q/\sqrt{2m}$ and $v_{2m} = \sqrt{\frac{2}{m}}\left|\frac{\varepsilon - \xi^2}{2\xi}\right|$.

If we define the oscillator strength $df_G/d\varepsilon$ as above

$$\frac{df_G}{d\varepsilon} = \frac{2m\varepsilon}{v_0 q^3} F(v_0/v_{2m}) \tag{14}$$

and

$$f_G = \int_{\epsilon_i}^{\infty} d\epsilon \, \frac{df_G}{d\epsilon} \tag{15}$$

This integral can be done analytically. Setting $\mathcal{E} = \frac{1}{2}mv_o^2\epsilon$, $q = mv_o\eta$, one finds $f_G = g_1 - g_2$ when $\eta^2 < \epsilon_i$ and $f_G = g_1 + g_2$ when $\eta^2 > \epsilon_i$. Here

$$g_1 = \frac{1}{2}\left(1 + \frac{1}{\eta}\right) - \frac{1}{\eta a^2}\left[1 - (1+a)e^{-a}\right]$$

$$g_2 = \frac{1}{a}\left[1 - \left(1 + \frac{a}{2}\right)e^{-a}\right] \tag{16}$$

where $a = 2\eta/|\epsilon_i - \eta^2|$. It may be shown that $f_G \to 1$ as $\eta \to \infty$ and $f_G \to \frac{2}{3\epsilon_i}$ as $\eta \to 0$. Figure (1) shows a plot of f_G vs. η from the expression given above for the case $\epsilon_i = 1$. It is seen that the distribution chosen by Gryzinski has the desirable effect of yielding a non-zero oscillator strength as $\eta \to 0$. However, it is clear that the value $2/3\epsilon_i$ attained in this limit has little physical significance. Further, as Burgess and Percival[4] and others have noted, the Gryzinski speed distribution has little basis in physical theory and should be regarded as empirical in character.

3. Hydrogenic Closed Shell Speed Distribution - Fock[13] has shown that the exact speed distribution corresponding to that of a closed shell of any principal quantum number in a hydrogenic atom is given by

$$f(v_2) = \frac{32}{\pi} \frac{v_o^5 v_2^2}{(v_o^2 + v_2^2)^4} \tag{17}$$

where $mv_o^2/2$ is the average kinetic energy of electrons in the shell. This distribution is normalized such that $\int_0^\infty f(v_2)\,dv_2 = 1$.

Averaging Eq. (1) over this distribution gives

$$\frac{d^2\bar{\sigma}}{dq\,d\varepsilon} = \int_{v_{2m}}^{\infty} dv_2\, f(v_2)\, \frac{d^2\sigma}{dq\,d\varepsilon} \tag{18}$$

where $v_{2m} = \sqrt{\frac{2}{m}}\left|\frac{\varepsilon - \xi^2}{2\xi}\right|$ originates from the energy-momentum conservation conditions (Eq. (2)) and $\xi = q/\sqrt{2m}$. The integration yields

$$\frac{d^2\bar{\sigma}}{d\eta\,d\epsilon} = \frac{2^{11}}{3}\,\frac{a_o^2}{\beta}\left(\frac{R_y}{E_o}\right)^2 \frac{\eta^2\,\theta(\epsilon-\epsilon_i)}{\left[(\epsilon-\eta^2)^2 + 4\eta^2\right]^3} \tag{19}$$

where the variables

$$\eta = \frac{q}{\sqrt{2mE_o}} \qquad Ry = e^2/2a_o = 13.6\ \text{eV}$$

$$\epsilon = \varepsilon/E_o \qquad a_o = \hbar^2/me^2 = 0.529\ \text{Å}$$

$$\epsilon_i = \varepsilon_i/E_o \qquad E_o = \tfrac{1}{2}mv_o^2$$

$$\beta = E_1/E_o$$

are employed.

The differential oscillator strength corresponding to this cross section may be written

$$\frac{df_{CH}}{d\epsilon} = \frac{2^8}{3\pi} \frac{\epsilon \eta^3 \theta(\epsilon - \epsilon_i)}{\left[(\epsilon-\eta^2)^2 + 4\eta^2\right]^3} \tag{20}$$

in terms of the new variables. The integral of this quantity may be done analytically; the result is

$$f_{CH} \equiv \int_{\epsilon_i}^{\infty} d\epsilon \frac{df}{d\epsilon} = \frac{2^8 \eta^3}{3\pi} \left[\frac{4 - \epsilon_i + \eta^2}{16 D^2} + \frac{3}{2^5 \eta^3} \left\{ \frac{\pi}{2} - \tan^{-1}\left(\frac{\epsilon_i - \eta^2}{2\eta} \right) \right\} - \frac{3}{2^7 \eta^2} \frac{\epsilon_i - \eta^2}{D} \right] \tag{21}$$

where $D = (\epsilon_i - \eta^2)^2 + 4\eta^2$. Figure 1 shows a plot of f_{CH} as a function of the momentum transfer variable η, choosing $\epsilon_i = 1$. It is seen that the velocity averaging process is successful in filling the η-ϵ plane with differential oscillator strength such that f_{CH} is non-zero everywhere save on the η=0 axis. f_{CH} tends asymptotically to unity and is slightly greater than zero (~ 1.002) in the region $2 \leq \eta \leq 5$. However, on the η=0 line there is difficulty, since $f_{CH} \sim \frac{64}{3\pi} \eta^3 / \epsilon_i^4$ for $\eta << 1$. Born approximation results with various atomic models leave little doubt that f_i should be non-zero there for optically allowed transitions.

III. Sum Rule-Constrained CBC Cross Sections

We wish to retain the analytical simplicity of the CBC cross sections, but we should prefer to use cross sections for which the GOS satisfies the

fundamental Bethe sum rule[11] and possibly higher-order sum rules.[1,14] The following simple procedure suggests itself in this connection. We note that optical oscillator strengths are known experimentally and theoretically for a number of atomic systems over a rather wide range of energies.[15] Optical oscillator strengths $f_n(0)$ (or $df(0)/d\varepsilon$ in the continuum) of an atom are equal to the GOS of that atom in the limit of zero momentum transfer; i.e.

$$f_n(0) = \lim_{q \to 0} \left\{ \frac{2m\varepsilon}{E_2 q^2} \left| F_n(q,\varepsilon) \right|^2 \right\} \tag{22}$$

Suppose that $f_n(0)$ and $\frac{d}{d\varepsilon} f(0)$ are known for a given atom and that one may use CBC GOS values in the region of large η for a given shell of that atom. We suggest that the following approximation to the true GOS of a given shell[16] should be useful;

$$\tilde{f}_n(q) = f_n(0) \left[1 - f_{CH}(q) \right] \tag{23}$$

in the region of discrete transitions and

$$\frac{d\tilde{f}(q)}{d\varepsilon} = \frac{df(0)}{d\varepsilon} \left[1 - f_{CH}(q) \right] + \frac{d f_{CH}(q)}{d\varepsilon} \tag{24}$$

in the continuum. That is, we propose an interpolation scheme for the GOS which reduces to the known optical oscillator strength for small momentum transfers and which goes over into the CBC cross section, using a closed shell

hydrogenic speed distribution, for large momentum transfer. There are at least two advantages to such a procedure: (1) the Bethe sum rule for f_n and $\frac{df}{d\varepsilon}$ is satisfied for all q; (2) the cross section resulting from this GOS yields a charged particle stopping power which reduces to the correct Bethe form for large (but non-relativistic) velocities of the charged particle. Clearly, one may choose other differential GOS functions than $\frac{df_{CH}}{d\varepsilon}$ for use in Eq. (23); however, they are plotted since the analytical simplicity of Eq. (20) is quite appealing. Also this form should be fairly accurate for inner shells, particularly if one employs experimental values of the ionization energy E_i of a given atomic shell and if one chooses the mean kinetic energy of electrons in that shell from Slater's rules.[17]

As an indication of the usefulness of the procedure described above, we have plotted in Fig. 2 the exact differential GOS of the H atom, $df_H/d\varepsilon$, the CBC GOS using Eq. (20), and $d\tilde{f}/d\varepsilon$ from Eq. (24) in which $\frac{df}{d\varepsilon}(0)$ is taken to be the exact optical oscillator strength of the H atom. All energies are expressed in terms of Ry = 13.6 eV and all momenta are expressed in units of $(a_o)^{-1} = (0.529\text{Å})^{-1}$. The various GOS's are plotted as a function of $\eta^2 = (a_o q)^2$ and for several values of $\epsilon = \mathcal{E}/\text{Ry}$. One sees from this plot that $df/d\varepsilon$ is superior to $df_{CH}/d\varepsilon$ and is a reasonable approximation to the exact GOS over the whole ε-η plane.

Summary

We have considered the GOS corresponding to various speed distributions in the CBC model. We find that the Gryzinski distribution, though unphysical,

yields a CBC cross section which satisfies the Bethe sum rule better overall than either that derived from the virial distribution or that derived from the hydrogenic closed-shell distribution. This fact may account in part for the generally good agreement between the Gryzinski theory and various experiments.[4]

In a succeeding paper we will present applications of the approximation indicated in Equations (23) and (24) to the construction of electron cross sections which satisfy the Bethe sum rule and yield mean excitation energies which are constrained to agree with experiment. Such procedures are of value in obtaining semi-empirical cross sections for complicated many-electron systems to use in the study of electron slowing-down in condensed matter.

REFERENCES

[1]For a recent review of this field see M. Inokuti, Rev. Mod. Phys. 43, 297 (1971). More recently Cooper and Kolbenstredt, Phys. Rev. A5, 677 (1972) have presented an approximate quantum model for such interactions.

[2]M. Gryzinski, Phys. Rev. 115, 374 (1959); Phys. Rev. 138, A305, A322, A336 (1965).

[3]P. D. Holt, in "Charged Particle Tracks in Solids and Liquids" published by The Institute of Physics and The Physical Society, (1970), p. 42.

[4]See e. g., A. Burgess and J. C. Percival in "Advances in Atomic and Molecular Physics," Vol. 4, Ed., D. R. Bates, Academic Press (1968) p. 109.

[5]L. C. Emerson, R. D. Birkhoff, V. E. Anderson and R. H. Ritchie, Phys. Rev. B7, 1798 (1973).

[6]J. J. Thomson, Phil. Mag. 23, 449 (1912).

[7]L. H. Thomas, Proc. Camb. Phil. Soc. 23, 714, 829 (1927).

[8]E. J. Williams, Nature 119, 489 (1927).

[9]Recent reviews of the development of CBC theory are given in reference (4), by L. Vriens in "Case Studies in Atomic Collision Physics I," North-Holland Publishing Co. (1969), p. 335, and by M. R. H. Rudge, Rev. Mod. Phys. 40, 564 (1968).

[10]J. D. Garcia, Phys. Rev. 177, 223 (1969).

REFERENCES

[11] H. A. Bethe, Hdbk. d. Physik 24-1, 714 (1933).

[12] L. Vriens and T. F. M. Bonsen, J. Phys. B1, 1123 (1968).

[13] V. Fock, Z. Physik 98, 145 (1935).

[14] U. Fano and J. E. Turner, NAS-NRC publication 1133.

[15] See, e.g., the paper of Stanton, (Physics Letters 38A, 131 (1972)) which compares optical oscillator strengths of a large number of atomic systems.

[16] We recognize that rigorous separation of the total GOS of an atom into independent contributions from each shell is not possible. Nevertheless, we suggest that such separation may not lead to large errors in the present framework.

[17] Robinson (Phys. Rev. 140 A764 (1965)) has found that by using experimental ionization energies and by choosing the mean kinetic energy from Slater's rules, together with an approximate recipe for correcting the CBC cross sections at small momentum transfer, one obtains quite good agreement with experimental ionization cross sections of the most weakly bound electrons in O, N, Ar, and Cl^-. Note, however, that he employs the virial speed distribution in his comparisons.

FIGURE CAPTIONS

Fig. 1. Integrated generalized oscillator strengths computed from the classical binary collision model plotted as a function of dimensionless momentum transfer η.

Fig. 2. Generalized oscillator strength for two different values of energy transfer ϵ plotted as a function of $\ell n(\eta^2)$, where η is momentum transfer. The quantity $df_H/d\epsilon$ is the exact GOS for the H atom, $df_{CH}/d\epsilon$ is the GOS computed from the CBC model by averaging over the momentum distribution of the H atom, and $d\tilde{f}/d\epsilon$ is computed from Equation 24 of the text.

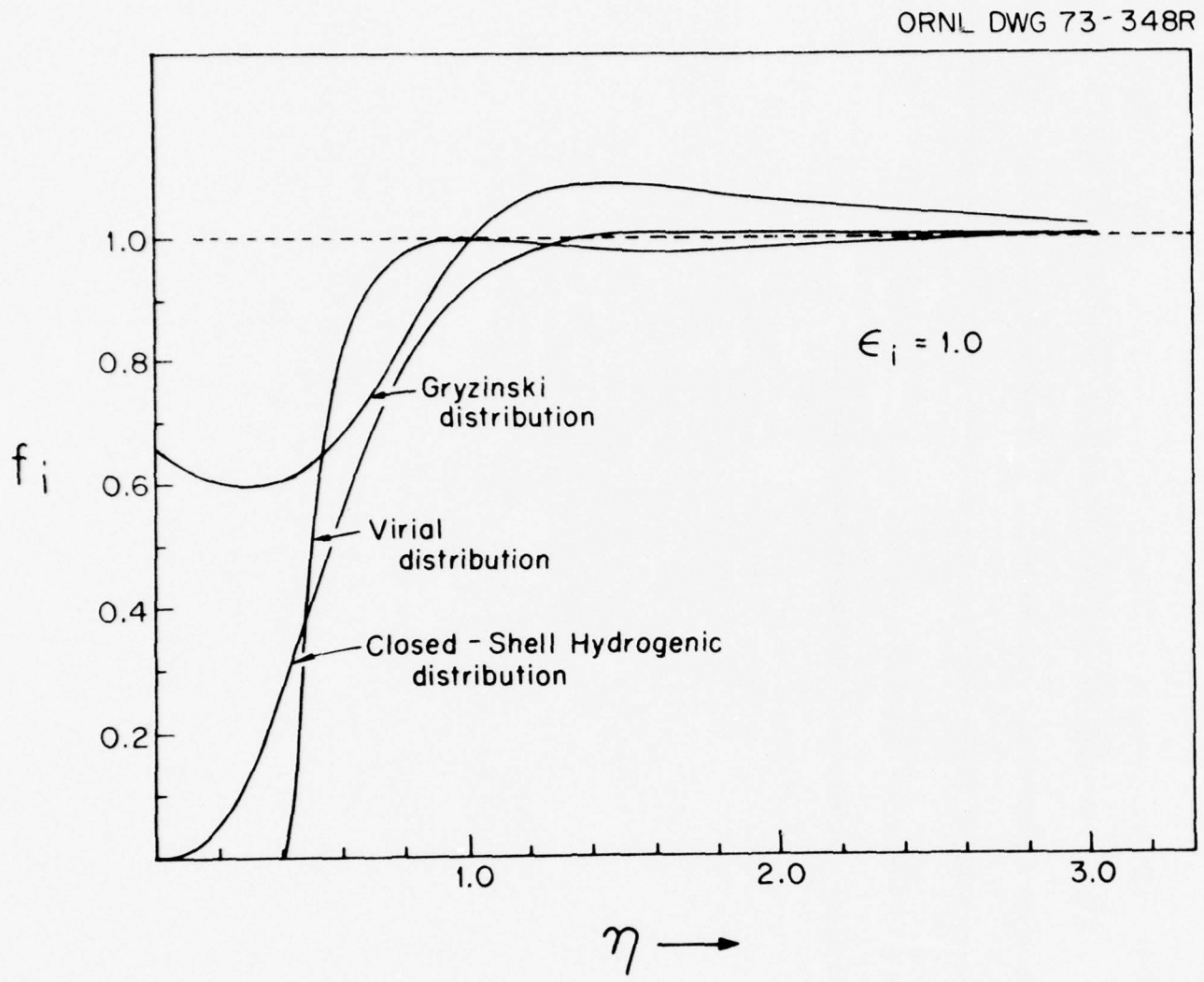

ORNL DWG 73-348R
1.0
0.8
0.6
0.4
0.2
f_i
$\epsilon_i = 1.0$
Gryzinski distribution
Virial distribution
Closed - Shell Hydrogenic distribution
1.0
2.0
3.0
η ⟶

Fig. 1

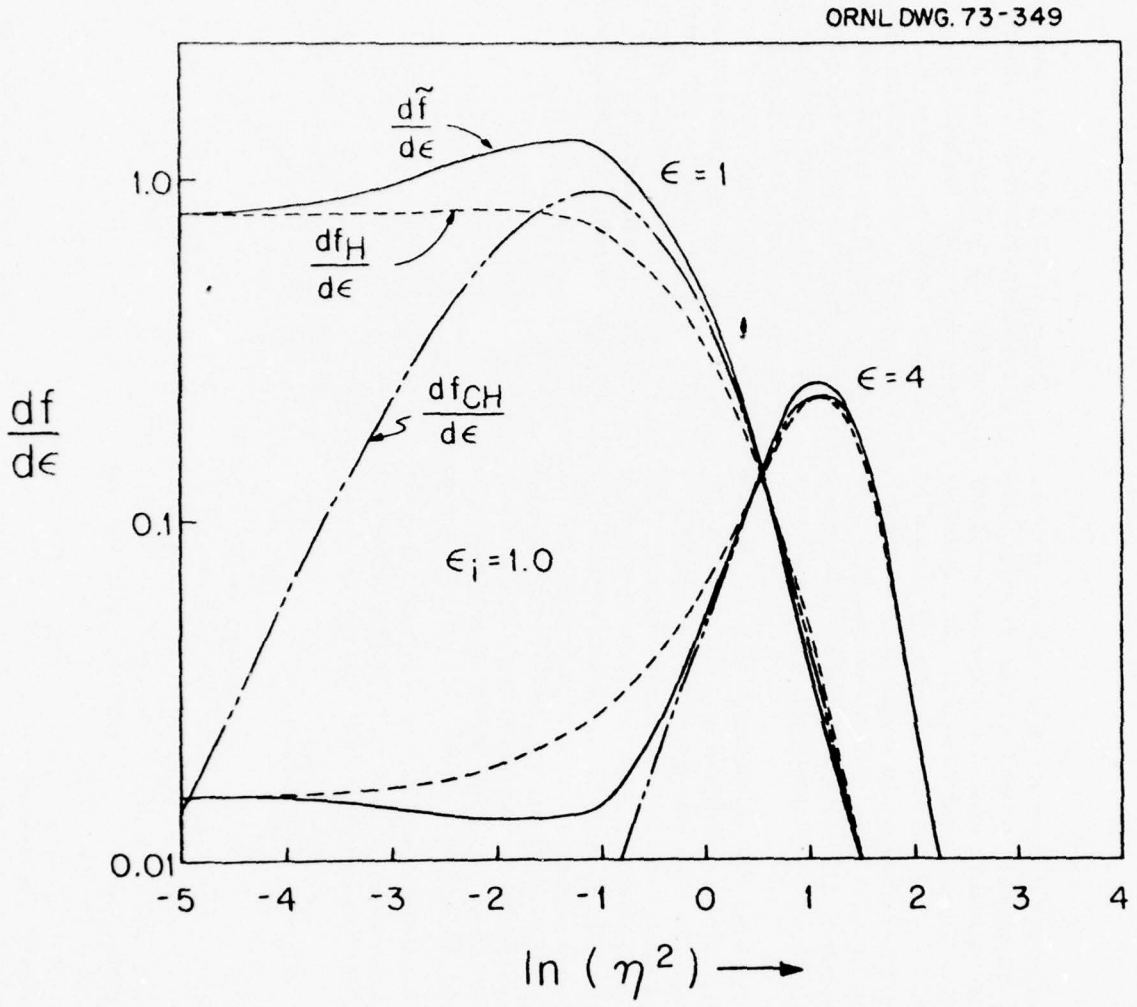

ORNL DWG. 73-349
$\frac{d\tilde{f}}{d\epsilon}$
$\epsilon = 1$
$\frac{df_H}{d\epsilon}$
$\epsilon = 4$
$\frac{df_{CH}}{d\epsilon}$
$\epsilon_i = 1.0$
$\frac{df}{d\epsilon}$
1.0
0.1
0.01
-5
-4
-3
-2
-1
0
1
2
3
4
$\ln(\eta^2) \longrightarrow$

Fig. 2

APPENDIX B-1

Electron Slowing- Down Studies in Al_2O_3

Reprinted from: Health Physics Division Annual Progress Report
for Period Ending July 31, 1973, ORNL-4903, pp. 103-104.

Because of its importance as an insulator and its ease of fabrication into forms suitable for experimental study, aluminum oxide was chosen for the investigation. The study has been carried out, concomitant with a theoretical investigation, using both polished and unpolished polycrystalline samples. It was necessary to dope the Al_2O_3 with a small amount of normal isotopic dysprosium which serves as the source of primary beta particles following activation by thermal neutron irradiation.

The target disks, containing 0.5 wt % dysprosium as the oxide, were fabricated by a coprecipitation technique. The disks were ground to final size using an aluminum oxide abrasive. Sources obtained in this manner exhibited a density of 87% of the theoretical value. The surfaces of the unpolished disks were covered with micropits and imperfections which had dimensions of the order of 0.001 in. The typical size of the individual crystals appeared to be under 0.005 in.

Results of the initial studies on the unpolished crystals were reported earlier. The electron flux inside the material is inferred from that measured in the vacuum environment outside by dividing by a suitable barrier transmission factor which takes the form

$$T(E) \approx 1 - \sqrt{E_A/(E + E_A)} \ ,$$

where E is the electron energy outside and E_A is the electron affinity, equal to the difference between the work function and the gap energy. There exists considerable uncertainty in the value of E_A. A literature survey on aluminum oxide revealed values extended from 0 for amorphous Al_2O_3 to 1.8 eV for the crystalline form. The electron affinity for our polycrystalline sources would presumably fall near the lower end of this range, since this form more nearly resembles the amorphous material. In our work we have somewhat arbitrarily chosen an E_A value of 0.5 eV.

The earlier studies were repeated using polished disks to eliminate possible effects of surface roughness on the experimentally determined flux. A diamond polishing compound was used to produce surfaces with a flatness of approximately one wavelength. The results for the electron flux inside the specimen, shown in Fig. 10.1, exhibit essentially the same shape as the results for the unpolished sources but are everywhere lower in absolute value. This difference is thought to be associated with the uncertainty in the thermal neutron flux in the irradiation facility rather than in the electron flux itself. The characteristics of the measured spectrum are similar to those found earlier for both metals and semiconductors. The most noteworthy difference is the somewhat more rapid buildup of secondary electrons at low energies in the case of the aluminum oxide.

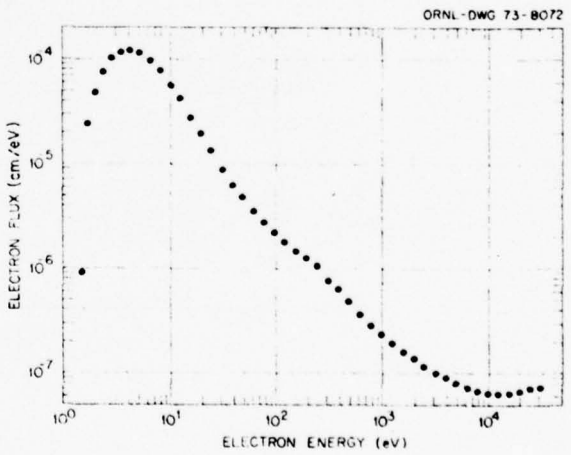


Fig. 10.1. Electron-slowing-down spectrum of aluminum oxide.

APPENDIX B-2

Electron Slowing- Down Studies in Al_2O_3

Reprinted from: Health Physics Division Annual Progress Report
for Period Ending July 31, 1974, ORNL-4979, p. 147.

Last year we reported[21] measurements of the electron slowing-down flux in polished aluminum oxide and assumed that the differences in flux values between these results and those obtained from our earlier studies using unpolished sources resulted from uncertainties in the thermal neutron flux at the time of irradiation rather than in the electron flux itself. We have now eliminated this uncertainty through an analysis of a set of flux monitors that were irradiated along with the set of polished source disks. An accurate value for the thermal flux was obtained from a cobalt-aluminum monitor, while corrections for the epithermal flux were obtained from simultaneous measurements using silver-aluminum monitors. Uncertainty in the ^{164}Dy cross section of $(2700 \pm 200) \times 10^{-24}$ cm^2 represents the largest uncertainty in the determination of the absolute secondary electron flux.

The electron slowing-down flux in aluminum oxide on the basis of this new neutron flux determination is shown in Fig. 22.12 over an energy range extending from 1.5 eV to 32 keV. The flux is slightly higher than that reported previously and reflects the more careful determination of the 2200-m/sec thermal neutron flux. Also shown in the figure is the spectrum calculated by using Monte Carlo techniques and employing inelastic cross sections obtained from a sum-rule-constrained classical binary collision model. Details of this calculation are discussed in the General Radiation Physics Section.

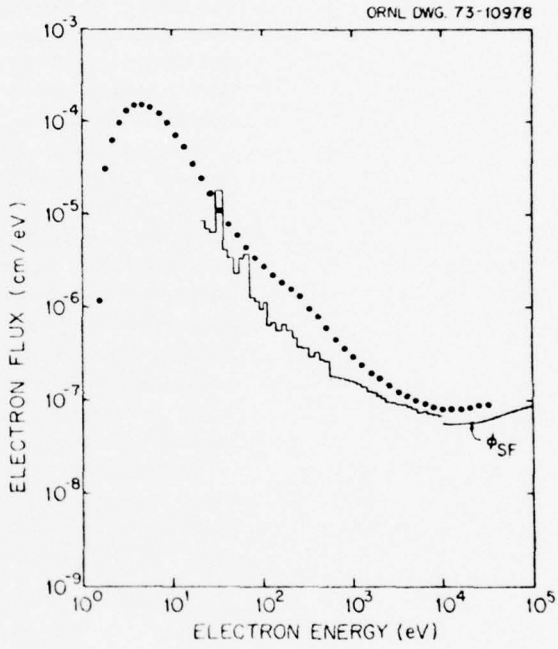


Fig. 22.12. Electron-slowing-down spectrum of aluminum oxide.

21. E. T. Arakawa et al., *Health Phys. Div. Annu. Progr. Rep. July 31, 1973*, ORNL-4903, pp. 103–4.

APPENDIX C

Reprinted from: Health Physics Division Annual Progress Report for Period Ending June 30, 1975, ORNL-5046, pp. 144-148.

THEORY OF THE LINEAR RESPONSE FUNCTION OF A MODEL INSULATOR[21]

Important progress has been made in understanding the properties of metals through study of the electron gas model. Here one ignores the detailed crystalline properties of the metal and concentrates on the dynamic properties of the conduction electrons. From this model, far-reaching conclusions have been drawn about collective modes, screening of impurity charges, and stopping power, to name only a few of the important phenomena in metals which have been treated on this basis.

There have been a few calculations of the dielectric response function of semiconductors, semimetals, and insulators. Most of the recent papers are concerned with the dielectric response function, ϵ, of specific solids. In an effort to develop a similarly simplified model for insulators which retains useful physical information about electronic properties, we have recently derived an expression for the linear response function of a randomly distributed assembly of molecules. This model would be expected to describe best the electronic properties of an insulating liquid.

The theoretical calculation starts with the polarization propagator, $\pi(\mathbf{r}_2, t; \mathbf{r}_1, 0)$, describing the ground-state expectation value for the process of pair creation at $(\mathbf{r}_1, 0)$ followed by destruction of a pair at $(\mathbf{r}_2, t)$. It is defined by

$$\pi(\mathbf{r}_2, t; \mathbf{r}_1, 0) = -\frac{i}{\Omega}\langle\Psi_0|T[\hat{\psi}^\dagger(\mathbf{r}_2, t)\,\hat{\psi}(\mathbf{r}_2, t)\,\hat{\psi}^\dagger(\mathbf{r}_1, 0) \times \hat{\psi}(\mathbf{r}_1, 0)]\,|\Psi_0\rangle\,, \quad (1)$$

where $|\Psi_0\rangle$ is the exact Heisenberg state vector of the system (we consider only the case $T = 0°K$), Ω is the volume of the system, and $\hat{\psi}(\mathbf{r}, t)$ is the wave destruction operator for electrons at $(\mathbf{r}, t)$. The wave operators may be expressed in occupation number representation as

$$\hat{\psi}(\mathbf{r}, t) = \sum_{l}\sum_{n \le n_F}^{\mathrm{OCC}} u_{nl}(r)\,\hat{a}_{nl}(t) + \sum_{\mathbf{k}}^{\mathrm{UNOCC}} u_{\mathbf{k}}(\mathbf{r})\,\hat{a}_{\mathbf{k}}(t)\,, \quad (2)$$

21. Research sponsored in part by the Defense Nuclear Agency, under subtask TA040, but does not reflect endorsement by the sponsor.

where $u_{n\mathbf{l}}(\mathbf{r})$ is the nth single-particle "orbital" on the ion core at position $\mathbf{l}$ and the a's are the usual creation operators. We take electrons to occupy independent orbitals centered on each of the ion cores, neglect overlap of orbitals on different ion cores, and will assume that there are n_F occupied orbitals on each core. With these assumptions we have $u_{n\mathbf{l}}(\mathbf{r}) = u_n(\mathbf{r} - \mathbf{l})$. Although not considered here, we could take a different distribution of orbitals on different cores. The excited states are taken to be OPW (orthogonalized plane wave) orbitals; that is,

$$u_{\mathbf{k}}(\mathbf{r}) = \frac{e^{i\mathbf{k}\cdot\mathbf{r}}}{\Omega^{1/2}} - \sum_{n<n_F} \sum_{\mathbf{m}} \langle n\mathbf{m}|\mathbf{k}\rangle \; u_{n\mathbf{m}}(\mathbf{r}) \,, \tag{3}$$

where $\langle \mathbf{r}|n\mathbf{m}\rangle \equiv u_{n\mathbf{m}}(\mathbf{r})$ and $\langle \mathbf{r}\,|\mathbf{k}\rangle \equiv e^{i\mathbf{k}\cdot\mathbf{r}}/\Omega^{1/2}$ for brevity. One may easily check that $u_{\mathbf{k}}(\mathbf{r})$ is orthogonal to all bound-state orbitals. The binding energies corresponding to these orbitals will be taken to fit experiment. Since we do not wish to assume that the system possesses any sort of crystal symmetry, it is not appropriate to use Bloch functions to represent electron states.

The Fourier representation of $\pi(\mathbf{r}_2, t; \mathbf{r}_1, 0)$ may be defined as

$$\pi_{\mathbf{q}_1,\mathbf{q}_2}(t) \equiv \int d^3r_1 \int d^3r_2 \, e^{-i(\mathbf{q}_1\cdot\mathbf{r}_1 + \mathbf{q}_2\cdot\mathbf{r}_2)} \, \pi(\mathbf{r}_2, t; \mathbf{r}_1, 0) \,. \tag{4}$$

If we abbreviate Eq. (2) as

$$\psi(\mathbf{r}, t) = \sum_{n,\mathbf{l}} u_{n\mathbf{l}}(\mathbf{r}) \hat{a}_{n\mathbf{l}}(t) \,, \tag{5}$$

Eq. (4) leads to

$$\pi_{\mathbf{q}_1,\mathbf{q}_2}(t) = -\frac{i}{\Omega} \sum_{s,\mathbf{l}} \sum_{u,\mathbf{m}} \sum_{v,\mathbf{p}} \sum_{w,\mathbf{q}} \int d^3r_1 \int d^3r_2 \, e^{-i(\mathbf{q}_1\cdot\mathbf{r}_1 + \mathbf{q}_2\cdot\mathbf{r}_2)} \times u^*_{s\mathbf{l}}(\mathbf{r}_2)\, u_{u\mathbf{m}}(\mathbf{r}_2)\, u^*_{v\mathbf{p}}(\mathbf{r}_1)\, u_{w\mathbf{q}}(\mathbf{r}_1) \times \langle \Psi_0 | T[\hat{a}^\dagger_{s\mathbf{l}}(t)\, \hat{a}_{u\mathbf{m}}(t) \hat{a}^\dagger_{v\mathbf{p}}(0)\, \hat{a}_{w\mathbf{q}}(0)\,] \, |\Psi_0\rangle \,. \tag{6}$$

To proceed, we need to approximate; we take $|\Psi_0\rangle$ to be the state vector of the noninteracting ground state ($|0\rangle$), and we take the state creation and annihilation operators also to have their noninteracting forms. Thus

$$\hat{a}_{s\mathbf{l}}(t) = e^{-i\omega_s t} \hat{a}_{s\mathbf{l}}(0) \equiv e^{-i\omega_s t} \hat{a}_{s\mathbf{l}} \,, \qquad \hat{a}^\dagger_{s\mathbf{l}}(t) = e^{i\omega_s t} \hat{a}^\dagger_{s\mathbf{l}}(0) \equiv e^{i\omega_s t} \hat{a}^\dagger_{s\mathbf{l}} \,, \tag{7}$$

where ω_s is the eigenenergy of an electron in the sth orbital located on any of the ions. We also find it convenient to make the assumption that the positions of the ion cores are completely random. Then we may replace the sum over $\mathbf{l}$ by an integral,

$$\sum_{\mathbf{l}} \to \frac{N}{\Omega} \int d^3 l \,,$$

where N is the number of ion cores in the volume Ω. With these assumptions we find

$$\pi^{(t>0)}_{\mathbf{q}_1,\mathbf{q}_2}(t) = -\frac{iN}{\Omega} \sum_s \sum_{\mathbf{p}} |\langle \mathbf{p} + \mathbf{q}_1 |s\rangle - \sum_n \langle \mathbf{p}|n\rangle \langle n|e^{-i\mathbf{q}_1\cdot\mathbf{r}}|s\rangle|^2 \, e^{-i(\omega_{\mathbf{p}} - \omega_s)t} \times \delta^3(\mathbf{q}_1 + \mathbf{q}_2) \tag{8}$$

for $t > 0$. For the case $t < 0$ it is only necessary to take the complex conjugate of the time-dependent exponential factor in Eq. (8). We now compute the frequency transform of the complete polarization propagator as

$$\pi_{\mathbf{q}_1,\mathbf{q}_2,\omega} = \int_{-\infty}^{\infty} dt \, e^{i\omega t} \, \pi_{\mathbf{q}_1,\mathbf{q}_2}(t) = -\frac{N}{\Omega} \delta^3(\mathbf{q}_1 + \mathbf{q}_2) \sum_s \sum_{\mathbf{p}}{}' \langle \mathbf{p} + \mathbf{q}_1 |s\rangle - \sum_n \langle \mathbf{p}\,n\rangle \langle n|e^{-i\mathbf{q}_1\cdot\mathbf{r}}|s\rangle|^2 \times \left(\frac{1}{\omega_{\mathbf{p}} - \omega_s - \omega - i\eta} + \frac{1}{\omega_{\mathbf{p}} - \omega_s + \omega - i\eta} \right) \,, \tag{9}$$

where η is a positive infinitesimal. Furthermore, in case the system has translational symmetry,

$$\pi_{\mathbf{q}_1,\mathbf{q}_2}(t) \to \delta^3(\mathbf{q}_1 + \mathbf{q}_2)\, \pi_{\mathbf{q}_1}(t);$$

in that case the dielectric response function $\epsilon_{\mathbf{q},\omega}$ is given in terms of

$$\pi_{\mathbf{q},\omega} = \int dt \, e^{i\omega t} \pi_{\mathbf{q}}(t)$$

as

$$\epsilon_{q,\omega} = 1 - v_q \pi_{q,\omega} \quad , \tag{10}$$

where $v_q = 4\pi/q^2$ is the Fourier transform of the Coulomb interaction energy. Note that atomic units are being used throughout. Thus we have

$$\epsilon_{q,\omega} = 1 + \frac{4\pi N}{q^2 \Omega} \sum_s \sum_p |F_{pqs}|^2 \times \left(\frac{1}{\omega_p - \omega_s - \omega - i\eta} + \frac{1}{\omega_p - \omega_s + \omega - i\eta} \right) \tag{11}$$

as the dielectric response function for our model insulator, where

$$F_{pqs} \equiv \int d^3 r \frac{e^{-i(p+q)\cdot r}}{\Omega^{1/2}} u_s(r) - \sum_n \int d^3 r_1 \frac{e^{-ip\cdot r_1}}{\Omega^{1/2}} u_n(r_1) \int d^3 r_2 e^{-iq\cdot r_2} \times u_n^*(r_2)\, u_s(r_2) \tag{12}$$

is the OPW form factor.

It is reasonable to look at the case where only a single ground-state orbital need be considered. This might be appropriate when all other orbitals are tightly bound. For an *s* orbital take

$$u_0(r) = \sqrt{\frac{\alpha^3}{\pi}}\, e^{-\alpha r}$$

as a properly normalized one. Then

$$F_{pq_0} = 8 \sqrt{\frac{\pi \alpha^5}{\Omega}} \left\{ \frac{1}{[\alpha^2 + (q+p)^2]^2} - \frac{16\alpha^4}{(\alpha^2 + p^2)^2 (4\alpha^2 + q^2)^2} \right\} . \tag{13}$$

The resulting response function is analytically quite manageable; it describes collective states and screening of impurity charges and at present is being used to determine electron inelastic mean free paths and energy loss rates in insulators.

APPLICATION OF THE MODEL INSULATOR THEORY TO Al_2O_3: THE LOW-ENERGY END OF THE ELECTRON SLOWING-DOWN SPECTRUM[22]

The theory described in the preceeding paper yields an analytical expression for the imaginary part of the dielectric response function of a model insulator and has been applied to compute the differential inelastic mean free path of a swift electron interacting with valence-band electrons in Al_2O_3. We assume that the dispersion relation for energetic electrons in the model insulator is given by $\omega_p = \beta p^2$, where $\beta = \frac{1}{2}$ if the energetic electron has the bare electron mass, and we consider only one bound state. Instead of using the conventional normalization for the excited-state OPW wave function, we require that the imaginary part of the dielectric response function, $\epsilon^{(2)}_{q,\omega}$, satisfy the usual sum rule:

$$\int_0^\infty \omega \epsilon^{(2)}_{q,\omega}\, d\omega = 2\pi^2 n \quad . \tag{1}$$

Here n is the density of ion cores, and we continue to work in atomic units. We find the sum-rule-constrained $\epsilon^{(2)}_{q,\omega}$ to be given by

$$\epsilon^{(2)}_{q,\omega} = \pi n \Gamma / \beta q \Lambda \quad , \tag{2}$$

where

$$\Gamma \equiv \frac{1}{3} \left\{ \frac{1}{[\alpha^2 + (q-p)^2]^3} - \frac{1}{[\alpha^2 + (q+p)^2]^3} \right\} - \frac{32\alpha^4}{(\alpha^2+p^2)^2 (4\alpha^2+q^2)^2} \left[\frac{1}{\alpha^2 + (q-p)^2} - \frac{1}{\alpha^2 + (q+p)^2} \right] + \frac{1024 pq \alpha^8}{(\alpha^2+p^2)^4 (4\alpha^2+q^2)^4} \quad , \tag{3}$$

$$\Lambda \equiv [\omega_B + \beta(q^2 + \alpha^2)] \left[\frac{1}{8\alpha^5} - \frac{32\alpha^3}{(4\alpha^2+q^2)^4} \right] \quad , \tag{4}$$

$$p = [(\omega - \omega_B)/\beta]^{1/2} \quad . \tag{5}$$

Here ω_B is the excitation energy of the single bound state. The procedure for using this model dielectric function to represent that of a real insulator will be to consider α and β as adjustable constants and match the optical dielectric function measured for that material. In the "optical limit," $q \to 0$, Eq. (2) becomes

$$\epsilon^{(2)}_{0,\omega} = \frac{512\pi}{3} n \frac{\alpha^7 p^3}{\beta(\omega_B + \beta\alpha^2)(\alpha^2+p^2)^6} \quad . \tag{6}$$

22. Research sponsored in part by the Defense Nuclear Agency, under subtask TA040, but does not reflect endorsement by the sponsor.

We have tried matching $\epsilon^{(2)}_{0,\omega}$ as given by Eq. (6) to the experimental values measured for Al_2O_3 by Arakawa and Williams.[23] Figure 17.11 shows a comparison of these results, where curve *A* represents the experimental results and curve *B* is obtained from our model with $\alpha = 0.78$, $\beta = 1/2$, and $\omega_B = 0.3309$. We used a density of 4.05 for corundum and took 15 valence electrons per Al_2O_3 unit. In effect we have assumed that the threshold for excitation of any of the valence electrons is 9 eV. We see that the agreement is quite reasonable. We could obtain excellent agreement by taking a combination of ground-state orbitals.

From the values of α, β, and ω_B determined in the "optical limit," the real part of the dielectric response function, $\epsilon^{(1)}_{q,\omega}$, was computed from $\epsilon^{(2)}_{q,\omega}$ using the Kramers–Kronig relations between the real and imaginary parts of an analytic function. Figure 17.12 shows a plot of the energy loss function, Im $(-1/\epsilon_{q,\omega})$, as a function of energy transfer ω for various values of momentum transfer q from these calculations, where q and ω are measured in atomic units. One sees a prominent plasmon resonance peaking at $\omega \sim 1$ (energy transfer ~ 27.2 eV) when $q \lesssim 1$. As q increases to larger values the loss function peaks at values of ω which increase and approach the quantity $\omega = q^2/2$, the energy-momentum relation of a free electron, as $q \to \infty$. Thus our model displays a smooth transition in response from collective behavior for small q to single-particle behavior for large q.

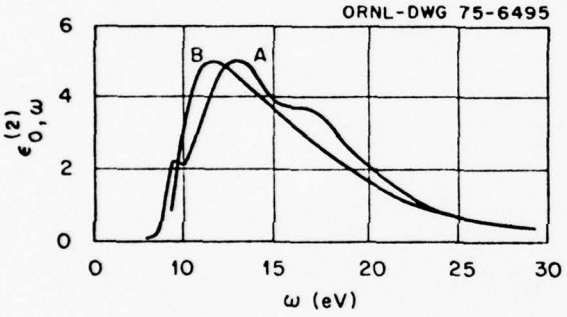


Fig. 17.11. The imaginary part of the dielectric response function of the model insulator in the "optical limit" (curve *B*) fitted to experimental results for Al_2O_3 (curve *A*).

The differential inverse mean free path, $d\mu/d\omega$, for an electron of velocity v interacting with a medium of dielectric response function $\epsilon_{q,\omega}$ is given by

$$\frac{d\mu}{d\omega} = \frac{2}{\pi v^2}\int_{v-\sqrt{v^2-2\omega}}^{v+\sqrt{v^2-2\omega}} \frac{dq}{q}\,\mathrm{Im}\left(\frac{-1}{\epsilon_{q,\omega}}\right) . \qquad (7)$$

This integral has been evaluated numerically as a function of v using the dielectric response function of a model insulator applied to Al_2O_3. The results may be fitted reasonably well for $v > 4.7$ with a function of the form

$$\frac{d\mu}{d\omega} = f(\omega)\ln(v/v_1) + g(\omega) \quad , \qquad (8)$$

where $f(\omega)$ is a function which describes mainly plasmon creation, $g(\omega)$ represents primarily interactions

23. E. T. Arakawa and M. W. Williams, *J. Phys. Chem. Solids* **29**, 735 (1968).

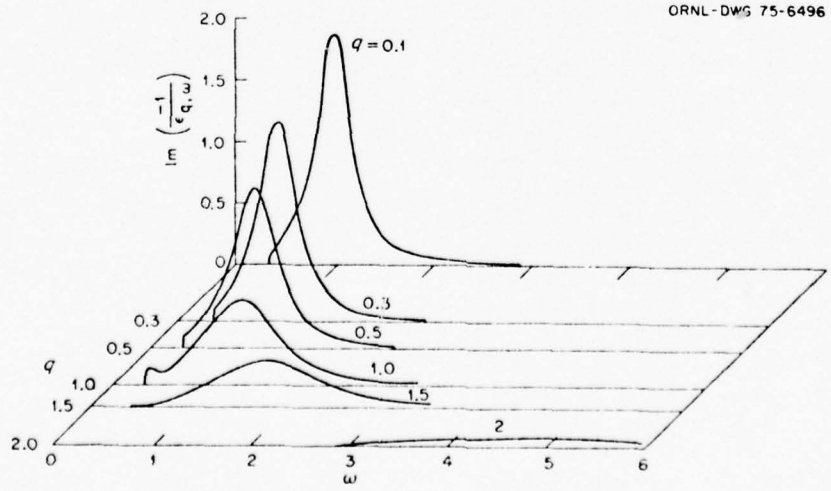


Fig. 17.12. The energy loss function as a function of momentum and energy transfer from the model insulator theory.

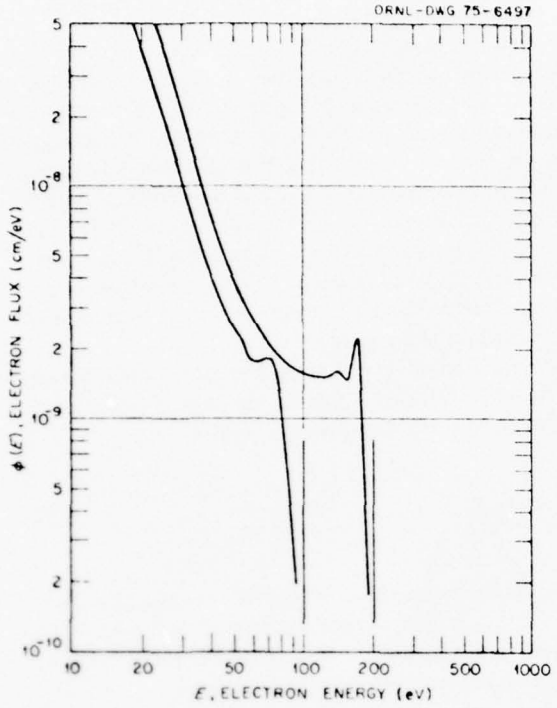


Fig. 17.13. Slowing-down spectrum generated by source electrons of 100 eV and 200 eV due to interaction with the valence band in Al_2O_3.

corresponding to large momentum transfers, and v_1 is an empirically determined constant. For values of $v < 4.7$ the function $d\mu/d\omega$ is stored in tabular form; double interpolation in these tables is carried out in a straightforward way for intermediate values of v and ω.

Figure 17.13 shows some preliminary results of a calculation of electron slowing-down spectra generated in our model insulator by electrons having energies of 100 and 200 eV. One sees a divergence in the flux $\phi(E)$ as the energy E approaches the threshold for excitation in the insulator. At the high-energy end of the spectrum there are several peaks just below the source energy spaced at intervals of ~ 28 eV. These are plasmon loss peaks and represent electrons which are degraded by the creation of one, two, etc., plasmons after being emitted from the source. These calculations are being extended to include inner-shell excitations.

These calculations show that it is possible to fit experimental data on optical dielectric functions of insulating materials using the model insulator theory. The dielectric response function determined in this way may then be used to calculate mean free paths, stopping powers, ranges, slowing-down spectra, etc. This model may thus prove to have wide applicability to the study of dynamic electron properties in insulating substances.

APPENDIX D

Reprinted from: Health Physics Division Annual Progress Report
for Period Ending June 30, 1976, ORNL-5171, pp. 174-178.

ELECTRON SLOWING-DOWN SPECTRA IN Al_2O_3

Theoretical calculations of electron slowing-down spectra for comparison with the Keplertron data require detailed estimates of differential inelastic cross sections for excitation of valence-band and inner-shell electrons for incident electron energies ranging from a few electron volts to about 10^6 eV. The work reported here involves the calculation of these quantities by (1) a model insulator theory[4,5] for the excitation of electrons from the valence band and (2) atomic generalized oscillator strengths (GOS), calculated by Manson[6] and McGuire[7] using the Hartree–Slater method, for the excitation of electrons from the aluminum L shell and oxygen K shell and by using hydrogenic wave functions[8,9] for the excitation of electrons from the aluminum K shell. These cross sections have been prepared for use in a numerical evaluation of a Boltzmann-type slowing-down-cascade equation. Contributions from Auger electrons to the slowing-down flux have been included in a straightforward manner.

Valence-Band Excitation

Since Al_2O_3 is a good insulator with a band gap of about 9 eV,[10] we represent the response of its valence electrons using a model insulator theory. In the previous annual report[11] this model was described in some detail, and the linear dielectric response function derived from the model was applied in a calculation of the low-energy end of the slowing-down spectrum in Al_2O_3.[4,5]

Given the dielectric response function of the model insulator, the differential inverse mean free path (DIMFP) is calculated from the equation[4]

$$\tau(E,\omega) \equiv \frac{d\mu}{d\omega} = \frac{2e^2}{\pi\hbar v^2}\int_{q_-}^{q_+}\frac{dq}{q}\,\mathrm{Im}\left(\frac{-1}{\epsilon_{q,\omega}}\right), \qquad (1)$$

where $v = \sqrt{2E/m}$ is the velocity of the incident electron and $q_\pm \equiv (\sqrt{2m}/\hbar)(\sqrt{E} \pm \sqrt{E-\hbar\omega})$. We assume here, also, that the energy–momentum relation of the swift electron in the solid does not differ appreciably from that of a free electron in a vacuum. Figure 30.3 shows a plot of the quantity $E\,\tau(E,\omega)$ vs ω for various values of E, with some quantities expressed in atomic units (a.u.). In this figure, $\tau(E,\omega)$ represents the DIMFP for loss of energy ω in the excitation of an electron from the valence band by an electron with energy E. One notes when $E \gg 1$ and $\omega \gg 1$ that $E\tau \sim \omega^{-2}$, corresponding to the differential cross section for energy transfer to a free electron. This valence band at 9 eV accounts for the response of 15 of the 24 valence electrons per Al_2O_3 unit in the solid. The remaining nine electrons are assumed to form a second tight-binding level at 29 eV and are also described using the model insulator theory.

Inner-Shell Excitation

Theoretical calculations of the cross sections for excitation of electrons from the inner shells of atoms in a solid will be based on two assumptions: (1) that the binding energies of the tightly bound inner shells are not changed substantially from the values appropriate for isolated atoms and (2) that widths of the energy bands corresponding to inner shells are narrow enough

4. C. J. Tung, R. H. Ritchie, J. C. Ashley, and V. E. Anderson, *Inelastic Interactions of Swift Electrons in Solids*, ORNL/TM-5188 (January 1976).
5. C. J. Tung and R. H. Ritchie, to be published.
6. S. T. Manson, *Phys. Rev. A* 6, 1013 (1972).
7. E. J. McGuire, Sandia research report No. SC-RR-70-406 (unpublished); E. J. McGuire, *Phys. Rev. A* 3, 267 (1971).
8. M. C. Walske, Ph.D. thesis, Cornell University, 1951; *Phys. Rev.* 101, 940 (1956).
9. E. Merzbacher and H. W. Lewis, *Handbuch der Physik*, vol. XXXIV, Springer-Verlag, Berlin, 1958.

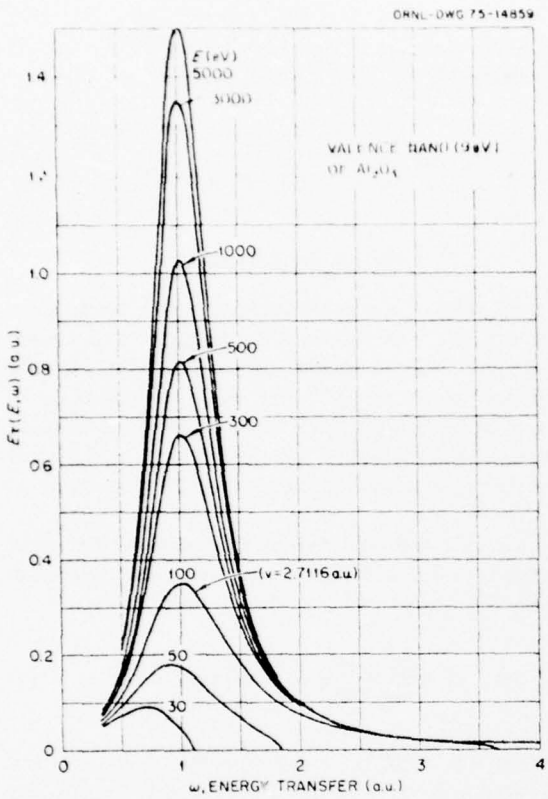


Fig. 30.3. Differential inverse mean free path, $\tau(E, \omega)$, for incident electrons of several energies interacting with the valence band (9 eV) of Al_2O_3.

to be neglected. With these assumptions, a theoretical determination of the cross sections for the excitation and ionization of inner shells may be obtained in the first Born approximation utilizing atomic GOS functions for such inner shells. The details of our calculations of DIMFPs for inner-shell excitation have been presented earlier and need not be repeated here.[12,13]

Auger Electrons

Auger electrons are produced when vacancies in a given shell are filled by electrons from a higher shell. The Auger transition results in a two-electron process. One electron fills the hole in the inner shell, while the excess of binding energy is transferred to a second electron, causing its emission as an Auger electron. To obtain Auger cascade transitions in Al_2O_3, we make the following assumptions: (1) that the Auger transitions occur only on a given ion (either aluminum or oxygen) and not between ions and (2) that the Auger transitions take place only from levels immediately above those in which holes exist.[14] With these assumptions, the transition to a vacancy in the aluminum K shell can be from either the aluminum L_1 shell ($2s$) or the aluminum $L_{2,3}$ shell ($2p$). We have used the transition from the aluminum $L_{2,3}$ shell to a vacancy in the aluminum K shell because selection rules tend to favor this transition. Also, calculation of the Auger electron kinetic energy for each transition and the number of Auger electrons created following the filling of a single hole in a given shell is straightforward. For example, the filling of a vacancy in the aluminum K shell from an electron in the aluminum $L_{2,3}$ shell will create an Auger electron having energy equal to $\hbar\omega_B^{Al,K} - 2\hbar\omega_B^{Al,L_{2,3}} \cong 1384$ eV, where $\hbar\omega_B$ is the binding energy of the indicated level, and will give rise to two holes in the valence band and an Auger electron with energy $\cong 63$ eV.

Electron Slowing-Down Cascade Equation and Its Solution

Spencer and Fano[15] and Spencer and Attix[16] have given a theoretical treatment of electron slowing-down spectra at energies high enough that detailed electronic structure of the material is not important. In their treatment, the Møller cross section for electron–electron scattering was employed to compute the delta-ray flux generated by electrons interacting with the medium. This delta-ray flux, when added to the flux of electrons slowing down from higher energies, gives the total flux in the medium at arbitrary energy. The Spencer–Fano approach, as originally employed, is strictly valid only for electron energies that are large compared with the binding energies of the most tightly bound electrons in the medium. Calculations at energies comparable with transition energies from inner shells require not only the detailed cross sections but also a different approach to the solution of the Boltzmann equation.[17,18]

Here our interest is in the energy dependence of the flux of electrons generated in a solid irrespective of their spatial distribution. The Boltzmann-type electron-

10. E. T. Arakawa and M. R. Williams, *J. Phys. Chem. Solids* 29, 735 (1968).
11. R. H. Ritchie et al., *Health Phys. Div. Annu. Prog. Rep. June 30, 1975*, ORNL-5046, pp. 144–48.
12. Ibid., pp. 154–55.
13. J. C. Ashley, C. J. Tung, and R. H. Ritchie, *IEEE Trans. Nucl. Sci.* NS-22, 2533 (1975).

number-balance integral equation for the flux may be written easily. Consider a very large medium containing an electron source density that is uniform in space and constant in time and produces $S(E)\,dE$ electrons in the interval of energy between E and $E + dE$ per unit volume. The electrons released from this source lose energy in collisions with other electrons in the medium. In the steady state, the number of electrons that enter a given interval of energy between E and $E + dE$ must equal the number scattered out. Thus, the electron slowing-down cascade equation in terms of the flux $\phi(E)$ may be written as

$$\phi(E)\int_0^\infty d\omega\,\tau(E,\omega) = \int_0^\infty d\omega\,\phi(E+\omega)\,[\tau(E+\omega,\omega) + \tau_s(E+\omega,E)] + S(E)\,, \qquad (2)$$

where $\tau(E, \omega)$ is the DIMFP that an electron with energy E may lose energy in the interval between ω and $\omega + d\omega$ and $\tau_s(E, E')$ is the DIMFP that an electron with energy E will produce a secondary electron in the interval of energies between E' and $E' + dE'$. This equation may be solved by standard numerical techniques,[4] given τ and τ_s for a solid of interest.

Numerical evaluation of $\phi(E)$ from Eq. (2) over the energy range of the Keplertron data[19] would require prohibitively large amounts of computer time, since it is necessary to use an energy mesh size comparable with or smaller than a few electron volts (the magnitude of valence-band excitation energy) in order to solve Eq. (2) accurately by direct methods. Hence, we have assumed that the Spencer–Fano (SF) flux[15] $\phi_{SF}(E)$ is sufficiently accurate down to $E_m \sim 10$ keV. We have determined an equivalent source density $S_{SF}(E)$ below E_m by computing an equivalent first-collision density in this range using $\phi_{SF}(E)$ and DIMFP functions from the model insulator theory and from the inner-shell cross section calculations. Figure 30.4 shows a plot of the Spencer–Fano flux for energies above 1 keV due to beta rays from neutron-activated ^{164}Dy uniformly distributed in the Al_2O_3 sample. The flux has been normalized to one electron created per cubic centimeter, so that the units of this normalized flux are centimeters per electron volt. In Fig. 30.5, we show the source density $S_{SF}(E)$ calculated using Eq. (2) with the Spencer–Fano flux $\phi_{SF}(E)$ and DIMFP functions for Al_2O_3. At high energies, most of the contribution to the equivalent source density, $S_{SF}(E)$, is from degraded Spencer–Fano flux electrons from higher energies. As electron energy decreases, the source density increases, since more and more secondary electrons are generated. The number of secondary electrons generated in the medium increases very rapidly as electron energies approach the threshold energy. In the bottom left corner of Fig. 30.5, a separate plot of the function for energies very close to E_m shows the general behavior of the function in that energy region.

Further details of the calculation of the slowing-down spectrum, given the equivalent source density, are rather lengthy and will not be repeated here (see ref. 4). Figure 30.6 shows a plot of a measured electron slowing-down flux in Al_2O_3 due to beta rays from neutron-activated ^{164}Dy uniformly distributed in the sample and the result of our corresponding calculations (solid line). For comparison, we show a Monte Carlo–computed spectrum[18] using semiclassical binary collision cross sections. The theoretical flux seems to confirm the Monte Carlo calculations but shows some discrepancy between experiment and theory in the energy range from 40 to 2000 eV. Efforts to understand these discrepancies are continuing. However, general agreement between theory and experiment in a broad energy range is clear.

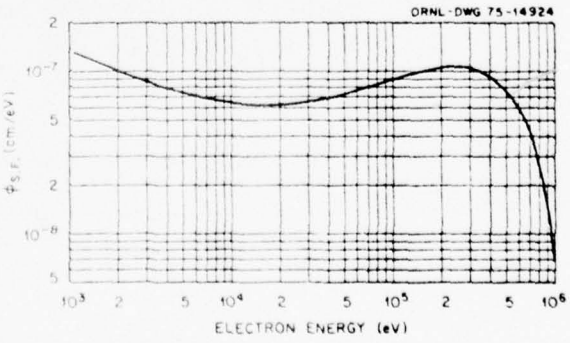


Fig. 30.4. Electron slowing-down spectrum above 1 keV in Al_2O_3, calculated using Spencer–Fano theory, due to beta rays from neutron-activated ^{164}Dy.

14. D. Penn, *Phys. Rev.* 128, 2093 (1962).
15. L. V. Spencer and U. Fano, *Phys. Rev.* 93, 1172 (1954).
16. L. V. Spencer and F. H. Attix, *Radiat. Res.* 3, 239 (1955).
17. L. C. Emerson, R. D. Birkhoff, V. E. Anderson, and R. H. Ritchie, *Phys. Rev. B* 7, 1798 (1973).
18. R. H. Ritchie, C. J. Tung, V. E. Anderson, and J. C. Ashley, *Radiat. Res.* 64, 181 (1975).
19. E. T. Arakawa et al., *Health Phys. Div. Annu. Prog. Rep. July 31, 1974*, ORNL-4979, p. 147.

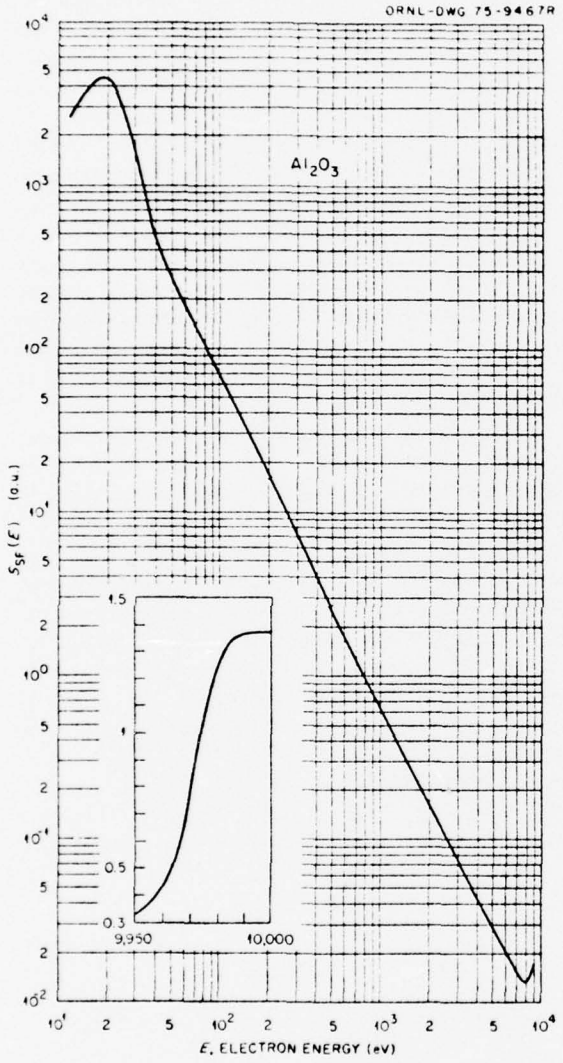


Fig. 30.5. First-collision electron source density, $S_{SF}(E)$, in Al_2O_3, calculated from differential inverse mean free path functions derived in this work, and from the Spencer–Fano flux for electron energy above 10 keV.

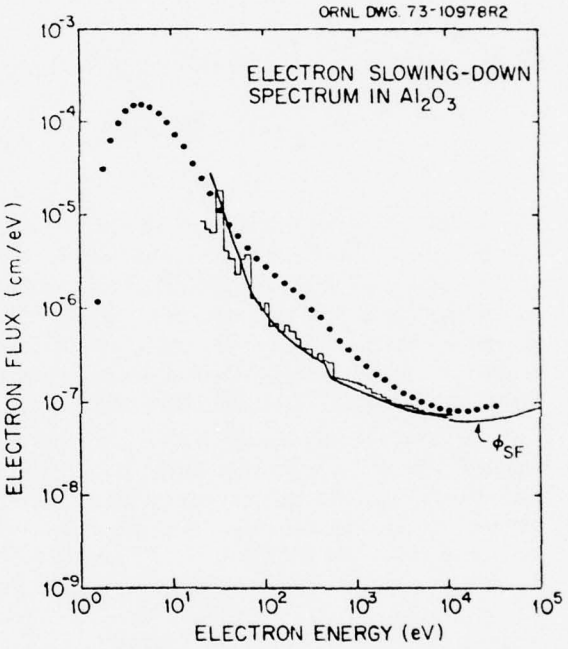


Fig. 30.6. Electron slowing-down spectrum in Al_2O_3. The solid curve shows the result of the present calculation. The points indicate experimental values. The histogram shows the result of a theoretical Monte Carlo calculation.

APPENDIX E-1

Reprinted from: Proceedings of IVth Int. Conf. on Vacuum UV Radiation Physics, Hamburg, 1974 (Pergamon-Vieweg) pp. 580-581.

6.13. Electron Attenuation Lengths in Carbon Films[1])

E. T. Arakawa, M. W. Williams, R. N. Hamm and R. D. Birkhoff
Health Physics Division, Oak Ridge National Laboratory, Oak Ridge, Tennessee 37830 USA

A. J. Braundmeier
Department of Physics, Southern Illinois University, Edwardsville, Illinois 62025

A method has been developed for obtaining electron attenuation lengths in solids from measurements of photoelectric yield as a function of photon angle of incidence [1]. Conventionally, electron mean free paths, or the directly measured quantities electron attenuation lengths, are determined from electron transmission measurements through thin films. However, when electron attenuation lengths are short, it is difficult to prepare sufficiently thin homogeneous films for these thin film measurements. Also, when energetic electrons interact with a solid, the points of origin and energies of secondary electrons are not well defined, and it is difficult to extract a meaningful electron attenuation length from such measurements. The method currently developed for obtaining electron attenuation lengths avoids these difficulties. Thick films of the solid under investigation are used, avoiding the problems associated with making very thin homogeneous films. Furthermore, the quantity analyzed is the photoelectric yield as a function of the photon angle of incidence relative to the photoelectric yield for normal incidence, so that absolute measurements are not required. Absolute photoelectric yields are difficult to measure accurately, but relative values are easy to obtain since virtually all photoelectrons emitted in any direction from the photoemitter can be collected if a sufficiently high potential difference is applied.

The experimental apparatus has been described previously. A grazing incidence scanning monochromator [2] is optically coupled to a stainless-steel high vacuum chamber [3]. The essential features of this chamber are a sample holder at the center of a cylindrical electron collector. The sample holder can be rotated through 360°, so that the angle of incidence of the photons can be varied. The cylindrical electron collector allows collection of virtually all photoelectrons emitted in any direction. Thick carbon films were obtained by vapor deposition from a carbon arc, in vacuum, directly onto a clean glass slide. After insertion of a carbon film, the experimental chamber was pumped down to $\sim 2 \times 10^{-7}$ torr.

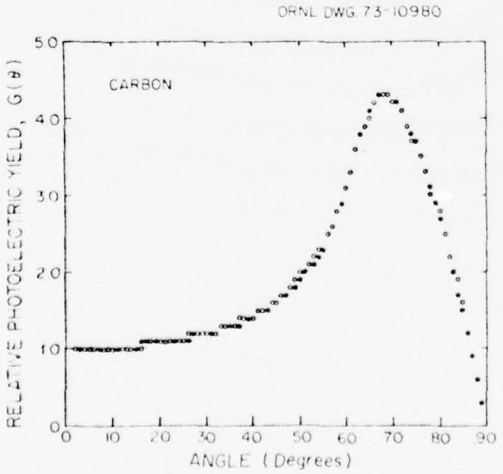


Fig. 1
Relative photoelectric yield vs. angle of incidence for a thick carbon film for photon energy of 51.87 eV. (○ measured values, ● least squares fit).

[1]) Research sponsored by the U. S. Atomic Energy Commission under contract with Union Carbide Corporation and in part by the Defense Nuclear Agency, under subtask TA 040, but does not reflect endorsement by the sponsor.

For each photon energy the total photoelectric yield was obtained in terms of the current going from the sample to the electron collector, as a function of photon angle of incidence, θ. The yield at angle θ, $Y(\theta)$, relative to the yield for normal incidence, $Y(0)$, was analyzed as a function of θ as described in Ref. [1]. For a given photon energy the ratio $Y(\theta)/Y(0) = G(\theta)$ shows a single maximum when plotted versus θ as shown in Fig. 1 if the film is infinitely thick and if its refractive index, n, is less than unity. For a small extinction coefficient, k, ($\lesssim 0.1$) these curves can be analyzed to yield n and either k or L where L is the electron attenuation length for the photoexcited electrons. The position of the maximum of $G(\theta)$ vs. θ is in the vicinity of θ_c where $\theta_c = \sin^{-1} n$ and hence yields the value of n while the magnitude of $G(\theta_c)$ is sensitive to k and L. In the present case we obtained values of k independently from measurements of reflectance as a function of photon angle of incidence and then used a two parameter least squares fitting procedure to obtain n and L from $G(\theta)$ vs. θ. Fig. 1 shows representative data points (shown by ○) for a photon energy of 51.87 eV. Using an independently measured value of k = 0.04 a least squares fit of this data to the theory (shown by ●) gave n = 0.89 and L = 2.4 Å. Since the reflectance vs. photon angle of incidence measurements yield both n and k values, we can make a consistency check by comparing the values of n obtained from the reflectance and from the photoelectric yield measurements.

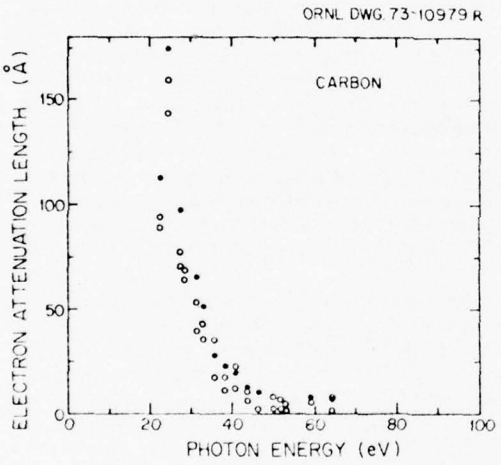


Fig. 2
Electron attenuation length for photoexcited electrons in carbon vs. incident photon energy.

The values obtained for the electron attenuation length of photoexcited electrons in carbon films are shown in Fig. 2 for photon energies from 20 to 64 eV. This is the range of energies for which the conditions $n \lesssim 1$ and $k \lesssim 0.1$ are satisfied for carbon.

Note added in proof: More recent experiments on the total photoelectric yield as a function of carbon film thickness lead us to suspect that the values of the electron attenuation lengths at the lower photon energies (20–30 eV) should be considerably less than shown in Fig. 2.

References

[1] *Arakawa, E. T., Hamm, R. N.* and *Williams, M. W.*, J. Opt. Soc. Am. 63, 1131 (1973).
[2] *Hanson, W. F., Arakawa, E. T.* and *Williams, M. W.*, J. Appl. Phys. 43, 1661 (1972).
[3] *Gesell, T. F.* and *Arakawa, E. T.*, Phys. Rev. Letters 26, 377 (1971).

APPENDIX E-2

Reprinted from: Health Physics Division Annual Progress Report for Period Ending June 30, 1975, ORNL-5046, pp. 127-128.

ELECTRON ATTENUATION LENGTHS IN CARBON FILMS[25]

Electron attenuation lengths, L, of photoexcited electrons in thick vapor deposited carbon films have been reported previously[26] over the range of photon energies from 20 to 64 eV. These values were derived from measurements of the total photoelectric yield, $Y(\theta)$, as a function of photon angle of incidence, θ. For a small extinction coefficient, k (<0.1), and a refractive index, n less than unity, the ratio $Y(\theta)/Y(0) = G(\theta)$ vs θ curves were analyzed to yield n and L. For each photon energy the position of the maximum of $G(\theta)$ vs θ, which occurs in the vicinity of θ_c, where $\theta_c = \sin^{-1} n$, yields a value of n while the magnitude of $G(\theta_c)$ is sensitive to both k and L. We measured k independently and hence obtained values of n and L by this method. As a consistency check, we compared the values of n obtained from reflectance and from photoelectric yield measurements on similar samples and obtained very good agreement. However, even though this consistency check was satisfactory, we still questioned the high values of L ($\sim$ 150 to 50 Å) obtained in the photon energy region of 20 to 30 eV. We thus decided to obtain values of L from measurements of the photoelectric yield, $Y(t)$, as a function of carbon film thickness, t. A wedge-shaped carbon film was deposited on a glass slide, and the metrical thickness as a function

---

25. Research sponsored in part by the Defense Nuclear Agency, under subtask TA040, but does not reflect endorsement by the sponsor.

26. E. T. Arakawa et al., *Health Phys. Div. Annu. Progr. Rep. July 31, 1974*, ORNL-4979, pp. 128, 129.

of position on the slide was obtained from a combination of transmittance and independent interferometric measurements. The experimental apparatus described previously[26] was used. In the same way as for the $Y(\theta)$ vs θ measurements, the carbon films were deposited in vacuum and exposed to the atmosphere on being transferred to the apparatus used for photoelectric measurements; then the values of $Y(t)$ were obtained with the experimental chamber pumped down to $\sim 2 \times 10^{-7}$ torr. For each constant incident photon energy, a $Y(t)$ vs t curve was plotted. Some representative curves of $Y(t)$ vs t for carbon on glass are shown in Fig. 16.8. It was found that for each photon energy from 10 to 64 eV, there was a rapid increase in $Y(t)$ in the vicinity of t = (10 to 15) Å with saturation of $Y(t)$ above this thickness. The complete analysis of photoelectric yield

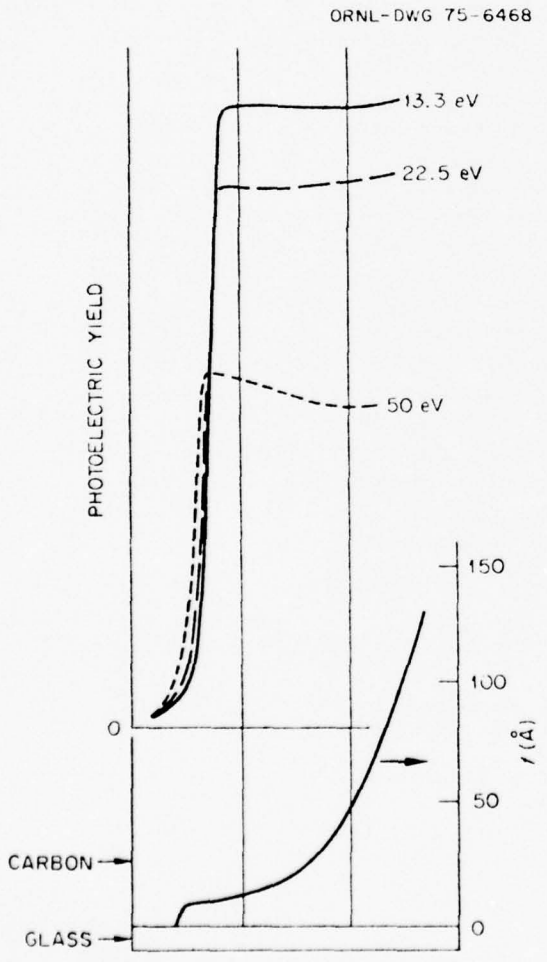


Fig. 16.8. Photoelectric yield vs carbon film thickness for constant incident photon energies.

measurements from such thin films is very complicated, requiring a knowledge of the homogeneity of the films and their effective optical properties in addition to a knowledge of the factors affecting the electron transport properties. Although a complete analysis of our $Y(t)$ vs t data for carbon has not yet been attempted, the values of L for photoexcited electrons in carbon appear to be much smaller in the region of 20 to 40 eV than the ones obtained[26] from the observations of $Y(\theta)$ vs θ. A theoretical analysis of the $Y(\theta)$ vs θ method has since been undertaken which showed that although reliable values of n can be obtained from $G(\theta)$ vs θ, to obtain L to ±1 Å requires that k be known to within ~1%. The uncertainty in the independently measured k values was much greater than this, leading to very large uncertainties in the calculated L values.

Electron attenuation lengths are known to be small in the region of 10 to 100 eV, and hence their accurate determination is difficult. At the same time, the values of these electron attenuation lengths in both metals and insulators are of great interest. We thus regard this as a continuing project. For the $Y(\theta)$ vs θ method, we plan to investigate various techniques whereby we can obtain extinction coefficients, k, to a higher accuracy than presently attainable since we have shown that the uncertainties associated with the values obtained for L are directly related to the uncertainties in the input values of k. For the $Y(t)$ vs t method, we plan to prepare and measure films of gold in ultrahigh vacuum for comparison with preliminary data already obtained on gold wedges prepared in vacuum but then exposed to air on transfer to the apparatus used to measure $Y(t)$ vs t. Gold is simpler to work with than carbon and should provide a check on the reliability of the experimental $Y(t)$ vs t curves obtained for carbon. Furthermore, experimental and theoretical studies of the electron attenuation lengths and the related electron mean free paths for gold have been reported in the literature. Data on the effective optical properties of gold as a function of film thickness are also available for evaporated gold films prepared under various conditions. A complete analysis of the $Y(t)$ vs t data for gold should thus be possible, providing a check on the reliability of this method. Ultimately, we hope to get completely consistent and reliable values of L in both metals and insulators.

APPENDIX F

To be published in the Physical Review.

Optical Properties of Polystyrene from the Near Infrared to the X-Ray Region and Convergence of Optical Sum Rules*

T. INAGAKI[+], R. N. HAMM, M. W. WILLIAMS, and E. T. ARAKAWA

Health Physics Division, Oak Ridge National Laboratory
Oak Ridge, Tennessee 37830

*Research sponsored by the Energy Research and Development Administration under contract with the Union Carbide Corporation, and in part by the Defense Nuclear Agency, under subtask TA040, but does not reflect endorsement by the sponsor.

[+]Also Department of Physics, The University of Tennessee, Knoxville, Tennessee. Present address, Department of Physics, Osaka Kyoiku University, Osaka, Japan.

By acceptance of this article, the publisher or recipient acknowledges the U.S. Government's right to retain a non-exclusive, royalty-free license in and to any copyright covering the article.

BEST AVAILABLE COPY

ABSTRACT

Optical functions of polystyrene in the form of thin films were determined for photon energies between 0.6 and 82 eV from transmission measurements. The results for k, the extinction coefficient, were combined with previous experimental results in the soft and hard X-ray regions up to 8050 eV. Analyses were made on several sum rules for the optical functions in this unusally wide energy range, including a sum rule for the refractive index, n, derived recently by Altarelli et al. Redistribution of the oscillator strength corresponding to 2.7% of the total electrons was found between the valence and core excitations of carbon. Using the complex dielectric function and the energy loss function obtained, the average photoexcitation energy and the average energy loss for fast charged particles over the entire oscillator strength distribution were evaluated to be 25.1 and 36.8 eV, respectively.

INTRODUCTION

The primary purpose of this paper is to examine in detail the response of electrons in a typical solid hydrocarbon to electromagnetic radiation over essentially the whole frequency range. This is achieved through sum rule calculations which are employed to determine the way in which the oscillator strength converges. In the past such calculations and their interpretation have suffered to a greater or lesser extent because the experimental data were generally unavailable over a wide enough energy range to give the desired certainty in the required extrapolations to infinite energy. To our knowledge there are just two previous studies[1] performed on experimental data which extends over a sufficiently large energy range. We know of no such analysis for any hydrocarbon.

In this study, we report the optical functions of polystyrene $-(C_8H_8)-$, in the form of thin solid films over the range of photon energies from 0.6 to 82 eV. The results for k, the extinction coefficient, are combined with the previous experimental data from 30 to 1550 eV taken by Lukirskii et al.[2] and those from 1490 to 8050 eV by Nordfors.[3] The combined spectrum of k covers substantially all the electronic excitations (more than 99.9% of the total oscillator strength), including the carbon core excitations starting at around 282 eV. Despite the recent progress in synchrotron radiation techniques, which make it possible to obtain optical spectra from the infrared to the hard X-ray region using a continuum photon source, similar data for any kind of material are still quite rare.

In addition to the well-known f-sum rules,[4] a detailed analysis is performed in this study on the refractive index, n, at high energies in order to employ a new sum rule for n which has been derived recently by Altarelli et al.[5] using the superconvergence theorem in high-energy physics. Since, as will be shown, the convergence of this sum rule is quite slow, it can be demonstrated and/or used only when the n values are available up to the extremely high energy region.

EXPERIMENTAL

Optical functions of polystyrene films between 0.6 and 82 eV were determined by the transmission method , details of which have been described previously.[6] In this method, the quantities determined experimentally are the transmittance, T, of a free-standing film as a function of photon energy over the whole range of photon energies, and the film thickness, d. In addition the values of n are measured directly over a limited energy region where the films are transparent. To derive the optical functions n and k at each energy, the

BEST AVAILABLE COPY

Kramers-Kronig relation between n and k is then utilized. An iterative computational procedure is carried out between the Kramers-Kronig relation and the explicit expression for transmittance which includes the correction factor for reflection effects at the film boundaries, until the values of n and k converge. n and k are thus determined self-consistently so that they reproduce the observed value of transmittance.

Self-supporting films of polystyrene were prepared by the same method as described previously.[7] Uniformity of film thickness was checked by measuring the transmittance at a suitable wavelength while scanning the whole film area. Determination of the film thickness, d, was made by observation of transmission maxima and minima due to interference in the transparent region. For the thinnest films, interference patterns could not be used as even the first minimum did not occur in the non-abosrbing region below 4.4 eV (above ~2800Å). In such cases the thickness was determined directly from the explicit expression for the transmittance in the transparent (k=0) region,[6]

$$T = \frac{\{4n/(1+n)^2\}^2}{1 - 2[(1-n)/(n+1)]^2 \cos(4\pi nd/\lambda) + [(n-1)/(n+1)]^4} \quad \ldots (1)$$

using the experimental values of T and n, where λ is the wavelength of the incident photons. The thicknesses of the five films used were found to be 230, 440, 570, 720, and 830 Å with about ±30 Å uncertainty. These values were adjusted, where necessary, within the limit of the experimental uncertainty so that the final results for n in the transparent region calculated from T and d agreed with the direcly measured values.

BEST AVAILABLE COPY

Refractive indices, n, between 2.0 and 4.4 eV, where polystyrene is transparent, were determined by the critical-angle, Brewster angle, and interference methods using separately prepared films. All these methods gave consistent results for n to within an error of ±0.5%. The average values were used in the thickness determination.

As is well-known,[8] polystyrene shows a weak absorption around 4.8 eV (∿2600 Å), which is a remnant of the forbidden absorption in benzene at about the same energy. Since this absorption was too weak to be observed even in the thickest of the films used in the observations described so far, an additional transmission measurement was performed in the vicinity of this band on a 4.50μ-thick film, and the extinction coefficient k for this band determined. The measurments were extended on this thick film down to 0.6 eV, where no further absorption was observed. This thick film was also used to determine the density of the polystyrene films. A known area of the film was cut out and weighed. The density was found to be (1.05±0.02) g/cm^3. This value agrees with the literature values[8] for bulk polystyrene: (1.042→1.065)g/cm^3. The tacticity of polystyrene in our films was not checked. It does not, however, seem to affect the results in the present spectral region.[9] Errors in the results obtained for (n-1) and k were estimated to be less than ±2%, except for the region above 60 eV.

The measurements described above were made with a Cary recording spectrophotometer (model 14) in the region 0.6→2 eV, a Seya-Namioka monochromator (McPherson model 235) in the region 2→15 eV, and a grazing-incidence monochromator (McPherson model 247) in the region 13→82 eV. Above 7.5 eV the measurements were made with line sources (hydrogen discharge and a condensed air spark) while below 7.5 eV continuum sources were employed.

RESULTS AND DISCUSSION

1. The extinction coefficient k.

The results for k between 0.6 and 82 eV are presented in Fig. 1 on a logarithmic plot. The spectrum exhibits structure below 10 eV due to molecular electronic excitations. Above 10 eV, the spectrum is essentially structureless, except for a broad absorption peak at around 14 eV. The absorption decreases rapidly and monotonically above this peak, and can be described by a straight line above 20 eV on a logarithmic plot. The best fit of the present k values between 20 and 60 eV to a straight line gave the expression

$$k(E) = 7.81 \times 10^{3}\, E^{-3.23}, \qquad (2)$$

where E is the photon energy in eV. Deviation found above 60 eV of the k values from the straight line fit seems to be due to experimental errors in the transmission measurements in that region, where the transmittances of thin films were quite high.

Also shown in Fig. 1 are the combined results for k obtained by Lukirskii et al.[2] and by Nordfors[3] extending to the hard X-ray region. These results were originally given by the expressions[2]

$$\mu(\lambda) = 0.40\lambda^{2.31} \qquad (3)$$

for $44\ \text{Å} < \lambda < 410\ \text{Å}$ and

$$\mu(\lambda) = 2.40\lambda^{2.68} \qquad (4)$$

for 8 Å < λ <44 Å, where μ is the linear absorption coefficient in cm^{-1} and λ is the wavelength of the photons in Å. In plotting these expressions in Fig. 1, they were converted into the forms

$$k(E) = 1.13 \times 10^{4} E^{-3.31} \qquad (5)$$

for 30 eV<E<282 eV and

$$k(E) = 2.21 \times 10^{6} E^{-3.68} \qquad (6)$$

for 282 eV<E<1550 eV, using the definition $\mu = 10^{8}(4\pi k/\lambda)$. The expressions (3) and (4) were deduced by Lukirskii et al.[2] from their experimental absorption measurements. The results of Nordfors[3] obtained in the region from 1490 to 8050 eV were found[10] to fit well to the expressions (4) or (6) for the higher energy region. Since, as will be shown, in the spectral region of their studies the refractive indices are quite close to unity, transmission measurements gave the absorption coefficient directly without taking into account reflection at the film boundaries. Their measurements were, however, made at only eight wavelengths from 30 to 282 eV, nine wavelengths from 282 to 1550 eV and five wavelengths[10] from 1490 to 8050 eV, employing the characteristic X-rays from various anode materials.

BEST AVAILABLE COPY

The jump in absorption at 282 eV is due to the carbon K-shell absorption edge, in the vicinity of which some fine structure should be found. The study of fine structure in core shell absorption edges using a continuum source of synchrotron radiation is of current interest, but such studies are not available for polystyrene. Despite the coarseness of Lukirskii et al.'s and Nordfors' data, their results seem to represent the essential features and correct order of magnitude of the absorption for polystyrene over a very wide range of photon energies. Indeed a fairly close fit is found between the present results and Lukirskii et al.'s results in the low energy region. The difference in k between the present result and their result is about 9% at 30 eV, and that between the extrapolation of the present result from 20 to 60 eV, which is shown by a dotted line in Fig. 1, and their result is about 8% at 282 eV. Two lines representing the extrapolations of the present results and their results below 282 eV cross at around 100 eV, indicating that the differences are not due to any systematic errors resulting from, for example, error in determination of the film thickness in either study, but due to random errors. Their original data at eight wavelengths below 282 eV, in fact, exhibit noticeable scatter from a straight line fit even on a logarithmic plot, but the discrepancy of their expression (5) from our expression (2) is well within the 10% experimental uncertainty claimed by them for their original data.

The results for k given in Fig. 1 provide basic data for comprehensive information about the electronic response of polystyrene to electromagnetic radiation. Before deriving the other optical quantities from these results, the validity of the k values obtained here was checked by evaluating the sum rule[11]

BEST AVAILABLE COPY

$$N_1(E) = \frac{4}{\pi} (m/4\pi n_o e^2\hbar^2) \int_o^E E' k(E')dE' \to N \; ; \; E \to \infty, \qquad (7)$$

where n_o is the molecular density and N is the total number of electrons in a molecule. Taking a monomeric unit $-(C_8H_8)-$ of polystyrene as a molecular unit, N is 56. In carrying out the integration (7), the k values above 8050 eV were assumed to be represented by expression (6) up to an infinite photon energy. This can be expected at least up to the MeV region, where photon-attenuations due to the Compton effect and pair-creation become appreciable.[12] In the region below 0.6 eV, where photoabsorption due to molecular vibrations occurs, the k values were assumed to be so small that the contribution of $E'k(E')$, in this low energy region, to $N_1(E)$ could be neglected.

The results of calculations of $N_1(E)$ are plotted in Fig. 2 as a function of E. Since in this study it was difficult to determine experimentally the density of the polystyrene film, ρ, with an uncertainty less that ±2%, the molecular density $n_o(=L\rho/M)$ was adjusted so that the value of $N_1(E)$ became equal to N in the limit of $E\to\infty$. (L is Avogadro's number and M is the molecular weight). This gave a film density of 1.040 g/cm^3, which is in excellent agreement with the measured value of (1.05±0.02) g/cm^3. Thus, in this check, the over-all validity of the k values was confirmed with an uncertainity of ±1%.

Further evaluations of $N_1(E)$ were made on the k values due to the valence and core excitations, separately. A saw-tooth like shape of the k spectrum in the logarithmic plot at high energy allows us to separate the absorption due to the core excitations from the total absorption. The separation was made simply by extrapolating the slope in Fig. 1 below the

K-shell edge to higher energies. This seems to be a quite plausible procedure. The results of $N_1^V(E)$ and $N_1^C(E)$, the contributions to $N_1(E)$ from the valence and core excitations, respectively, are given in Fig. 2. It is noted that a redistribution of electron numbers corresponding to 1.51 electrons is found between the valence and core excitations. $N_1^V(E)$ and $N_1^C(E)$ should tend to 40 and 16, the numbers of valence and core electrons, respectively, in the limit $E \to \infty$, if there is no oscillator strength coupling between them. The fact that the oscillator strengths for inner shells are considerably smaller than their numbers of electrons has been known since the early days of X-ray spectroscopy.[13] In addition the magnitude of the oscillator strength redistribution between the outer and inner shells has been known, in general, to become larger as the atomic number becomes bigger. It is further to be noted that the effective numbers of electrons as plotted in Fig. 2 as functions of photon energy E do not saturate until a few thousand eV. This is so even for the valence electrons showing that even at these high energies the contribution of valence excitations to the oscillator strength is not negligible.

The analyses presented above were performed on the present results between 0.6 and 60 eV. In the region from 60 to 282 eV, the extrapolation of the present results between 20 and 60 eV expressed by Eq. (2) was used, instead of Lukirskii et al.'s result given by Eq. (5) for the reason mentioned earlier. Expression (2) was also used to represent the absorption by valence electrons above 282 eV. If we used Lukirskii et al.'s expression (5) for the absorption by valence electrons above 60 eV, no substantial change is found in the results for the film density and the oscillator strength redistribution. In all further analyses presented below, therefore our expression (2) was used for the absorption by valence electrons above 60 eV.

BEST AVAILABLE COPY

BEST AVAILABLE COPY

Some uncertainties in the sum rule calculations may arise from the ambiguity of the k data in the vicinity of the carbon K-absorption edge at around 282 eV. In the present analyses, a step-like edge was assumed at 282 eV as given by Lukirskii et al. Since such a sharp K-edge has been observed for polypropylene [14] $(-(C_3H_6)-)$, an organic polymer similar to polystyrene, at 283 eV using a continuum of soft X-ray photons from a synchrotron, the threshold energy used in the present analyses seems to be reasonable. A ±2 eV deviation of the threshold energy from 282 eV results in changes of only ± 0.003 g/cm^3 and ∓ 0.13 electrons in the results for the film density and the oscillator strength redistribution, respectively. Thus, although to evaluate the uncertainty involved in the present results we have to wait for a precise observation of the carbon K-edge structure in polystyrene the present results seem to be sufficiently correct with uncertainties which are probably less than those suggested.

2. The refractive index n.

The refractive index n(E) at a photon energy E can be determined by the Kramers-Kronig relation

$$n(E) - 1 = \frac{2}{\pi} \int_0^\infty \frac{E'k(E')}{E'^2 - E^2} dE' , \qquad (8)$$

using the experimental values of k at all energies. In the present case, the experimental k values in the region from 0.6 to 8050 eV are available, and in the regions outside these energies the values extrapolated as

described earlier in the sum rule calculation can be used. n(E), therefore, can be determined with little uncertainty at all energies. Just as k can be separated into the valence and core contributions, n(E)-1 is also separable. The results of $n^V(E)-1$ and $n^C(E)-1$, the contributions to n(E)-1 from the valence and core excitations, respectively, are presented in Figs. 3 and 4, respectively.

Both $n^V(E)-1$ and $n^C(E)-1$ become almost constant in the regions far below the absorption onsets. It is to be noted that the values of $n^C(E)-1$ below about 100 eV are smaller than those of $|n^V(E)-1|$ in that region by a factor 10^3 or so, showing that the contribution of the core excitation to the refractive index is negligibly small in this low energy region. The singularity appearing in $n^C(E)-1$ at the carbon K-edge is due to the present approximation of a step-like onset for the K-shell absorption. At high energies, $n^V(E)-1$ and $n^C(E)-1$ tend to zero.

As will be shown later in the Appendix, if the k(E) values are expressed for $E \geq E_1$ by a form

$$k(E) = \alpha E^{-\beta} \tag{9}$$

as has indeed been found in the present results for $E_1 \simeq 20$ eV, n(E)-1 for $E \geq 10E_1$ can be written as

$$n(E)-1 = -E_p^2/2E^2 - Q(\beta)k(E) \tag{10}$$

with an accuracy much better than 99%, where E_p^2 is a constant defined by the sum rule (7) as

$$E_p^2 = \frac{4}{\pi} \int_0^\infty E' k(E') dE'$$

$$= (4\pi n_o e^2 \hbar^2/m)\ N_I \qquad (11)$$

and $Q(\beta)$ is a quantity which depends only on the exponent β in the expression (9). The plot of $Q(\beta)$ vs β given in the Appendix, Figure 12 shows that for $\beta > 2$ as in the present results, $n(E)-1$ goes asymptotically to

$$n(E)-1 = -E_p^2/2E^2 \qquad (12)$$

at high energies. This form of $n(E)-1$ is that of a free-electron gas in the high energy limit. In the present case, using the expressions $k^v(E) = 7.81 \times 10^3 E^{-3.23}$ and $k^c(E) = 2.21 \times 10^6 E^{-3.68} - 7.81 \times 10^3 E^{-3.23}$, $n^v(E)-1$ and $n^c(E)-1$ were obtained for $E \geq 200$ eV and $E \geq 2820$ eV, respectively, as

$$n^v(E)-1 = -(E_p^v)^2/2E^2 - 1.78 \times 10^3/E^{3.23}, \qquad (13)$$

$$n^c(E)-1 = -(E_p^c)^2/2E^2 - 1.85 \times 10^6/E^{3.68} + 1.78 \times 10^3/E^{3.23}, \qquad (14)$$

where $(E_p^v)^2 = (4\pi n_o e^2 \hbar^2/m) \times 41.51$ and $(E_p^c)^2 = (4\pi n_o e^2 \hbar^2/m) \times 14.49$. The detailed behavior of $n^v(E)-1$ and $n^c(E)-1$ at high energies relative to the free-electron expressions $n_F^v(E)-1 = -(E_p^v)^2/2E^2$ and $n_F^c(E)-1 = -(E_p^c)^2/2E^2$, respectively, are shown in the inserts of Figs. 3 and 4.

The results of $(n^v(E)-1)/(n_F^v(E-1)$ and $(n^c(E)-1)/(n_F^c(E)-1)$ given here exhibit quite similar behaviors and show that monotonic convergences of $n^v(E)-1$ and $n^c(E)-1$ to the respective free-electron values start at about 100 eV

BEST AVAILABLE COPY

and 900 eV, respectively. It is to be noted, however, that the deviation of $n^c(E)-1$ values from the free-electron values is considerably larger than that of $n^v(E)-1$ over the entire high energy region. The relatively close fit of the $n^v(E)-1$ values to the free-electron values above 40 eV in Fig. 3 has to be considered fortuitous. As is shown in the Appendix, Figure 12, this close fit is due to the relatively small value of $Q(\beta)$ in Eq. (10) for $\beta=3.23$, the exponent for absorption of the valence electrons.

A simple and interesting sum rule

$$S(E) = \int_0^E \{n(E') - 1\}dE' \to 0; \; E \to \infty \qquad (15)$$

has been derived recently by Altarelli et al.[5] for the refractive index n(E) of isotropic media including conductors. This sum rule asserts that the average value of the refractive index over the whole spectral range is equal to unity. In the derivation of this sum rule, the only assumption made was that in the high energy limit the medium responds like a free-electron gas, i.e.,

$$n(E) + ik(E) \simeq 1-E_p^2/2E^2. \qquad (16)$$

As we have already seen, this is indeed the case for the present results. S(E) evaluated from $n^v(E)-1$ and $n^c(E)-1$ are given in Fig. 5 as functions of photon energy E up to 10^4 eV. Both $S^v(E)$ and $S^c(E)$ converge slowly to zero at high energies. The analytical expressions (13) and (14) allow us to extend the integrations $S^v(E)$ and $S^c(E)$ up to infinity. It was found that both $S^v(E)$ and $S^c(E)$ converge exactly to zero in the limit of $E \to \infty$.

BEST AVAILABLE COPY

For a high energy E, above which the behavior of n(E)-1 can be represented by the free-electron expression (12), S(E) may be approximated by

$$S_F(E) = -\int_E^\infty \{n(E')-1\}dE' \simeq E_p^2/2E \qquad (17)$$

This form describes the asymptotic behavior of S(E) in the high energy limit. $S_F(E)$ from the valence and core contributions are presented in Fig. 5 and compared with the results for S(E). S(E) is described well by $S_F(E)$ over a wide range in the high energy region. Relative deviations between S(E) and $S_F(E)$ are, however, about the same as those found in the results for $(n(E)-1)/(n_F(E)-1)$ at corresponding energies as shown in the inserts of Figs. 3 and 4.

Before closing this subsection, we present in Fig. 6 the results of n(E)-1, in the region where n(E)-1 is negative, on logarithmic plots, together with the free-electron values. These plots are of help in evaluating the complex dielectric function and the energy loss function, which will be presented in the following section.

3. The complex dielectric function ε and the energy loss function $\mathrm{Im}(-1/\varepsilon)$.

The imaginary part of the complex dielectric function $\varepsilon(=\varepsilon_1+i\varepsilon_2)$ and the energy loss function $\mathrm{Im}(-1/\varepsilon)$ for fast charged particles were calculated from the values of n and k, and are presented in Fig. 7 on logarithmic plots, together with the values of 2k. Among these three spectra, substantial

BEST AVAILABLE COPY

differences are found only in the low energy region. Deviations of the $\mathrm{Im}(-1/\varepsilon)$ spectrum from ε_2, found in the low energy region, describe the so-called collective effect,[15] i.e. charged particle density fluctuations brought about by fast charged particles incident on condensed matter. In Fig. 7,

regularities in the displacement of the low energy structures should be noted. All three peaks found in the low energy region shift to higher energies in order of ε_2, 2k and $\mathrm{Im}(-1/\varepsilon)$, and their peak heights decrease also in this order.

For ε_2 and $\mathrm{Im}(-1/\varepsilon)$, there exist the well-known f-sum rules,[4]

$$N_2(E) = \frac{2}{\pi}\,(m/4\pi n_o e^2\hbar^2)\int_o^E E'\varepsilon_2(E')dE' \to N;\ E\to\infty, \qquad (18)$$

$$N_3(E) = \frac{2}{\pi}\,(m/4\pi n_o e^2\hbar^2)\int_o^E E'\,\mathrm{Im}\{-1/\varepsilon(E')\}dE' \to N;\ E\to\infty, \qquad (19)$$

The results of $N_2(E)$ and $N_3(E)$ are shown in Fig. 8 as functions of photon energy E, together with that of $N_1(E)$ which has already been presented in Fig. 2. It was found that all these numbers of effective electrons converge to the same value in the high energy limit. As has been seen, k and n-1 are separable into the valence and core contributions. Generally, ε_2 and $\mathrm{Im}(-1/\varepsilon)$ are not separable, as by definition they include the cross terms between the valence and core contributions. In the case of $|n^V-1|$ and $|n^C-1|\ll 1$, and k^V and $k^C \ll 1$, however, it can be shown that ε_2 and $\mathrm{Im}(-1/\varepsilon)$ are separable. This can be seen from the results shown in Fig. 7, where ε_2 and $\mathrm{Im}(-1/\varepsilon)$ are in agreement with 2k in the high energy region; thus they can be separated into the valence and core contributions in the same manner as the k spectrum. $N_1(E)$, $N_2(E)$ and $N_3(E)$ for the valence and core contributions are plotted in Fig. 8. Because of the close agreement among 2k, ε_2 and $\mathrm{Im}(-1/\varepsilon)$, no substantial differences were found in the N(E) values in the high energy region.

BEST AVAILABLE COPY

Detailed spectra for ϵ_1, ϵ_2, and $\mathrm{Im}(-1/\epsilon)$ in the low energy region are presented in Figs. 9 and 10 on linear plots. The general spectral features given here agree well with results from earlier studies[9,16,20] obtained below 20 eV. Considerable numerical disagreements are, however, found between the present results and some of the earlier ones. Apparently, the discrepancies can be attributed to poor experimental accuracy and large uncertainties in data analysis in the earlier studies. Four absorption bands can be distinguished below 11 eV in the ϵ_2 spectrum shown in Fig. 9; at around 4.8, 5.8, 6.3, and 9.5 eV. The interpretation of these structures and the corresponding structures in $\mathrm{Im}(-1/\epsilon)$ have already been described by many authors.[9,16-20] The spectral features in the extreme ultraviolet above 10 eV given in Fig. 10 are quite simple and are marked only by the broad peaks at 12.5 eV in ϵ_2 and at 21.7 eV in $\mathrm{Im}(-1/\epsilon)$. These features are typical of many organic solids.[6,7,21,22] The spectrum for $\mathrm{Im}(-1/\epsilon)$ shown here agrees well with that from characteristic electron energy loss measurements[16,23] on thin polystyrene films.

4. The average photoexcitation energy and the average energy loss.

The present results, extending substantially over the region from zero to infinite photon energy, allow us to evaluate the average photoexcitation energy and the average energy loss suffered by fast charged particles. These quantitites are of key importance in radiation physics which deals with the interaction of high energy ionizing radiations with matter.

Shown in Fig. 11 are the results of the photoexcitation energy $\bar{E}_2(E_0)$ and the energy loss $\bar{E}_3(E_0)$ averaged over the spectral region from E_0 to infinity, i.e.,

$$\bar{E}_2(E_o) = \int_{E_o}^{\infty} E\varepsilon_2(E)dE \Big/ \int_{E_o}^{\infty} \varepsilon_2(E)dE, \qquad (20)$$

$$\bar{E}_3(E_o) = \int_{E_o}^{\infty} E\ \mathrm{Im}\{-1/\varepsilon(E)\}dE \Big/ \int_{E_o}^{\infty} \mathrm{Im}\{-1/\varepsilon(E)\}dE. \qquad (21)$$

Such plots of $\bar{E}_2(E_o)$ and $\bar{E}_3(E_o)$ as functions of E_o are of help in evaluating the contribution of excitations in a particular energy range to the average excitation energy and energy loss. Since, in the present results, the onset of valence absorption was found at 4.5 eV, the values of $\bar{E}_2(E_o)$ and $\bar{E}_3(E_o)$ at E_o = 4.5 eV give the average excitation energy and energy loss, respectively, over the entire oscillator strength distribution. $\bar{E}_2$ and $\bar{E}_3$ at E_o = 4.5 eV were found to be 25.1 and 36.8 eV, respectively. This difference can be attributed to an energy loss associated with the creation of collective oscillations due to the interaction of fast charged particles with matter. Photons generally do not excite collective oscillations in experimental systems designed for the measurement of k.

From the definition of the energy loss function,[15] the average energy loss $\bar{E}_3(E_o)$ obtained here should be considered to be that due to a single energy loss event associated with zero transverse momentum-transfer from the fast charged particle to the medium. Therefore, it cannot be compared directly with similar quantities such as the mean excitation potential, (I), appearing in the well-known Bethe-Bloch formula[24,25] for the stopping power or the so-called W-value, the average energy for an ion-pair creation. It may be worthwhile, however, to note that I = 63.5 eV was obtained by

BEST AVAILABLE COPY

Sternheimer[26] for polystyrene, and W = 37 eV was reported by Mathieu et. al.[27] for liquid cyclohexane, which may be considered to be a model system for solid polystyrene.

The variations of $\bar{E}_2(E_o)$ and $\bar{E}_3(E_o)$ shown in Fig. 11 as functions of E_o are no more than a few eV for $E_o \leq 10$ eV, showing that the contributions of such low energy excitations to the average excitation energy and energy loss are relatively small. This result will apply to other condensed hydrocarbons, as substantial differences of the oscillator strength distribution for these materials have been found[21] only in the region below about 10 eV. Also shown in Fig. 11 is $\bar{E}_1(E_o)$ defined by

$$\bar{E}_1(E_o) = \int_{E_o}^{\infty} Ek(E)dE \; / \int_{E_o}^{\infty} k(E)dE. \qquad (22)$$

As is well-known, Ek(E) for condensed media cannot be considered to give the oscillator strength distribution in a strict sense. It has been found for many hydrocarbons,[9,28,29] however, that except for molecular Rydberg fine structure the k spectrum in the gas phase agrees well with that in the condensed phase, apart from a constant factor corresponding to the ratio of molecular densities between these two phases. This is particularly so in the region above 10 eV, where most of the excitation energy and energy loss occurs. $\bar{E}_1(E_o)$ shown here, therefore, can be regarded as representing approximate values of $\bar{E}_2(E_o)$ and $\bar{E}_3(E_o)$ in the low density limit i.e. for gas phase hydrocarbons, since ϵ_2 and $\mathrm{Im}(-1/\epsilon)$

BEST AVAILABLE COPY

in the low density limit agree with 2k over the whole spectral range. $\bar{E}_1^{v}(E_o)$, $\bar{E}_2^{v}(E_o)$ and $\bar{E}_3^{v}(E_o)$ presented in Fig. 11 are the respective average excitation energy and energy loss derived from the valence excitation only. Here, one may see how much the core excitations contribute to the average excitation energy and energy loss.

Finally the values of the extinction coefficient k obtained and used in this study are tabulated in Table I for further use.

5. Concluding remarks.

It was found in the present study that the convergence of all sum rules associated with the optical constants of polystyrene are quite slow, and the almost perfect saturations do not occur until the keV region. This is for a material having one of the simplest of all electronic configurations. Experimentally, the f-sum rules have provided useful criteria for consistency checks of the optical constants. It has been shown, however, that the f-sum rules are applicable only when the experimental data cover all electronic excitations including the innermost core excitations. In applying the f-sum rules for a particular shell, difficulties arise from, in addition to the slow convergences, the fact that a non-negligible amount of oscillator strength coupling always occurs between the inner and outer shell electrons. If experimental data cover only a part of the total oscillator strength distribution as is so in most cases, the oscillator strength for a particular shell, to which the f-sum rules should converge, can not be known a priori without knowing those for the remaining shells.

BEST AVAILABLE COPY

It has been proposed recently by Altarelli et al.[5] that the S(E) sum rule for the refractive index given by Eq. (15) may be used as a saturation criterion and/or as a consistency check for the optical constants obtained experimentally. The present results for S(E) shown in Fig. 5, indeed, converge to the free-electron values $S_F(E)$ given by Eq. (17) much faster than the f-sum rules converge. Differences between S(E) and $S_F(E)$, however, are not negligibly small up to quite high energies. Further, E_p^2 for a particular shell in the expression for $S_F(E)$, which is proportional to the oscillator strength, can not be known until the convergence of the f-sum rule is attained. Practically, the new sum rule for S(E), if applied to a particular shell, is subject to the same uncertainty as the f-sum rules.

APPENDIX

Let us assume that the extinction coefficient k(E) at photon energy E is expressed by

$$k(E) = \alpha E^{-\beta} \qquad \text{(A1)}$$

for $E \geq E_1$ as is generally found for high photon energies, where α and β are positive constants. According to a Kramers-Kronig relation, the refractive index n(E) at photon energy E is given by

$$n(E) - 1 = \frac{2}{\pi} \int_0^\infty \frac{E' k(E')}{E'^2 - E^2} \, dE'. \qquad \text{(A2)}$$

Dividing the integration into three regions, and, then, allowing less than 1% error to the first and third regions, n(E)-1 can be written as

$$n(E)-1 = \frac{2}{\pi}\left\{\int_0^{0.1E} \frac{E'k(E')}{E'^2-E^2}\,dE' + \int_{0.1E}^{10E} \frac{E'k(E')}{E'^2-E^2}\,dE' + \int_{10E}^{\infty} \frac{E'k(E')}{E'^2-E^2}\,dE'\right\}$$

$$= \frac{2}{\pi}\left\{-\frac{1}{E^2}\int_0^{0.1E} E'k(E')dE' + \int_{0.1E}^{10E} \frac{E'k(E')}{E'^2-E^2}\,dE' + \int_{10E}^{\infty} \frac{k(E')}{E'}dE'\right\}. \quad (A3)$$

Now, if we confine ourselves to the case of $E \geq 10E_1$. The first integral can be written as

$$\frac{2}{\pi}(1/E^2)\left\{-\int_0^{\infty} E'k(E')dE' + \int_{0.1E}^{\infty} E'k(E')dE'\right\}. \quad (A4)$$

The first integral in (A4) should be a constant from the sum rule , and the second one is calculable analytically, as the expression (A1) holds for this region. Thus, the integrals in (A4) become

$$-E_p^2/2E^2 + \frac{2}{\pi}\,\frac{10^{\beta-2}}{\beta-2}\,k(E), \quad (A5)$$

where E_p^2 is defined by

$$E_p^2 = \frac{4}{\pi}\int_o^{\infty} E'k(E')dE' \quad (A6)$$

The third integral in Eq. (A3) is also calculable analytically and is given by

$$\frac{2}{\pi}\,\frac{10^{-\beta}}{\beta}\,k(E) \quad (A7)$$

Finally, the second integral in Eq. (A3) is also calculable as the expression (A1) holds for this region. However, the functional dependence of this integral on E can be obtained easily without carrying out the integration. Using the similarity of the expression (A1) in logarithmic scale, the integral region from 0.1E to 10E can be shifted to an arbitrary region, for example, from $0.1E_2$ to $10E_2$. This shift introduces a factor $(E/E_2)^{-\beta}$, i.e.,

$$\frac{2}{\pi}\int_{0.1E}^{10E} \frac{E'k(E')}{E'^2-E^2}\,dE' = \frac{2}{\pi}(E/E_2)^{-\beta}\int_{0.1E_2}^{10E_2} \frac{E'k(E')}{E'^2-E_2^2}\,dE' \qquad (A8)$$

Since this shift of integral region is valid for any $E_2(\geq E)$, the integral

$$\frac{2}{\pi}(1/E_2)^{-\beta}\int_{0.1E_2}^{10E_2} \frac{E'k(E')}{E'^2-E_2^2}\,dE' \qquad (A9)$$

should be a constant. Thus, the second integral in Eq. (A3) can be written as

$$\frac{2}{\pi}\,P(\beta)k(E) \qquad (A10)$$

where $P(\beta)$ defined by

$$P(\beta) = (1/E_2)^{-\beta}\int_{0.1E_2}^{10E_2} \frac{E'^{-\beta+1}}{E'^2-E_2^2}\,dE' \qquad (A11)$$

is a quantity depending only on β. Summing up (A5), (A7), and (A10), we have for $E \geq 10E_1$

$$n(E)-1 = -(E_p^2/2E^2) + \frac{2}{\pi}\left\{\frac{10^{\beta-2}}{\beta-2} + P(\beta) + \frac{10^{-\beta}}{\beta}\right\} k(E) \qquad \text{(A12)}$$

$$= -(E_p^2/2E^2) - Q(\beta)k(E)$$

Values of $Q(\beta)$ obtained from a numerical calculation of $P(\beta)$ are plotted in Fig. 12 as a function of β. $Q(\beta)$ becomes zero at $\beta=3.06$ and goes to negative infinity in the limit of $\beta \to 2$. Such an analytical expression for $n(E)-1$ for the high energy region is quite useful in analyses of optical data as has been shown in this study, and can be applicable for any kind of material, as the expression (A1) involves a general behavior of k due to high energy absorptions.

REFERENCES

1. H. R. Philipp and H. Ehrenreich, J. Appl. Phys. 35, 1416 (1964); M. Altarelli and D. Y. Smith, Phys. Rev. B 9, 1290 (1974).

2. A. P. Lukirskii, V. A. Fomichev, and I. A. Brytov, Opt. Spectry. (USSR) 20, 202 (1966).

3. B. Nordfors, Arkiv Fysik 11, 587 (1957).

4. P. Nozieres and D. Pines, Phys. Rev. 113, 1254 (1959).

5. M. Altarelli, D. L. Dexter, H. M. Nussenzveig, and D. Y. Smith, Phys. Rev. B 6, 4502 (1972).

6. T. Inagaki, R. N. Hamm, E. T. Arakawa, and L. R. Painter, J. Chem. Phys. 61, 4246 (1974).

7. T. Inagaki, R. N. Hamm, E. T. Arakawa, and R. D. Birkhoff, Biopolymers 14, 839 (1975).

8. R. H. Boundy and R. F. Boyer, Styrene, Its Polymers, Copolymers, and Derivatives (Reinhold Publishing, New York, 1952).

9. R. H. Partridge, J. Chem. Phys. 47, 4223 (1967).

10. Apparently, the results cited in the figure in Lukirskii et al.'s paper (Ref. 1) as the results by Nordfors (Ref. 2) are not Nordfor's results, but those of empirical calculations by J. A. Victoreen (J. Appl. Phys. 20, 1141 (1949)). Despite this erroneous citation, the original data taken by Nordfors at five wavelengths from 8.23 Å to 1.54 Å were found to fit well to the expression (4) or (6).

11. F. Stern, Solid State Physics, edited by F. Seitz and D. Turnbull (Academic, New York, 1963), Vol. 15, p. 341.

12. W. Heitler, The Quantum Theory of Radiation (The Oxford University Press, 1954), Chap. 7.

13. A. H. Compton and S. K. Allison, X-Rays in Theory and Experiment (D. van Nostrand, New York, 1936), p. 542.

14. W. Hayes and F. C. Brown, Phys. Rev. A 6, 21 (1972).

15. H. Raether, Springer Tracts in Modern Physics, edited by G. Höhler (Springer, Berlin, 1965), Vol. 38, p. 85.

16. N. Swanson and C. J. Powell, J. Chem. Phys. 39, 630 (1963); Phys. Rev. 145, 195 (1966).

17. J. G. Carter, T. M. Jelinek, R. N. Hamm, and R. D. Birkhoff, J. Chem. Phys. 44, 2266 (1966).

18. J. T. Shapiro and R. P. Madden, J. Opt. Soc. Am. 58, 771 (1968).

19. W. L. Buck, B. R. Thomas, and A. Weinreb, J. Chem. Phys. 48, 549 (1968).

20. S. Onari, J. Phys. Soc. Jpn. 26, 500 (1969).

21. T. Okabe, J. Phys. Soc. Jpn. 35, 1496 (1973).

22. M. Isaacson, J. Chem. Phys. 56, 1803 (1972).

23. R. E. Lavilla and H. Mendlowitz, J. Phys. (Paris) 25, 114 (1964).

24. H. A Bethe, Handbuch der Physik (Springer, Berlin , 1933), Vol. 24, p. 273.

25. F. Block, Z. Physik 81, 363 (1933).

26. R. M. Sternheimer, Phys. Rev. 103, 511 (1956).

27. J. Mathieu, D. Blanc, P. Caminade, and J. P. Patau, J. Chim. Phys. 64, 1679 (1967).

28. E. E. Kock and M. Skibowski, Chem. Phys. Letters 9, 429 (1971).

29. M. Yoshino, J. Takeuchi, and H. Suzuki, J. Phys. Soc. Jpn. 34, 1039 (1973).

FIGURE CAPTIONS

Fig. 1. The extinction coefficient k for polystyrene as a function of photon energy E. Dotted line is extrapolation of the present results between 20 and 60 eV.

Fig. 2. Effective number of electrons $N_1(E)$ per monomeric unit of polystyrene obtained from the extinction coefficient k as a function of photon energy E. $N_1^V(E)$ and $N_1^C(E)$ represent the contributions from the valence and core electron excitations, respectively.

Fig. 3. The refractive index for polystyrene due to the valence electron excitations as a function of photon energy E. Dashed curve represents the free-electron values.

Fig. 4. The refractive index for polystyrene due to the carbon core electron excitations as a function of photon energy E. Dashed curved represents the free-electron values.

Fig. 5. The sum rule S(E) for the refractive index n of polystyrene as a function of photon energy E. $S^V(E)$ and $S^C(E)$ represent the contributions from the valence and core electron excitations, respectively. $S_F^V(E)$ and $S_F^C(E)$ represent the corresponding free-electron values.

Fig. 6. The refractive index n for polystyrene in the region where n-1 is negative as a function of photon energy E. n^V and n^C represent the contributions from the valence and core electron excitations, respectively. n_F, n_F^V, and n_F^C represent the corresponding free-electron values.

Fig. 7. Twice the extinction coefficient k, the imaginary part of the complex dielectric function $\epsilon(=\epsilon_1 + i\epsilon_2)$ and the energy loss function $\mathrm{Im}(-1/\epsilon)$ for polystyrene as functions of photon energy E.

Fig. 8. Effective number of electrons $N_1(E)$, $N_2(E)$, and $N_3(E)$ per monomeric unit of polysytrene obtained from the extinction coefficient k, the imaginary part of the complex dielectric function $\epsilon(=\epsilon_1+i\epsilon_2)$ and the energy loss function $\mathrm{Im}(-1/\epsilon)$, respectively, as functions of photon energy E. $N^V(E)$ and $N^C(E)$ represent the contributions from the valence and core electron excitations, respectively.

Fig. 9. The real and imaginary parts of the complex dielectric function $\epsilon(=\epsilon_1+i\epsilon_2)$ and the energy loss function $\mathrm{Im}(-1/\epsilon)$ for polysytrene as functions of photon energy E.

Fig. 10. The real and imaginary parts of the complex dielectric function $\epsilon(=\epsilon_1+i\epsilon_2)$ and the energy loss function $\mathrm{Im}(-1/\epsilon)$ for polysytrene as functions of photon energy E.

Fig. 11. The average photoexcitation energy $\bar{E}_2$ and the average energy loss $\bar{E}_3$ for polystyrene over the spectral range from E_0 to infinity as functions of E_0. $\bar{E}_1$ may represent $\bar{E}_2$ and $\bar{E}_3$ in the low density limit. $\bar{E}_1^V$, $\bar{E}_2^V$, and $\bar{E}_3^V$ represent the corresponding values due to the valence electron excitations only.

Fig. 12. Dependence of $Q(\beta)$ on the exponent β.

Table I. The extinction coefficient k for polystyrene as a function of photon energy E.

E(eV)	k	E(eV)	k
0.6		11.0	0.586
:	0.00000	11.5	0.636
4.4		12.0	0.681
4.5	0.0011	12.5	0.713
4.6	0.0089	13.0	0.730
4.7	0.0103	13.5	0.743
4.8	0.0103	14.0	0.748
4.9	0.0092	14.5	0.747
5.0	0.0072	15.0	0.741
5.1	0.0054	16.0	0.702
5.2	0.0041	17.0	0.646
5.3	0.0043	18.0	0.590
5.4	0.0292	19.0	0.531
5.6	0.183	20.0	0.473
5.8	0.330	22.0	0.361
6.0	0.431	24.0	0.276
6.2	0.825	26.0	0.211
6.4	1.023	28.0	0.164
6.6	0.884	30.0	0.129
6.8	0.694	35.0	0.0806
7.0	0.524	40.0	0.0542
7.3	0.354	45.0	0.0375
7.6	0.239	50.0	0.0247
7.9	0.206	55.0	0.0192
8.2	0.220	60.0	0.0136
8.6	0.264	:	a
9.0	0.344	282	
9.5	0.425	:	b
10.0	0.474	8050	
10.5	0.523		

a. $k=7.81\times10^{3}E^{-3.23}$ (Extrapolation of k between 20 and 60 eV).

b. $k=2.21\times10^{6}E^{-3.68}$ (Refs. 2 and 3).

FIGURE 1

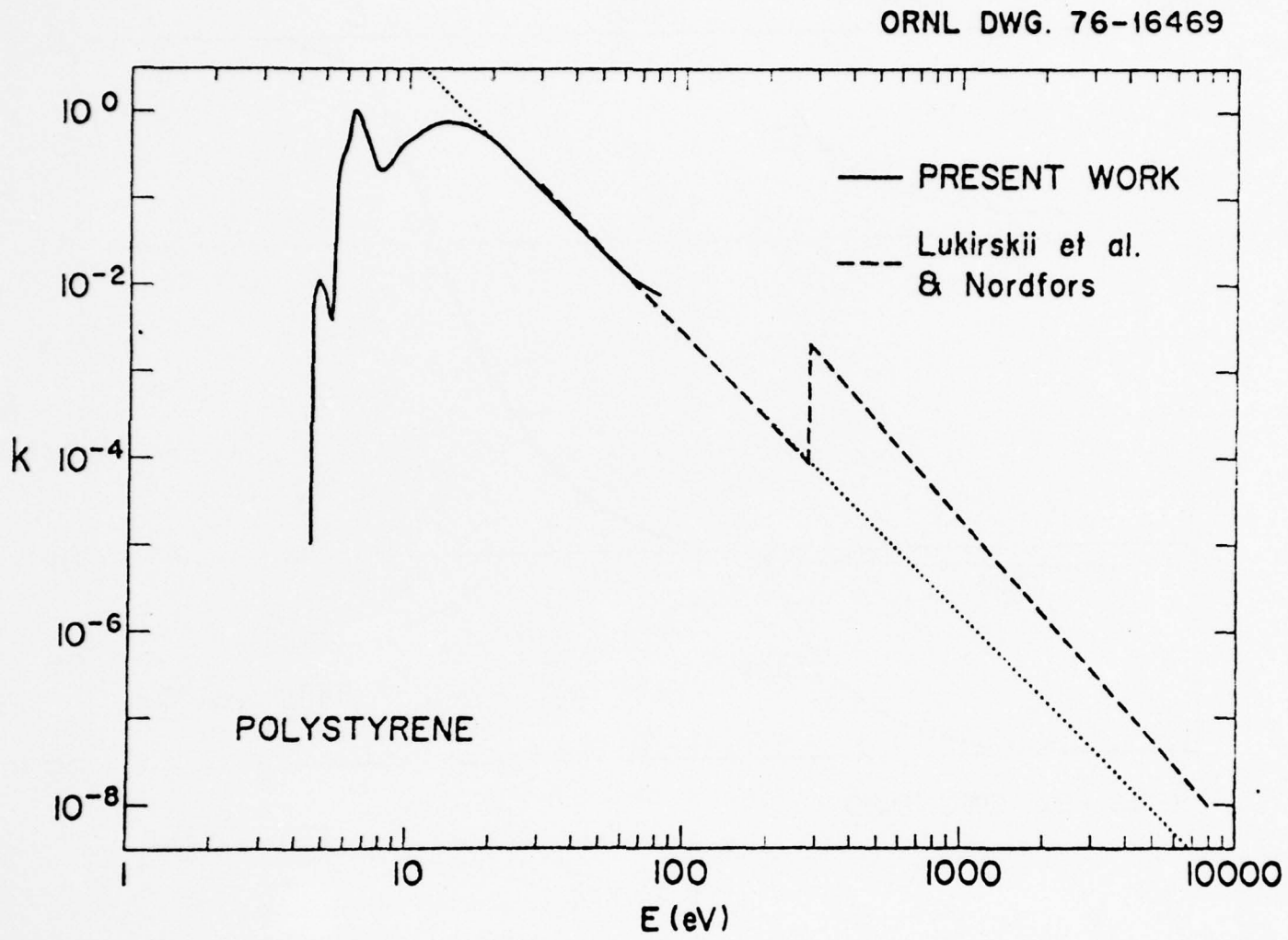

ORNL DWG. 76-16469
PRESENT WORK
Lukirskii et al.
& Nordfors
POLYSTYRENE
k
10^{0}
10^{-2}
10^{-4}
10^{-6}
10^{-8}
1
10
100
1000
10000
E (eV)

FIGURE 2

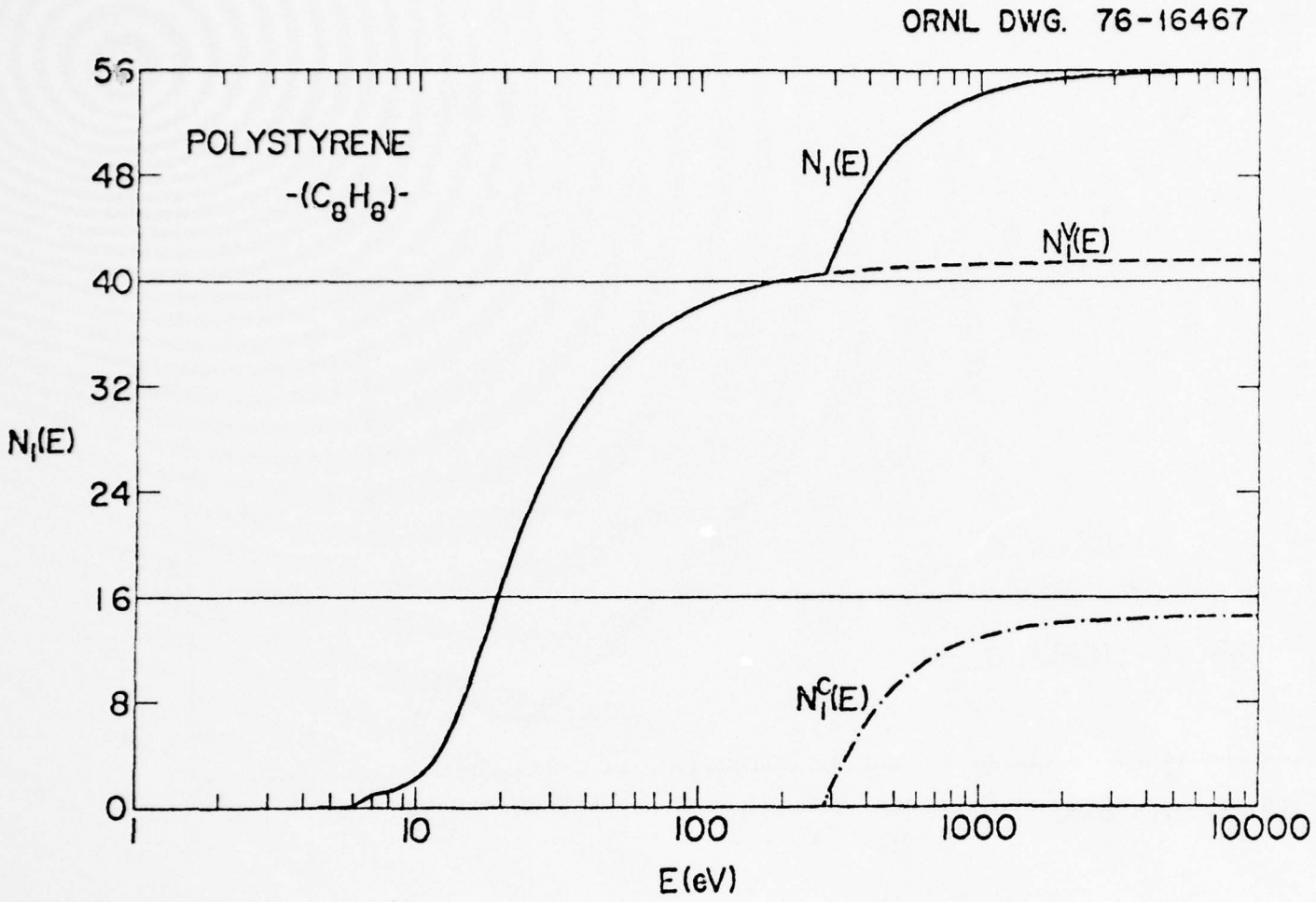

ORNL DWG. 76-16467
POLYSTYRENE
-(C8H8)-
N1(E)
N1V(E)
N1C(E)
56
48
40
32
24
16
8
0
1
10
100
1000
10000
E(eV)

FIGURE 3

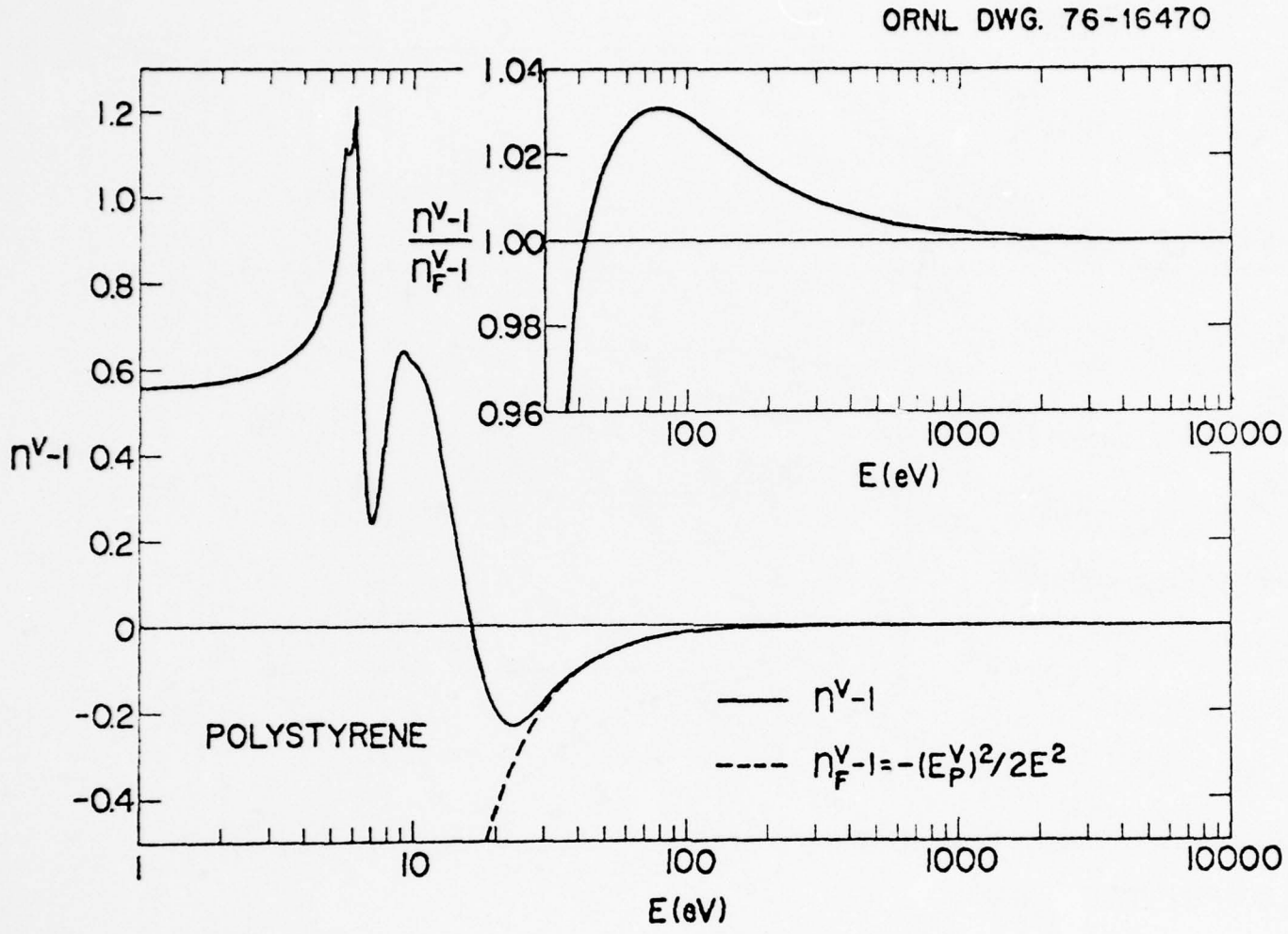

ORNL DWG. 76-16470
n^v-1
$\frac{n^v-1}{n_F^v-1}$
E(eV)
POLYSTYRENE
n^v-1
$n_F^v-1=-(E_p^v)^2/2E^2$
E(eV)

FIGURE 4

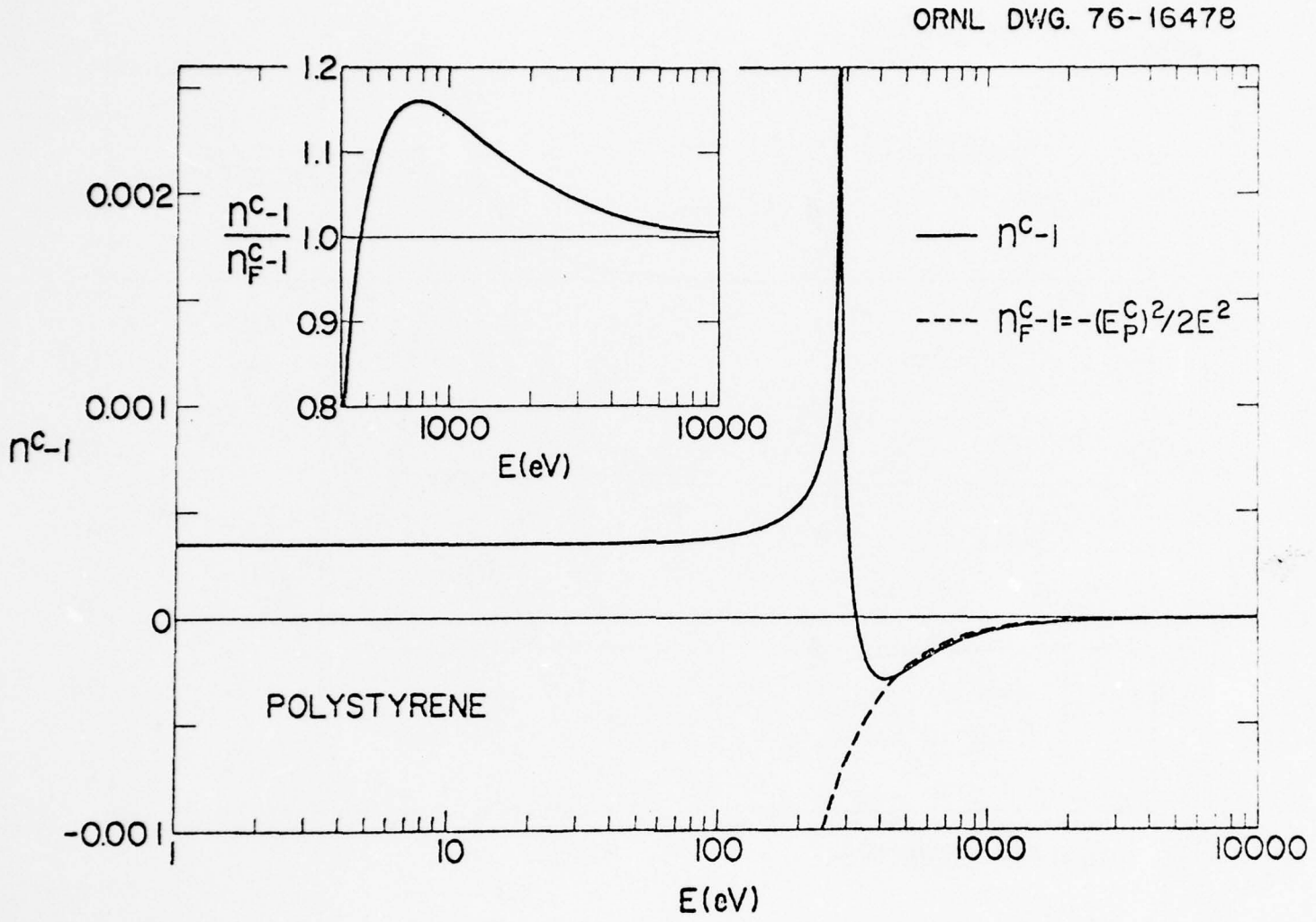

ORNL DWG. 76-16478
1.2
1.1
1.0
0.9
0.8
$\frac{n^c-1}{n_F^c-1}$
1000
10000
E(eV)
0.002
0.001
0
-0.001
n^c-1
n^c-1
$n_F^c-1=-(E_p^c)^2/2E^2$
POLYSTYRENE
1
10
100
1000
10000
E(eV)

FIGURE 5

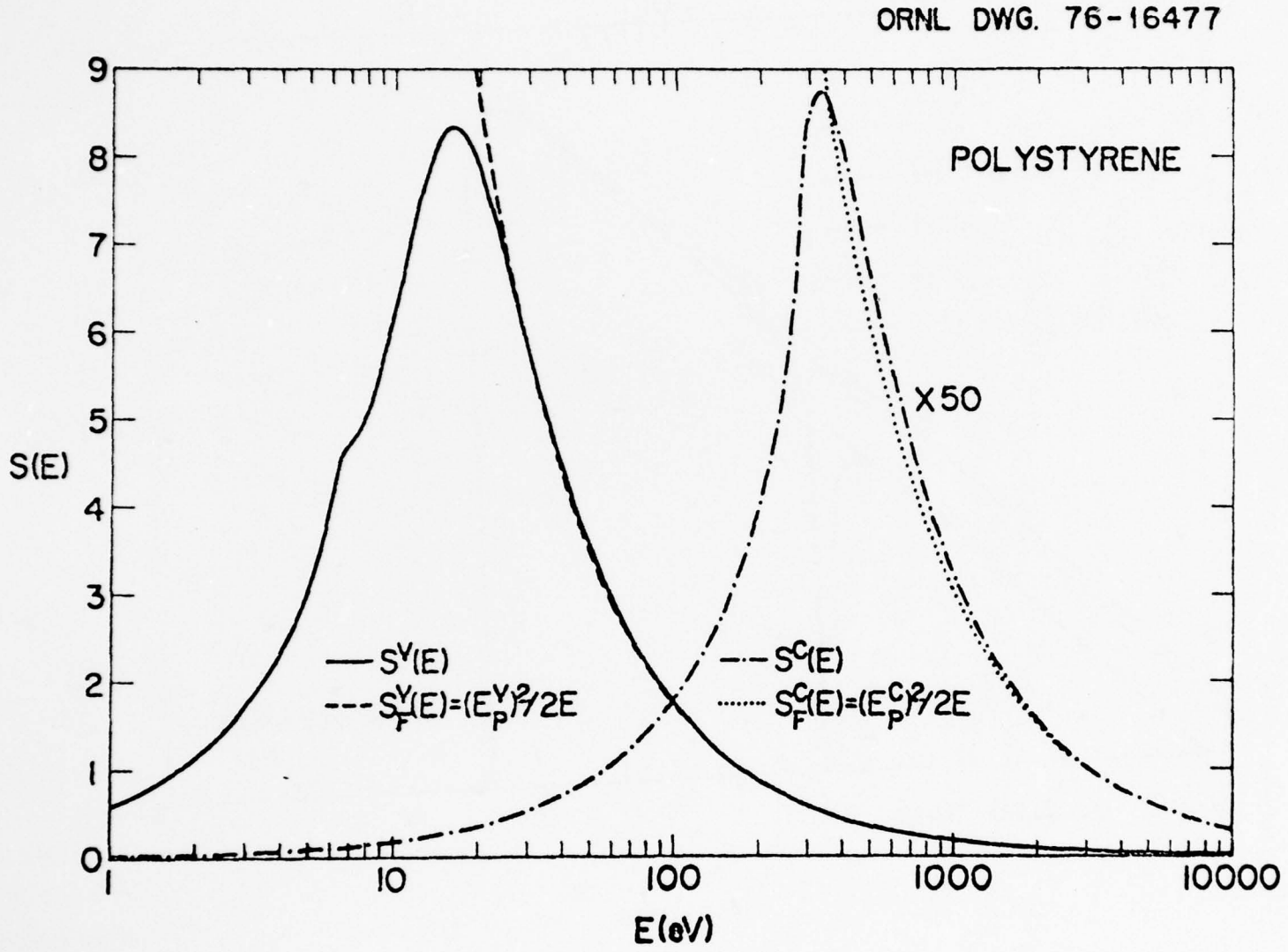
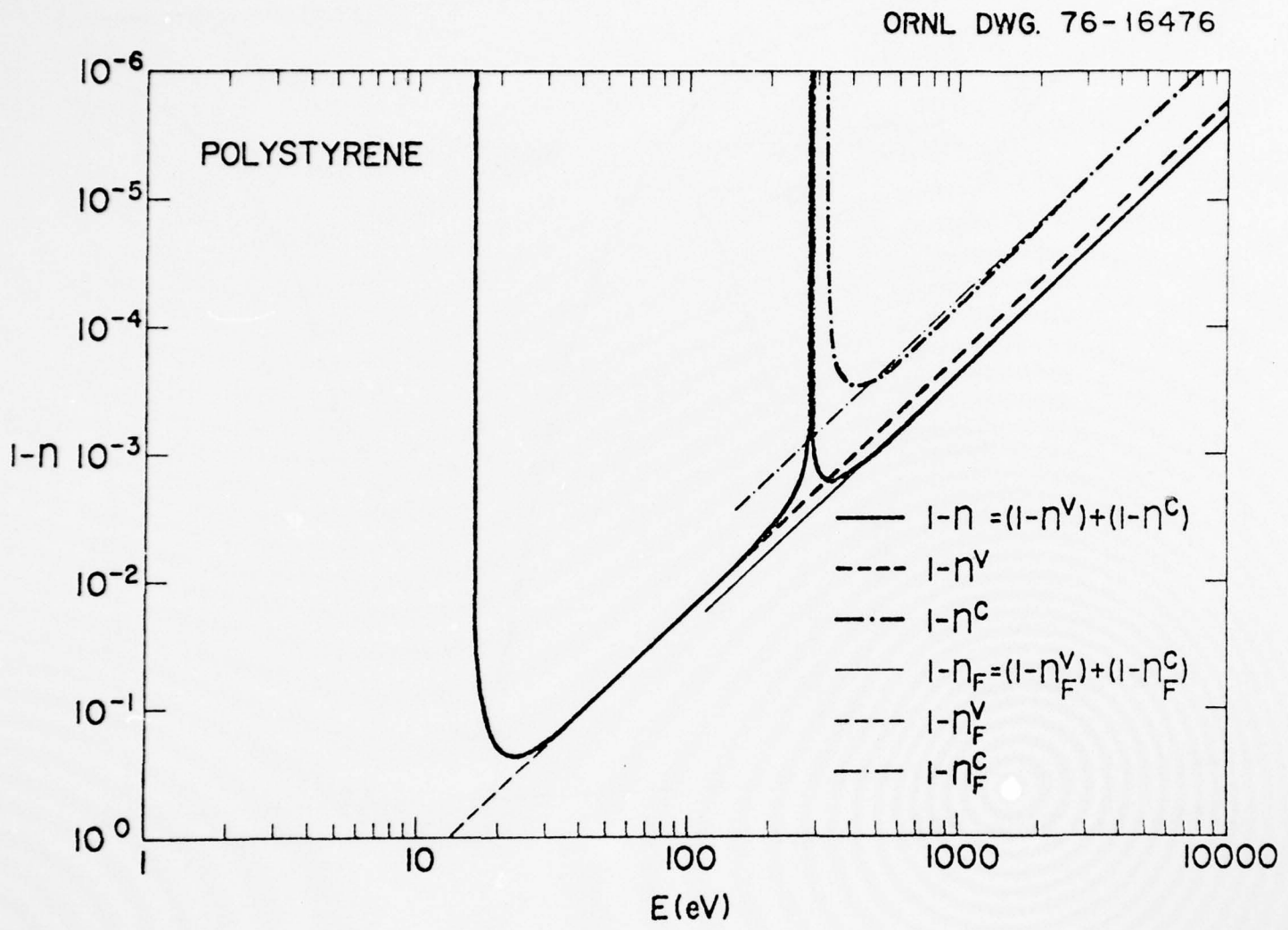
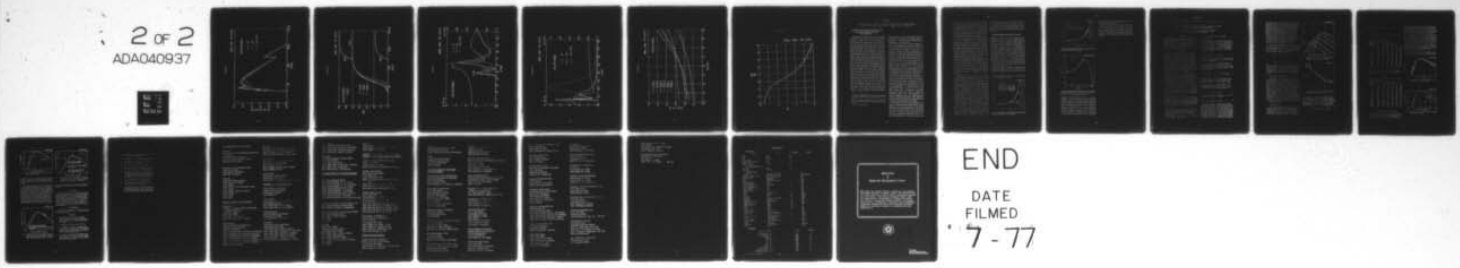

ORNL DWG. 76-16477
POLYSTYRENE
X50
S(E)
E(eV)
$S^V(E)$
$S_F^V(E)=(E_p^V)^2/2E$
$S^C(E)$
$S_F^C(E)=(E_p^C)^2/2E$
0
1
2
3
4
5
6
7
8
9
1
10
100
1000
10000

FIGURE 6


ORNL DWG. 76-16476
POLYSTYRENE
1-n
10^{-6}
10^{-5}
10^{-4}
10^{-3}
10^{-2}
10^{-1}
10^{0}
1
10
100
1000
10000
E(eV)
$1-n = (1-n^V)+(1-n^C)$
$1-n^V$
$1-n^C$
$1-n_F=(1-n_F^V)+(1-n_F^C)$
$1-n_F^V$
$1-n_F^C$

AD-A040 937 ROME AIR DEVELOPMENT CENTER GRIFFISS AFB N Y F/G 7/5
STUDIES OF ELECTRON INTERACTIONS WITH COMMUNICATIONS MATERIALS.(U)
FEB 77 J C ASHLEY, M W WILLIAMS
UNCLASSIFIED RADC-TR-77-74 NL

2 OF 2
ADA040937



END

DATE
FILMED
7-77

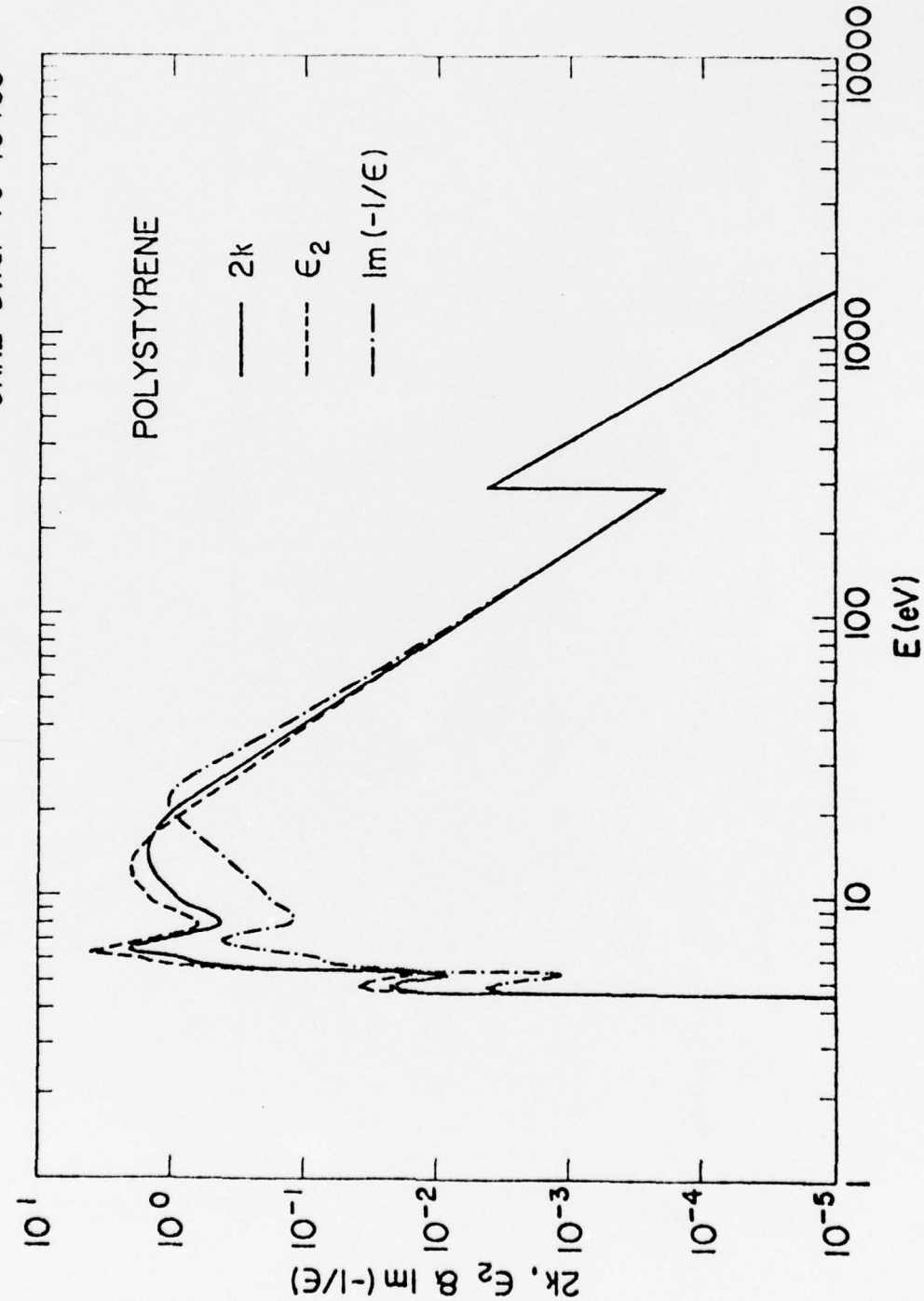

ORNL DWG. 76-16468
POLYSTYRENE
2k
ϵ_2
Im (-1/ϵ)
2k, ϵ_2 & Im (-1/ϵ)
E (eV)
10^{1}
10^{0}
10^{-1}
10^{-2}
10^{-3}
10^{-4}
10^{-5}
1
10
100
1000
10000

FIGURE 7

FIGURE 8

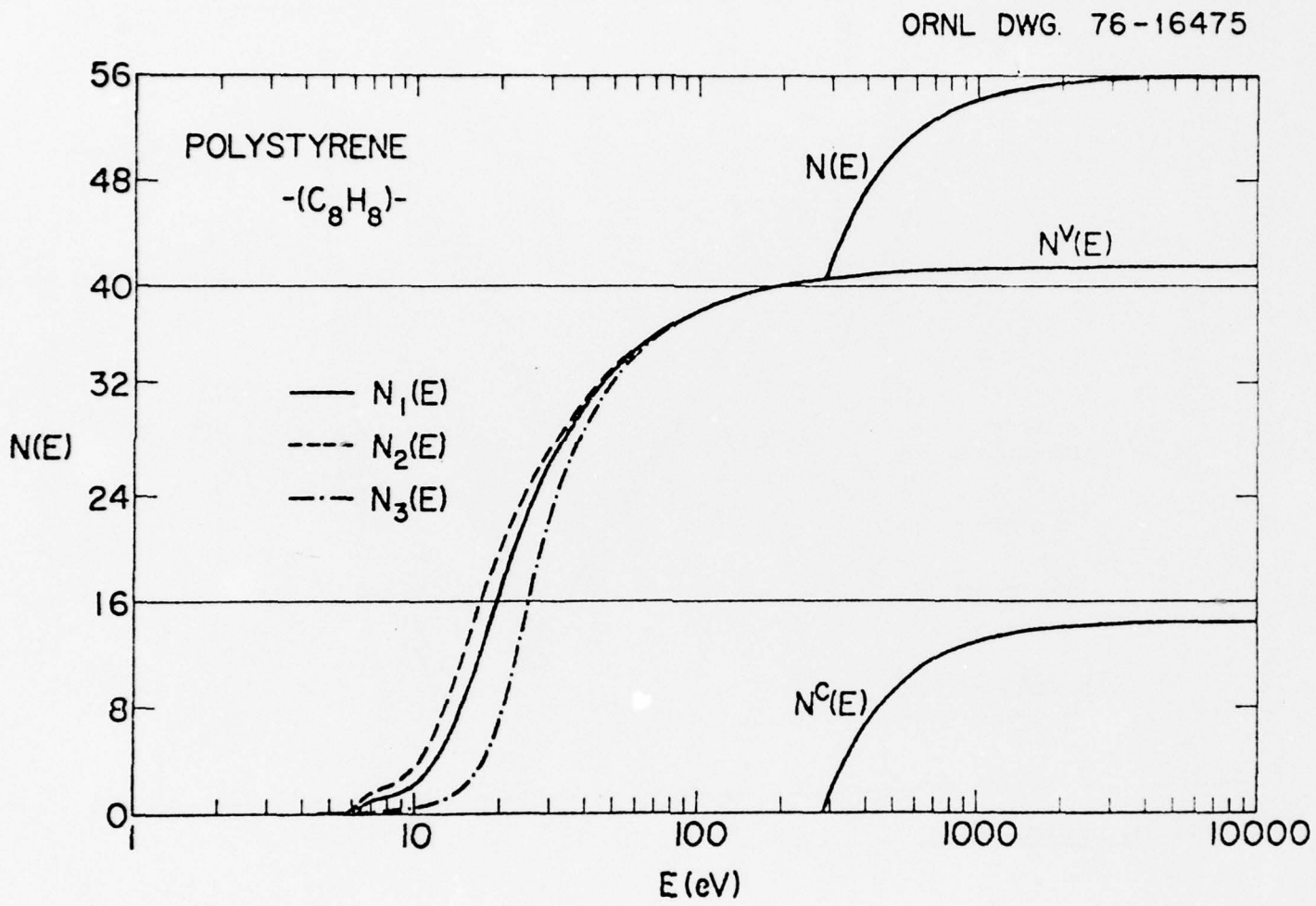

ORNL DWG. 76-16475
POLYSTYRENE
-(C8H8)-
N(E)
N^V(E)
N1(E)
N2(E)
N3(E)
N^C(E)
56
48
40
32
24
16
8
0
1
10
100
1000
10000
N(E)
E(eV)

FIGURE 9

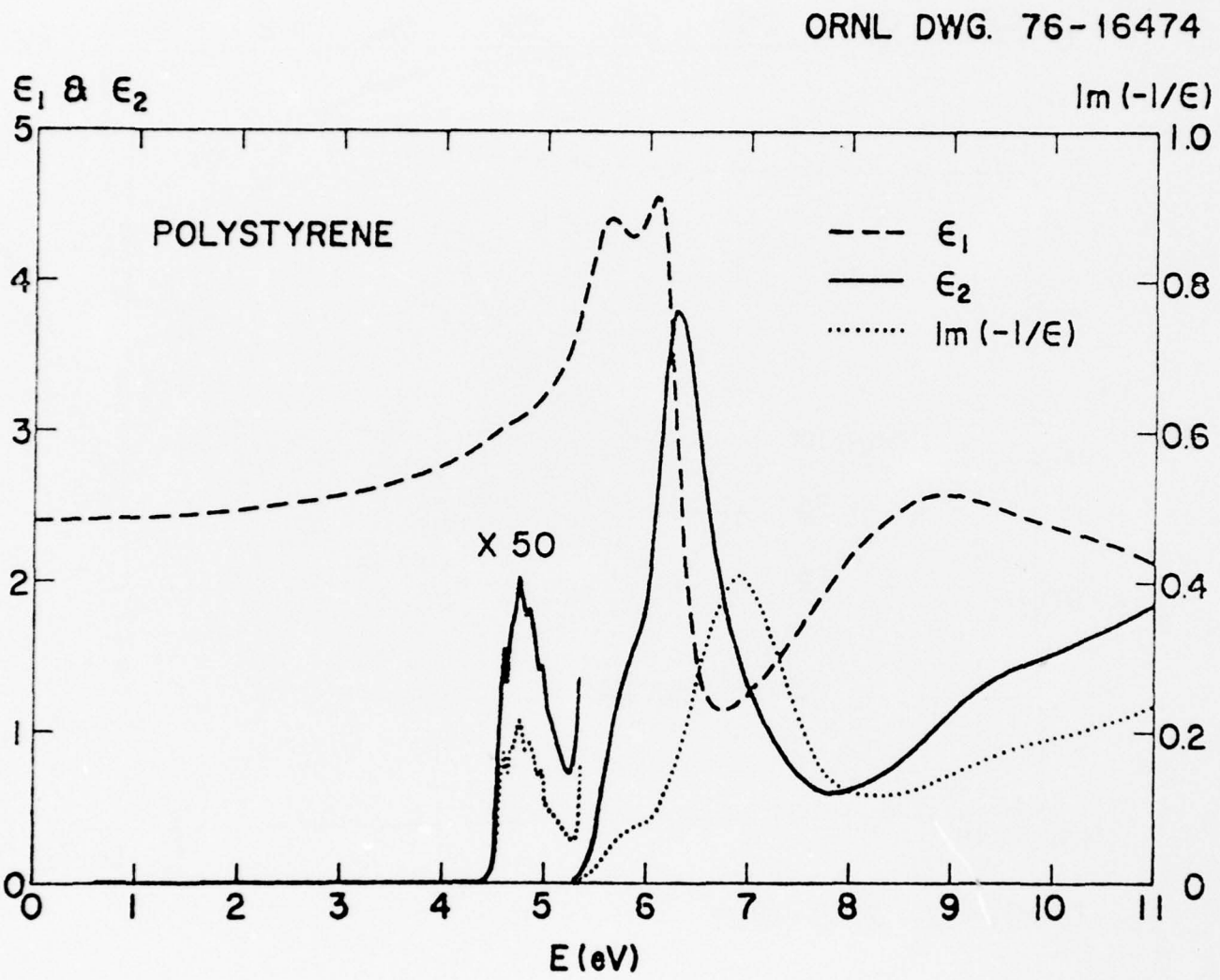
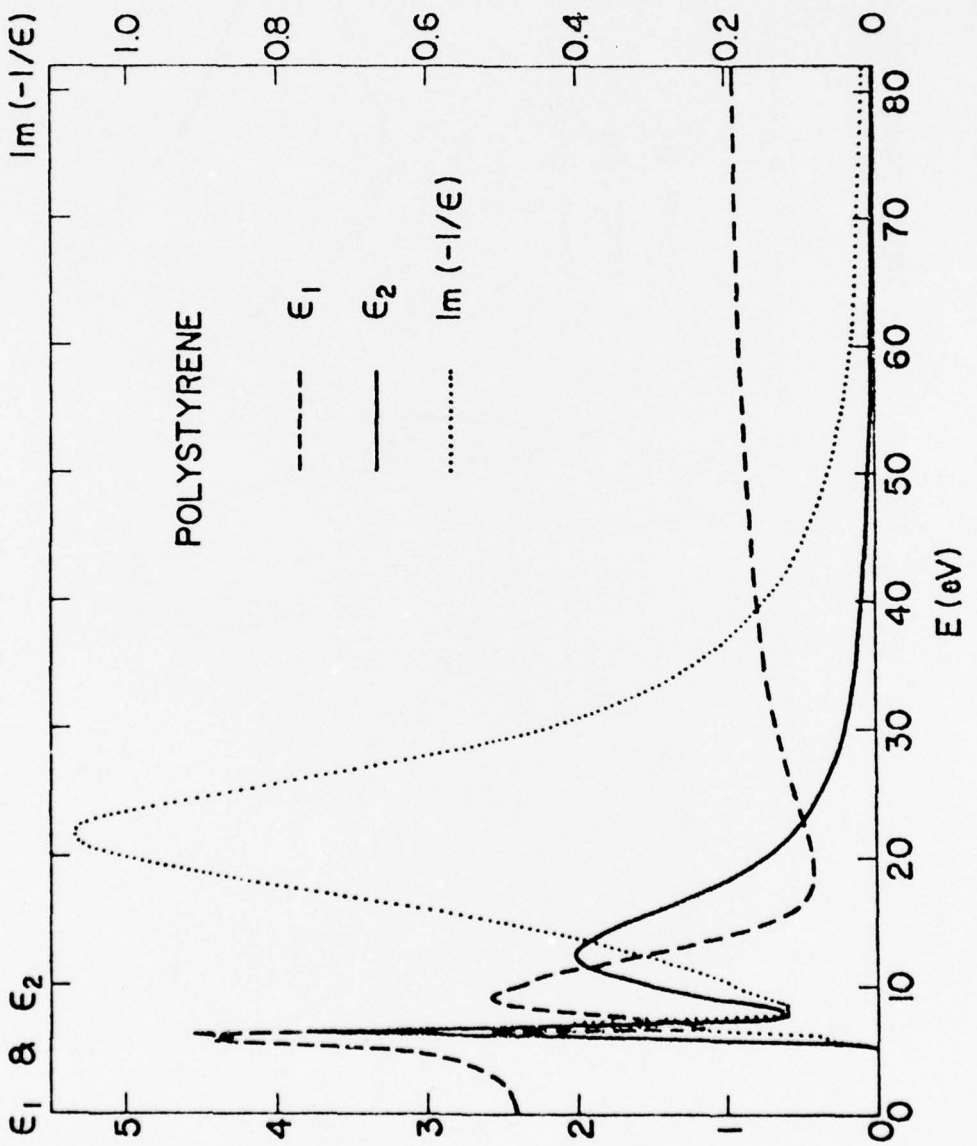

ORNL DWG. 76-16474
ε1 & ε2
Im (-1/ε)
POLYSTYRENE
ε1
ε2
Im (-1/ε)
X 50
E (eV)
0
1
2
3
4
5
6
7
8
9
10
11
0.2
0.4
0.6
0.8
1.0

FIGURE 10


ORNL DWG. 76-16473
POLYSTYRENE
ϵ_1
ϵ_2
Im (-1/ϵ)
ϵ_1 & ϵ_2
Im (-1/ϵ)
E (eV)
0
1
2
3
4
5
0
10
20
30
40
50
60
70
80
0
0.2
0.4
0.6
0.8
1.0

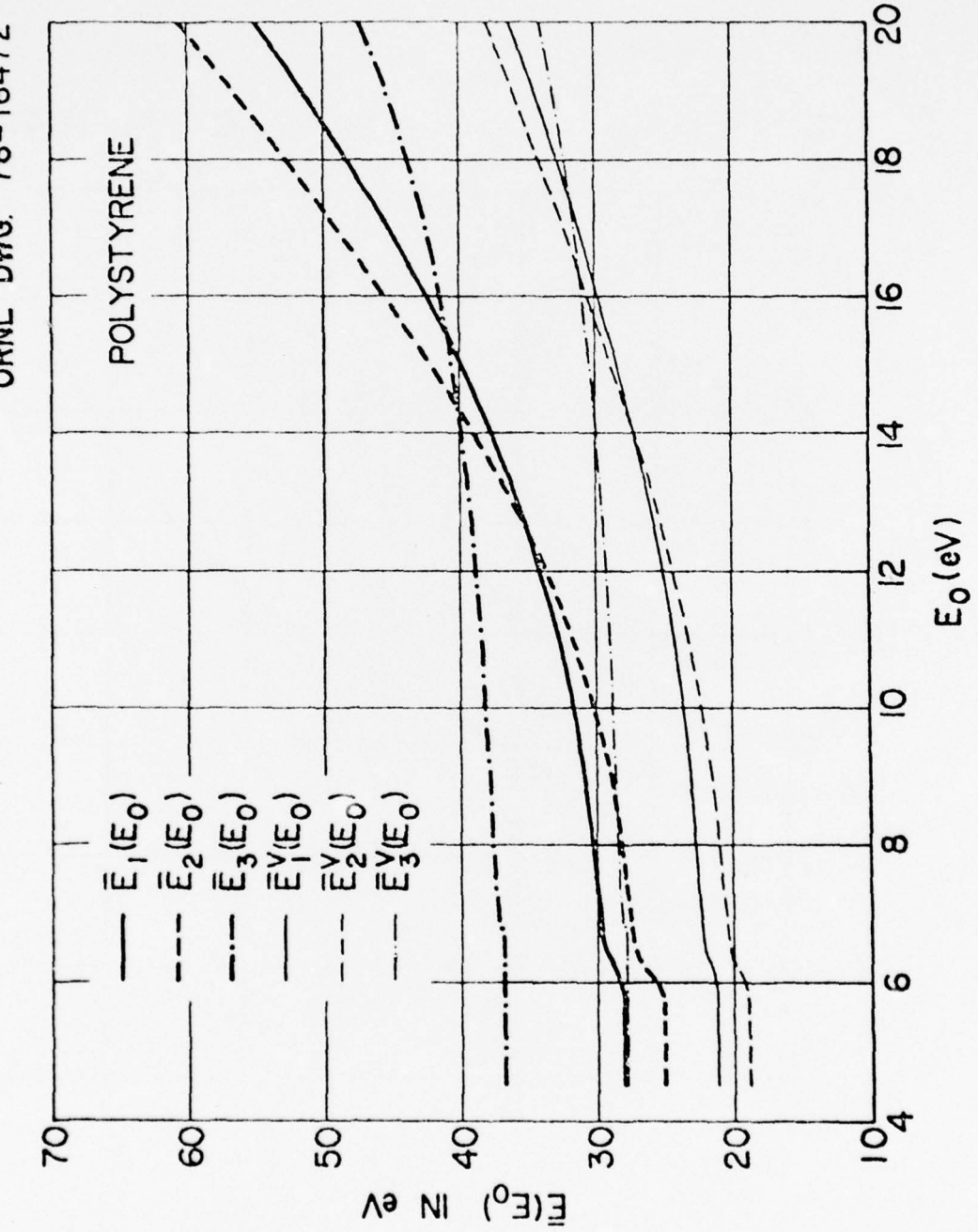
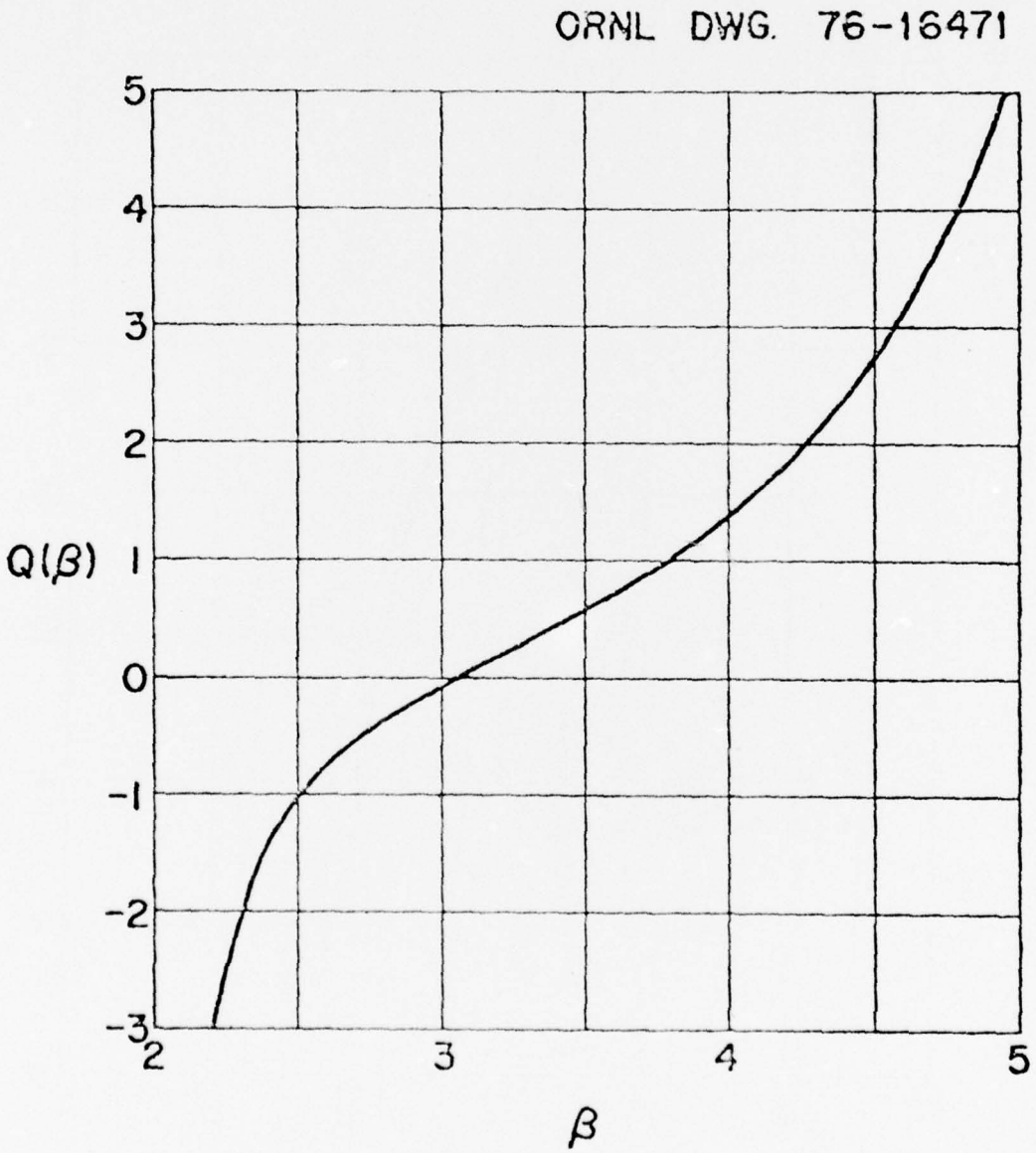

ORNL DWG. 76-16472
POLYSTYRENE
$\bar{E}_1(E_0)$
$\bar{E}_2(E_0)$
$\bar{E}_3(E_0)$
$\bar{E}^V_1(E_0)$
$\bar{E}^V_2(E_0)$
$\bar{E}^V_3(E_0)$
$E_1(E_0)$ IN eV
E_0 (eV)
70
60
50
40
30
20
10
4
6
8
10
12
14
16
18
20

FIGURE 11

FIGURE 12



APPENDIX G

Reprinted from: Health Physics Division Annual Progress Report
for Period Ending June 30, 1976, ORNL-5171, pp. 160-162.

ELECTRON ATTENUATION LENGTHS IN THE VACUUM ULTRAVIOLET AND SOFT X-RAY REGIONS[12]

Considerable time has been spent this year reviewing attempts, both by us[13] and by others as reported in the literature, to obtain electron attenuation lengths, L, from observations of photoelectron yield in the ultraviolet and soft x-ray regions. There is great theoretical and practical interest in the related quantities, the mean free path of electrons in the bulk of a solid and the escape depth, range, or attenuation length for electrons emitted across the surface. Observations on electrons with energies from a few electron volts above the Fermi energy to about 200 eV are of particular interest, as theories predict a variation with energy of the electron mean free path which has a minimum in the region of 50 to 100 eV for most materials. It is just this energy region which has been least studied and where, consequently, there are relatively few published values for electron mean free paths in solids. In the ultraviolet and soft x-ray regions, materials are either strongly or moderately absorbing over at least part of the energy range. At the same time, electron attenuation lengths, L, are short, $\lesssim 10$ Å, over much of the region. Measurement of these short attenuation lengths requires special techniques. Two methods frequently used to measure electron attenuation lengths are obviously not applicable in this case. Electron transmission measurements require homogeneous self-supporting thin films. For very short attenuation lengths, it would seem to be impossible to prepare such films which are sufficiently thin. The use of Auger electrons generated in a substrate to determine electron attenuation lengths in deposited overlayers is subject to a practical lower limit of about 200 eV for the electron energies available. It appeared that photoemission was a promising approach to obtaining L in this energy range.

Over the past several years, we have attempted to obtain electron attenuation lengths from observations of the total photoelectric yield, $Y(\theta)$, as a function of the photon angle of incidence, θ. Last year[13] we reported that a theoretical analysis showed large uncertainties in the L values calculated from our observation of $G(\theta)$ vs θ, where $G(\theta) = Y(\theta)/Y(0)$. These observations were for thick vapor-deposited carbon films over the range of photon energies from 20 to 64 eV, where L is known to be small. In fact, for any material, if L is about 10 Å or less, as is generally thought over the range of electron energies from about 10 eV to about 1000 eV, then to obtain L to ± 1 Å, $G(\theta)$, the extinction coefficient k, and the polarization P of the incident photons must each be known to about 1%. For our observations, both $G(\theta)$ and P are reproducible and can be obtained to ±1%. However, for materials which are moderately to strongly absorbing, a limit of error on k of ±1% is unattainable at this time. In attempting to calculate L from observations of $G(\theta)$ vs θ, inaccuracies may also result if the sample is not homogeneous with a clean, smooth, planar surface. In addition, there are still questions concerning the theory by which L is related to the measured $G(\theta)$ vs θ. Different theories yield significantly different L values for the same input data.[14] Finally, since the definition of L assumes homogeneous media and L may be considered a macroscopic quantity even if the experimental and theoretical problems are dealt with satisfactorily, there remains the philosophical question of the significance of L values that are calculated to be comparable with or less than the surface roughness of the sample.

It was thought that an alternative method of obtaining L from photoemission measurements would be analysis of $Y(t)$ vs the film thickness t. The range of film thickness required depends on the optical properties of the film and the value of L of the emitted electrons. For a strongly absorbing film and small L, the thicknesses available should range from $t < L$ to $t = \infty$. For weakly absorbing films, one does not need to have

12. Research sponsored in part by the Defense Nuclear Agency, under Subtask TA040, but does not reflect endorsement by the sponsor.

13. E. T. Arakawa et al., *Health Phys. Div. Annu. Prog. Rep. June 30, 1975*, ORNL-5046, pp. 125-28, and previous reports in this series.

14. K. L. Kliewer, preprint.

films with $t < L$, but small enough thicknesses should be used that the first, and strongest, structure in $Y(t)$ vs t is accurately specified. Furthermore, these films need to be homogeneous and continuous and to have smooth interfaces with the substrate and with vacuum in order for $Y(t)$ vs t to yield meaningful L values. A literature survey showed that using currently available techniques for making thin films, all films are discontinuous for t less than about 50 to 300 Å, the thickness at which continuity occurs depending on the method of preparation. In many cases, values of L calculated from observations on ultrathin films would be more dependent on the method of film preparation, and hence film structure, than on the basic electronic properties of the material of the film. Thus this method is generally unsuitable for the determination of L values in the uv and soft x-ray region. In view of this conclusion, some L values obtained by this method and published in the literature turn out to be meaningless, except insofar as they set upper bounds on the actual values of L.

Examination of variations of these two methods, such as $G(\theta)$ vs θ for thin films of known thickness, or the ratio of photoelectric yields for a thin film illuminated from the front and from the back through the substrate, as a function of film thickness, reveals that all methods for L involving photoelectric yield measurements appear subject to the same limitations when L is small and the material is moderately to strongly absorbing.

In conclusion, when the medium is strongly absorbing, techniques involving thick films must be used to determine L values. However, to obtain L to ±1 Å when L is less than about 10 Å requires that k be known to within ±1%. For strongly absorbing materials in the energy range of interest, k cannot presently be measured to this accuracy. Thus L cannot be obtained with any meaningful degree of accuracy. When the medium is weakly absorbing and L is short, both thick- and thin-film techniques can be used, but data should be interpreted with great care. Films should not be employed that are so thin that they are not continuous. Effective L values calculated from observations on such films are dependent on film structure and hence are not characteristic of the material. When effective L values can be obtained by a method employing thin films that are thick enough to be continuous and homogeneous, they should be corrected for size effects so that the electron attenuation lengths obtained correspond to those for electrons escaping across a planar interface between the semi-infinite medium and vacuum. Using currently developed experimental techniques, for weakly absorbing material L values can be obtained, but it is extremely difficult to get values accurate to even ±10% by any photoemission technique. Finally, especially for short attenuation lengths, the theories of photoemission employed in their derivation need to be refined.

PHOTOEMISSION FROM THICK SAMPLES[12]

Although, as described in the preceding section, observations of $G(\theta)$ vs θ from a thick sample cannot be analyzed for electron attenuation lengths when the sample is strongly absorbing, the relative yields for a given photon energy are found to be characteristic of the material. Generally, $G(\theta)$ vs θ is reproducible to ±1% and is relatively insensitive to surface conditions. These data, currently unavailable in the open literature, are of practical interest in the development of improved photoemitters in the vacuum ultraviolet and soft x-ray regions. Over the past several years we have obtained observations of $G(\theta)$ vs θ for insulators such as polystyrene and amorphous carbon, semiconductors such as silicon, and metals such as gold and aluminum at selected energies in the range of photon energies from about 20 to about 80 eV.

Representative data for carbon have been presented previously.[15] Representative data for insulators, semiconductors, and metals are given in Figs. 29.3–29.5. As

15. E. T. Arakawa et al., *Health Phys. Div. Annu. Prog. Rep. July 31, 1974*, ORNL-4979, pp. 128–29.

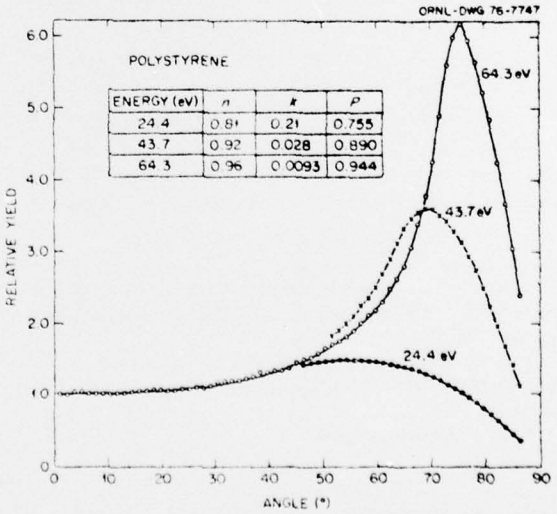


Fig. 29.3. Relative photoyield vs angle of incidence for three different energies of photons on polystyrene.

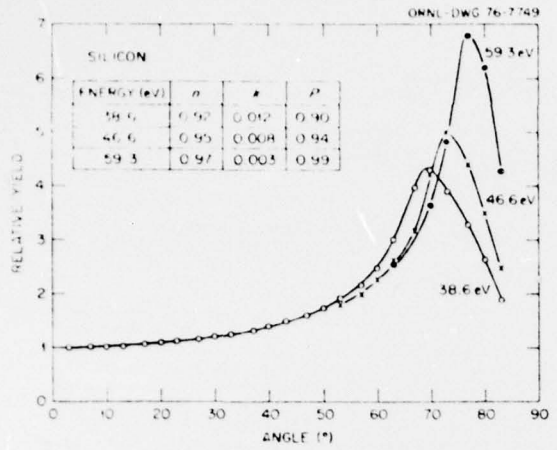


Fig. 29.4. Relative photoyield vs angle of incidence for three different energies of photons on silicon.

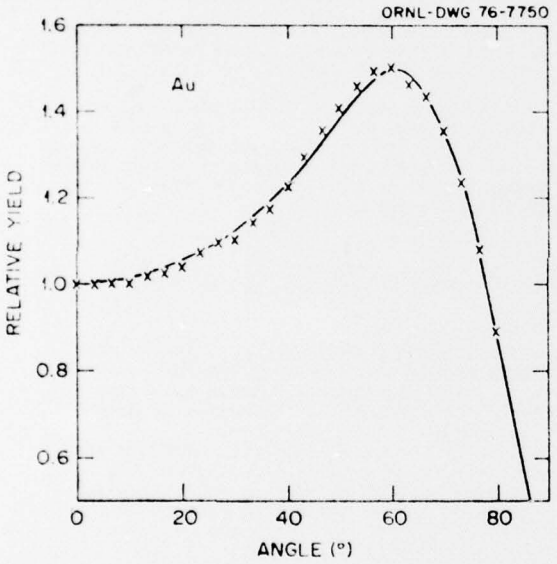


Fig. 29.5. Relative photoyield vs angle of incidence for 39-eV photons on gold. At 39 eV, the optical functions of gold are n = 0.77 and k = 0.41. The polarization was P = 0.87.

expected,[13] the characteristics of $G(\theta)$ vs θ are dependent in each case at any given energy on the optical functions, n and k, of the material at that energy and the polarization of the incident light. The refractive index, n, determines the position of the maximum in $G(\theta)$ by the relationship $n \cong \sin \theta_m$, while the extinction coefficient, k, and electron attenuation length, L, determine the magnitude of $G(\theta_m)$. Since for all the data presented it is believed that L is small and for any practical interpretation cannot vary by more than a factor of 10, the magnitude of $G(\theta_m)$ is seen to be dominated by the value of k.

In view of the conclusion reached in the previous section, namely, that our $G(\theta)$ vs θ data in the region from 20 to 80 eV cannot be analyzed at the present time to yield meaningful L values, all of our accumulated $G(\theta)$ vs θ data are currently being prepared for publication without attempting to obtain the associated L values.

APPENDIX H

To Be Published in IEEE Trans. Nucl. Sci., December 1976.

CALCULATIONS OF MEAN FREE PATHS AND STOPPING POWERS OF LOW ENERGY ELECTRONS (≤ 10 keV) IN SOLIDS USING A STATISTICAL MODEL*

J. C. Ashley, C. J. Tung†, R. H. Ritchie, and V. E. Anderson‡
Health Physics Division, Oak Ridge National Laboratory
Oak Ridge, Tennessee 37830

Abstract

A statistical model is described and employed to calculate inverse mean free paths and stopping powers for electrons of energies from a few eV to 10 keV above the Fermi level in Al, Si, Ni, Cu, Ag, and Au. Brief tables of mean free paths and stopping powers for these solids are presented. In some cases graphical displays of inverse mean free paths and stopping powers are also included. The calculations based on this model are discussed and compared with previous work.

I. Introduction

A quantitative description of the interaction of electrons with matter over a large range of energies is a subject of basic importance in a wide variety of theoretical and applied areas. From the theoretical standpoint, calculations of energy loss and range of electrons in many different materials have formed the basis of at least two extensive tabulations.[1,2] Both of these works are restricted to electron energies ≥ 10 keV and are based on the Bethe theory of stopping power including various modifications and corrections (e.g. density-effect corrections). We feel that calculations of mean free paths, energy loss, etc. for electrons of energy ≤ 10 keV, based on the best currently available theoretical models, will provide useful guides for interpretation of experimental data as well as input for calculations in applied areas.

Earlier tabulations of inverse mean free paths, stopping powers, CSDA ranges, and straggling for Al and Al_2O_3 [3], and Si and SiO_2 [4] involved the use of various models to describe the extended electron states of a solid (valence band or conduction band), and theoretical calculations of atomic, generalized oscillator strengths (GOS's)[5] to describe excitation of electrons from the inner shells of the atoms in the solids. Where detailed, a priori GOS calculations such as in Ref. 5 are not available, one must depend on calculations based on classical binary collision cross sections, hydrogenic wavefunctions, etc. to approximate the excitation of the inner-shell electrons. Although the inner shells are not very important in calculations of inverse mean free paths of electrons for energies <10 keV, the inner-shell electrons do contribute significantly to the stopping power for incident electron energies ≳500 eV.[3,4,6]

Instead of dividing the electrons in the solid into two distinct groups (e.g. inner-shell and valence band) we will present here an alternative approach in which the response of all of the electrons in the solid are treated in a comprehensive manner within the framework of a single model. A model that has been developed for this purpose is the "electron gas statistical model", or "statistical model" for brevity.

*This research was sponsored in part by the Defense Nuclear Agency under subtask TA040 and in part by the Energy Research and Development Administration under contract with Union Carbide Nuclear Corporation.
†Postdoctoral Fellow, University of Tennessee, Knoxville Tennessee 37919
‡Computer Sciences Division, Oak Ridge National Laboratory, Oak Ridge, Tennessee 37830

II. Electron Gas Statistical Model

A. General Theory

A charged particle passing through a solid interacts with a large number of electrons simultaneously and it is thus appropriate to speak of a mean free path of the charged particle against energy loss to the solid. Assuming the effect of the charged particle on the medium may be treated in first Born approximation, the inverse mean free path differential in momentum transfer, $\hbar k$, and energy transfer, $\hbar\omega$, for a particle of velocity v is given by

$$\frac{d^2\mu}{dk\,d\omega} = \frac{2e^2}{\pi\hbar v^2}\,\frac{1}{k}\,\mathrm{Im}\left[\frac{-1}{\epsilon(k,\omega)}\right] \qquad (1)$$

where $\epsilon(k,\omega)$ is the exact dielectric response function of the solid.[7,8] We assume in this work that the solid is isotropic and homogeneous.

For our calculations of inverse mean free paths and stopping powers, it is sufficient to compute inverse mean free paths differential in energy transfer only. This differential inverse mean free path (DIMFP) for energy loss $\hbar\omega$ by an electron with energy $E = mv^2/2$ in the solid is given by

$$\tau(E,\hbar\omega) = \frac{d\mu}{d(\hbar\omega)} = \frac{1}{\pi a_0 E}\int_{k_-}^{k_+}\frac{dk}{k}\,\mathrm{Im}\left[\frac{-1}{\epsilon(k,\omega)}\right] \qquad (2)$$

where $\hbar k_\pm = \sqrt{2m}\,[\sqrt{E} \pm \sqrt{E-\hbar\omega}]$ and $a_0 = \hbar^2/me^2$. This expression assumes that the energy-momentum relation for a swift electron in the solid does not differ appreciably from that of a free electron in vacuum.

Given $\epsilon(k,\omega)$ for the solid, the quantities of interest here follow directly from $\tau(E,\hbar\omega)$. The inverse mean free path of the electron, μ, is given by integrating over allowed energy transfers as

$$\mu(E) = \int d(\hbar\omega)\;\tau(E,\hbar\omega). \qquad (3)$$

The rate of energy loss of the electron, or the stopping power of the medium, is given by

$$S(E) = dE/dx = \int d(\hbar\omega)\;\hbar\omega\;\tau\;(E,\hbar\omega). \qquad (4)$$

Since exact dielectric response functions for solids are not available, various models and approximations must be employed to calculate quantities which may be compared with experimental measurements. For example, the electron gas model[7,8] for the response of the conduction-band electrons in metals has been used quite widely. The uniform electron density assumed in this model leads to results in many cases which agree quite well with experiment. In the case of aluminum, for example, calculations of electron inelastic mean free paths yield excellent agreement with experiment.[9] The model which is used here, the electron gas statis-

tical model, incorporates the relative simplicity of the electron gas model but is applicable to a larger class of materials. Such a statistical approach, pioneered by Jens Lindhard, has met with considerable success when applied to the calculation of charged-particle energy loss in many different materials.[10] Basically the approach involves the assumption that the stopping medium is characterized by a space-varying density of electrons, $n(\vec{r})$, and that the contribution of those electrons in a small volume element d^3r at $\vec{r}$ to the stopping process is the same as the same number of free electrons in an electron gas at the same density. The total stopping power, for example, is then computed by averaging over the $n(\vec{r})$ distribution appropriate to a given medium. The contribution of the inner-shell electrons to the electron energy loss is included in a statistical fashion in the averaging process.

The DIMFP for an electron gas of uniform density n, $\tau(E,\hbar\omega,n)$, is calculated from Eq. (2) and used to evaluate $\mu(E,n)$ and $S(E,n)$. These quantities are calculated for a large number of values of n for use in the average over the $n(\vec{r})$ distribution. The inverse mean free path $\langle\mu(E)\rangle$ and stopping power $\langle S(E)\rangle$ calculated on the basis of this statistical model are obtained from

$$\langle\mu(E)\rangle \equiv \int d^3r\ \mu(E,n(\vec{r}))\ /\ \int d^3r \qquad (5)$$

and

$$\langle S(E)\rangle \equiv \int d^3r\ S(E,n(\vec{r}))\ /\ \int d^3r \qquad (6)$$

where the integration is carried out over some appropriate volume of the solid. The electron gas model will be discussed briefly in Part B, and the spherically symmetric electron density distributions n(r) calculated in a Wigner-Seitz cell using a relativistic Hartree-Fock method, which were used to evaluate the averages indicated in Eqs. (5) and (6), will be described briefly in Part C.

B. Electron Gas of Uniform Density

The dielectric response function of a uniform density electron gas in the form derived by Lindhard[7] has been used extensively. The equation for $\varepsilon(k,\omega)$ can be found in Reference 7 and will not be repeated here. Instead we present graphically an example of the results of calculations required for the averages indicated in Eqs. (5) and (6). In Figure 1 we show the stopping power in atomic units as a function of incident electron energy for electron gases of several uniform densities. The curves are labeled by the "one electron radius" r_s which is related to the uniform density n by $1/n \equiv 4\pi a_0^3 r_s^3/3$ where $a_0 \equiv \hbar^2/me^2 = 0.529$ Å. The stopping power in atomic units may be converted to units of eV/Å by multiplying by 27.2/0.529 = 51.4. Similar calculations have been carried out for μ. The limits on the integrations in Eqs. (3) and (4) for these calculations are given by $0 \leq \hbar\omega \leq E-E_F(n)$, where $E_F(n)$ is the Fermi energy for the uniform electron density n. In terms of the "one electron radius", the Fermi energy is given by $E_F = (e^2/2a_0)\ (9\pi/4)^{2/3}\ r_s^{-2}$.

C. Calculation of n(r)

For the calculation of electron density as a function of position in the solid we have used an existing computer program which employs relativistic self-consistent-field calculations[11] to evaluate the spherically symmetric electron density n(r) in a Wigner-Seitz sphere around an atomic nucleus. As an example of this type of calculation we show in Figure 2 the

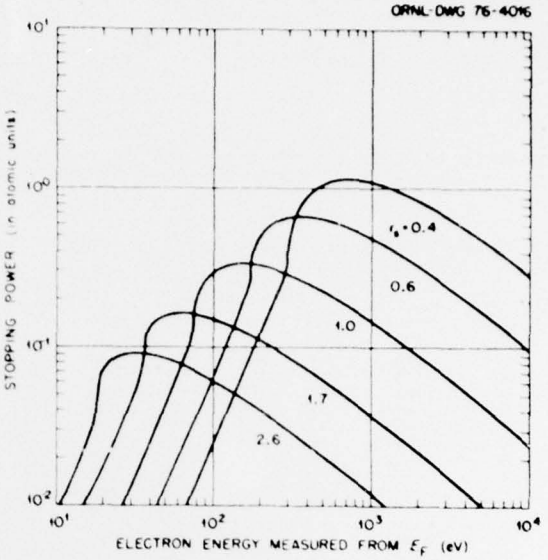


Fig. 1 Stopping power of an electron gas for several values of uniform, electron gas density as a function of incident electron energy.

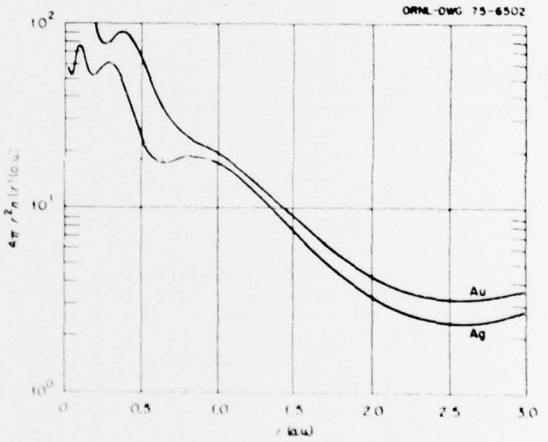


Fig. 2 Electron densities in Au and Ag computed by a relativistic Hartree-Fock procedure using the Wigner-Seitz boundary condition.

density $4\pi r^2 n(r)$ as a function of r for Ag and Au. These densities represent, approximately, the number of electrons per unit radius of a spherical shell of radius r centered about each nucleus in the respective solids. Atomic units are used here, e.g., all lengths are expressed in units of a_0. Given these computed electron densities, the inverse mean free path and stopping power are calculated at fixed values of E from

$$\langle\mu(E)\rangle = \int_0^{r_{WS}} dr\ r^2\ \mu(E,n(r))\ /\ \int_0^{r_{WS}} dr\ r^2 \qquad (7)$$

and

$$-S(E) = \int_0^{r_{WS}} dr\, r^2\, S(E,n(r)) \Big/ \int_0^{r_{WS}} dr\, r^2 \quad (8)$$

In Table I we present the mean free paths $1/\sigma_{in}$ of electrons in the six solids Al, Si, Ni, Cu, Ag, and Au as calculated from Eq. (7) using the statistical model.

Table I

Inelastic mean free paths of electrons in six solids calculated using a statistical model.

Electron energy above Fermi energy (eV)	Mean free path, $1/\sigma_{in}$ (Å)					
	Aluminum	Silicon	Nickel	Copper	Silver	Gold
10	25.9	25.0	46.6	36.5	32.6	40.8
15	15.0	14.5	26.5	20.9	18.8	23.3
20	10.1	9.30	18.0	14.5	12.4	16.1
30	4.13	4.19	10.3	6.48	5.51	7.58
40	3.57	3.57	5.15	4.47	4.40	4.88
60	3.68	3.66	4.04	4.02	4.10	4.18
80	4.03	4.02	4.02	4.14	4.25	4.20
100	4.44	4.44	4.20	4.39	4.51	4.39
150	5.50	5.51	4.82	5.11	5.24	5.00
200	6.51	6.56	5.44	5.82	5.93	5.61
300	8.46	8.57	6.72	7.26	7.35	6.90
400	10.3	10.5	7.89	8.53	8.65	8.10
600	13.8	14.1	10.2	11.1	11.2	10.5
800	17.1	17.5	12.4	13.4	13.7	12.7
1,000	20.2	20.7	14.4	15.6	16.0	14.8
2,000	35.0	36.0	24.1	26.1	27.0	24.5
4,000	62.2	64.1	41.9	45.5	46.7	42.1
6,000	87.6	90.5	58.5	63.5	65.1	58.5
8,000	112	116	74.3	80.7	82.8	74.3
10,000	136	140	89.7	97.4	99.9	89.6

Table II presents the stopping powers for the same six materials included in Table I for incident electron energies from 10 eV to 10 keV, as calculated from Eq. (8).

Table II

Stopping powers of six solids for electrons calculated using a statistical model.

Electron energy above Fermi energy (eV)	Stopping power (eV/Å)					
	Aluminum	Silicon	Nickel	Copper	Silver	Gold
10	0.248	0.257	0.138	0.176	0.197	0.158
15	0.648	0.668	0.363	0.463	0.517	0.415
20	1.31	1.45	0.719	0.892	1.06	0.802
30	4.80	4.60	1.90	3.10	3.56	2.64
40	6.06	6.00	5.07	5.32	5.09	4.99
60	6.41	6.44	7.66	6.87	6.39	6.89
80	6.19	6.18	8.40	7.36	6.90	7.67
100	5.86	5.82	8.57	7.45	7.04	7.94
150	5.15	5.03	8.44	7.31	7.08	8.08
200	4.69	4.50	8.33	7.24	7.20	8.20
300	4.02	3.76	7.82	6.84	6.91	7.79
400	3.64	3.35	7.59	6.69	6.72	7.51
600	3.03	2.73	6.89	5.97	5.87	6.59
800	2.63	2.36	6.01	5.42	5.19	5.93
1,000	2.44	2.19	5.72	5.27	4.82	5.74
2,000	1.64	1.48	4.05	3.80	3.44	4.37
4,000	0.998	0.891	2.64	2.47	2.43	3.27
6,000	0.736	0.657	1.98	1.86	1.84	2.51
8,000	0.590	0.526	1.60	1.50	1.49	2.05
10,000	0.495	0.442	1.35	1.27	1.26	1.75

III. Comparisons With Other Calculations

As an initial test of the model described here we compared the mean free paths and stopping powers calculated for Al and Si with our earlier tabulated results.[3,4] For the mean free paths we find the predictions of the statistical model to be ≲10% smaller than our earlier more detailed calculations in the energy region 100 eV to 10^4 eV. More specifically the electron mean free paths in Si are ≲3% less than the values predicted from Ref. 4 for 60 eV ≤E≤ 10^4 eV, while for Al we find electron mean free paths ≲5% less than the values predicted from Ref. 3 for 300 eV ≤E≤ 10^4 eV. For energies ≲ 100 eV, larger differences are found as we go to lower energies. At E = 10 eV, the results here are ≲50% of our earlier results.[3,4] This difference is due principally to the neglect of exchange effects between the incident electron and electrons of the medium in the statistical model. For the stopping power, the statistical model predictions are ≲20% larger than our earlier results for 100 eV ≤E≤ 10^4 eV with larger differences occuring for E<100 eV, again due to neglect of exchange effects. A comparison with our earlier, published results for the stopping power of Al not including exchange effects[6] shows agreement to within ≲10% for the broad energy range 10 eV to 10^4 eV.

We show in Figures 3-5 the stopping power of Au, Ag, Cu, and Ni calculated from the statistical model; results from Bethe-Bloch theory[2] are shown for E>10^4eV.

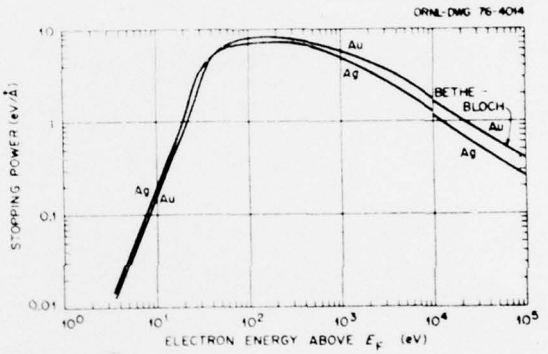


Fig. 3 Stopping power of Au and Ag for electrons calculated using a statistical model.

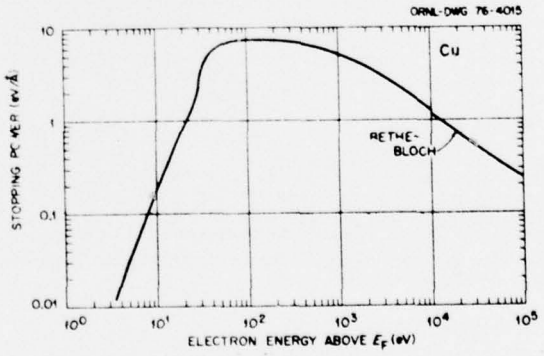


Fig. 4 Stopping power of Cu for electrons calculated using a statistical model.

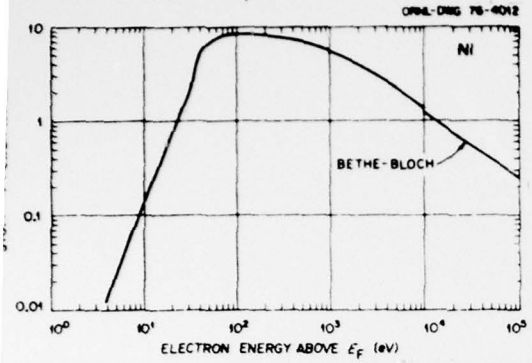


Fig.5 Stopping power of Ni for electrons calculated using a statistical model.

or these four solids the stopping powers calculated on he basis of the statistical model agree with the predictions of Bethe-Bloch theory[2] to better than 10% at =10 keV; (Ni, 9% larger; Cu and Ag, 8% larger; Au, 4% arger).

For the energy range 200 eV $\leq E \leq$2000 eV, mean free aths have been calculated by Penn[12] using an electron as model including exchange and correlation effects in n approximate way, and with approximate corrections for inner-shell contributions. The best agreement with the statistical model calculations is found for Al where Penn's results are 5% smaller at E=200 eV, with the difference decreasing to a constant value of ~3% for E≥1000 eV. For Si, Penn's mean free path is 12% smaller at E=200 eV and ~8% smaller for E≥600 eV. For the other solids, for the same energy range, Penn's results are smaller than ours by ~20% for Ni, Au, and Ag, and ~30% for Cu. We display in Figures 6 and 7 the results of our statistical model calculations for the inverse mean free path of electrons in Cu and Ni.

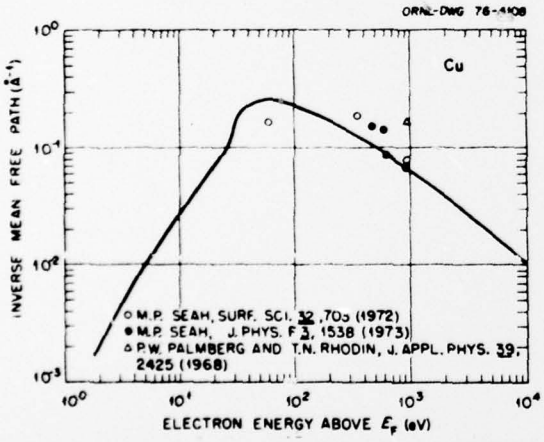


Fig. 6 Inverse mean free path of electrons in Cu calculated using a statistical model. Experimental measurements of attenuation length were taken from the references shown in the figure.

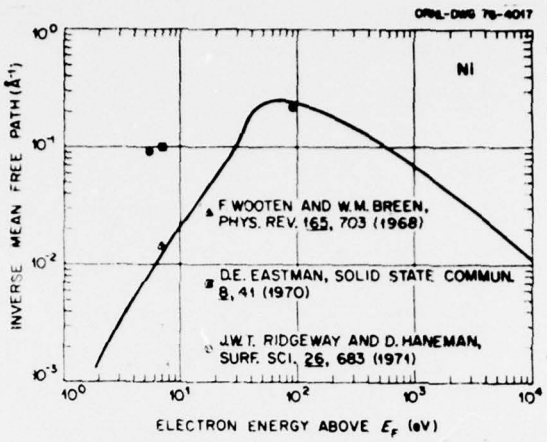


Fig. 7 Inverse mean free path of electrons in Ni calculated using a statistical model. Experimental measurements of attenuation length were taken from the references shown in the figure.

Also shown are experimental measurements of attenuation lengths taken from the references indicated on the figures.

IV. Conclusions

We have described a statistical model which may be used with some confidence to calculate mean free paths and stopping powers for elemental solids where more detailed calculations, as e.g. in References 3 and 4, are unavailable. For the region of electron energies $\lesssim 10^4$ eV, reliable determinations of such electron interaction parameters are important for studies of low energy electron diffraction, electron transport, etc. A more extensive tabulation, including ranges and straggling, for this energy region for Ni, Cu, Ag, and Au is available.[13]

V. Acknowledgement

The authors are grateful for continuing advice and assistance from E. A. Burke and J. N. Bradford in connection with this work.

References

1. M. J. Berger and S. M. Seltzer in "Studies in Penetration of Charged Particles in Matter" (National Academy of Sciences-National Research Council, Washington, D.C., 1964. Publ. No. 1133) pp. 205-268.

2. L. Pages et al., Atomic Data 4, 1-127 (1972).

3. J. C. Ashley, C. J. Tung, V. E. Anderson, and R. H. Ritchie, "Inverse Mean Free Path, Stopping Power, CSDA Range, and Straggling in Aluminum and Aluminum Oxide for Electrons of Energy ≤10 keV," AFCRL-TR-75-0583 (December 1975).

4. C. J. Tung, J. C. Ashley, V. E. Anderson, and R. H. Ritchie, "Inverse Mean Free Path, Stopping Power, CSDA Range, and Straggling in Silicon and Silicon Dioxide for Electrons of Energy ≤10 keV," RADC-TR-76-125 (April 1976).

5. S. T. Manson, Phys. Rev. A6, 1013-1024 (1972); S. T. Manson (private communication).

6. J. C. Ashley, C. J. Tung, and R. H. Ritchie, IEEE Trans. Nucl. Sci. NS-22, 2533-2536 (1975).

7. J. Lindhard, K. Dan. Vidensk. Selsk. Mat.-Fys. Medd. 28, No. 8, 1-57 (1954).

8. R. H. Ritchie, Phys. Rev. 114, 644-654 (1959).

9. R. H. Ritchie, et al., Rad. Res. 64, 181-204 (1975); C. J. Powell, Surf. Sci. 44, 29-46 (1974).

10. J. Lindhard, M. Scharff, and H. E. Schiøtt, K. Dan. Vidensk. Selsk. Mat.-Fys. Medd. 33, No. 14 (1963); E. Bonderup, K. Dan. Vidensk. Selsk. Mat.-Fys. Medd. 35, No. 17 (1967); E. Bonderup and P. Hvelplund, Phys. Rev. A4, 562-569 (1971).

11. T. C. Tucker, et al., Phys. Rev. 178, 998-1108 (1969); Phys. Rev. 174, 118-124 (1968).

12. D. R. Penn, Phys. Rev. B 13, 5248-5254 (1976); J. Electron Spectrosc. 9, 29-40 (1976).

13. J. C. Ashley, C. J. Tung, R. H. Ritchie, and V. E. Anderson, "Inverse Mean Free Path, Stopping Power, CSDA Range, and Straggling in Ni, Cu, Ag, and Au for Electrons of Energy <10 keV Calculated From a Statistical Model", RADC-TR-76-220 (June 1976).

DEPARTMENT OF DEFENSE

Director
Armed Forces Radiobiology Research Institute
Defense Nuclear Agency
National Naval Medical Center
Bethesda, MD 20014

Defense Documentation Center
Cameron Station
Alexandria, VA 22314
Attn: TC (12 cys)

Director
Defense Nuclear Agency
Washington DC 20305
Attn: RAEV
Attn: STTL, Tech Library (3 cys)
Attn: DDST
Attn: DDST, Peter H. Haas
Attn: RATN
Attn: STVL
Attn: STSI

DEPARTMENT OF THE ARMY

Director
Ballistic Missile Defense Advanced Technical Center
Huntsville Office
P.O. Box 1500
Huntsville AL 35807
Attn: RDMH-O, F. M. Hoke

Commander
Harry Diamond Laboratories
2800 Powder Mill Road
Adelphi MD 20783
Attn: AMXDO-RBG, Robert E. McCoskey
Attn: AMXDO-RB, Edward E. Conrad
Attn: AMXDO-RBF, John E. Thompkins
Attn: AMXDO-RBI, John A. Rosado
Attn: AMXDO-RC, Robert B. Oswald, Jr.
Attn: AMXDO-RDH, Paul A. Caldell
Attn: George Merkel

Director
US Army Ballistic Research Labs
Aberdeen Proving Ground MD 21005
Attn: AMXBR-RL, Mr. Harrison
Attn: AMXRD-BRD, Dr. Eccleshall

Commander
US Army Electronics Command
Fort Monmouth NJ 07703
Attn: AMSEL-NL-D
Attn: AMSEL-TN-N, Dr. E. Both
Attn: AMSEL-WL-D

Commander
US Army Nuclear Agency
Fort Bliss TX 79916
Attn: ATCN-W, LTC Leonard A. Slaga

DEPARTMENT OF THE NAVY

Chief of Naval Research
Department of the Navy
Arlington VA 22217
Attn: Code 422

Commander
Naval Electronics Laboratory Center
San Diego CA 92152
Attn: Code 3200, H. F. Wong
Attn: Code 3100, E. E. McCown

Superintendent
Naval Postgraduate School
Monterey CA 93940
Attn: Code 2124 Tech Rpts Library

Director
Naval Research Laboratory
Washington DC 20375
Attn: Code 5210, John E. Davey
Attn: Code 4004, Emanual L. Brancato
Attn: Code 5216, Harold L. Hughes
Attn: Code 6460, Dean L. Mitchell
Attn: Code 6631, James C. Ritter
Attn: Code 6603F, Richard L. Statler

Commander
Naval Surface Weapons Center
White Oak, Silver Spring, MD 20910
Attn: Code 730, Technical Library
Attn: Code 431, John H. Malloy

Director
Strategic Systems Project Office
Navy Department
Washington DC 20376
Attn: NSP-2342, Richard L. Coleman
Attn: NSP-230, David Gold
Attn: NSP-27331, Phil Spector

DEPARTMENT OF THE AIR FORCE

Hanscom AFB MA 01731
Attn: RADC/ETSD, R. P. Dolan
Attn: RADC/ETSD, F. D. Shepherd
Attn: RADC/ETSR, E. A. Burke
Attn: AFGL/SURRP (13 copies)
Attn: AFGL/SURRA (5 copies)
Attn: AFGL/SUOLA S29 (2 copies)
Attn: RADC/ETO/E. Cormier
Attn: RADC/ETSR/C. McCartney (5 cys)

Air Force Institute of Technology, AU
Wright-Patterson AFB OH 45433
Attn: ENP, Charles J. Bridgeman

Air Force Weapons Laboratory (AFSC)
Kirtland AFB NM 87117
Attn: ELP, TREE Section
Attn: SAA
Attn: SAY

SAMSO
P.O. Box 92960
Worldway Postal Center
Los Angeles CA 90009
Attn: DYS, Maj Larry A. Darda
Attn: DYS, Maj Heilman
Attn: DYS, Capt W. Mercer
Attn: RSSE, Ltc Kenneth L. Gilbert
Attn: RSE
Attn: XRS

SAMSO
Norton AFB CA 92409
Attn: MNNH, Capt William M. Carra
Attn: MNNH, Capt Saleh

UNITED STATES ENERGY RESEARCH AND DEVELOPMENT ADMINISTRATION

Los Alamos Scientific Laboratory
P.O. Box 1663
Los Alamos NM 87545
Attn: Doc Con for Donald R. Westervelt

Sandia Laboratories
Livermore Laboratory
P.O. Box 969
Livermore CA 94550
Attn: Doc Con for Kenneth A. Mitchell, 8157
Attn: Doc Con for J. A. Mogford, 8111
Attn: Doc Con for Theodore A. Dellin
Attn: Doc Con for Kenneth W. Dolan

Sandia Laboratories
P.O. Box 5800
Albuquerque NM 87115
Attn: Doc Con for J. V. Walker, 5620
Attn: Doc Con for D. F. Hartman
Attn: Doc Con for F. N. Coppage, 1830
Attn: Doc Con for J. A. Hood, 2110
Attn: Doc Con for C. N. Vittitoe, 5223
Attn: Doc Con for J. E. Gover, 1935
Attn: Doc Con for C. J. MacCallum

University of California
Lawrence Livermore Laboratory
P.O. Box 808
Livermore CA 94550
Attn: Walter W. Hofer, L-153
Attn: William J. Hogan, L-531
Attn: Leroy M. Erickson, L-24
Attn: Hans Kruger, L-94

OTHER GOVERNMENT

Department of Commerce
National Bureau of Standards
Washington DC 20234
Attn: Robert C. Placious, Appl Rad Div
Attn: Judson C. French

NASA
600 Independence Avenue SW
Washington DC 20546
Attn: Code Res Guid Con & Info Sys

NASA
Lewis Research Center
21000 Brookpark Road
Cleveland OH 44135
Attn: Library

DEPARTMENT OF DEFENSE CONTRACTORS

Aeronutronic Ford Corporation
Western Development Labs Div
3939 Fabian Way
Palo Alto CA 94303
Attn: Donald R. McMorrow, MS G30

Aerospace Corporation
P.O. Box 92957
Los Angeles CA 90009
Attn: R. Mortensen
Attn: L. W. Aukerman
Attn: William W. Willis
Attn: Library
Attn: Melvin J. Bernstein
Attn: J. Benveniste

Battelle Memorial Institute
505 King Avenue
Columbus OH 43201
Attn: STOIAC

Bell Telephone Laboratories, Inc.
Mountain Avenue
Murray Hill NJ 07974
Attn: R. D. Taft, 2B-181
Attn: H. A. Jarrell, WH-2F-153

Boeing Company, The
P.O. Box 3707
Seattle WA 98124
Attn: A. R. Lawrey, MS 2R-00

Communications Satellite Corp.
950 L'Enfant Plaza, South, S.W.
Washington DC 20024
Attn: Richard A. Arndt

General [illegible]
Valley Forge Space Center
P.O. Box 8555
Philadelphia PA 19101
Attn: Daniel Edelman

General Electric Company
Re-Entry & Environmental Systems Div
P.O. Box 7722
3198 Chestnut St
Philadelphia PA 19101
Attn: John W. Palchefsky, Jr.
Attn: Robert V. Benedict

General Electric Co.
Tempo-Center For Advanced Studies
816 State St. (P.O. Drawer QQ)
Santa Barbara CA 93102
Attn: DASIAC

Honeywell Inc. (Aerospace Div)
13350 U.S. Highway 19
St. Petersburg FL 33733
Attn: Harrison H. Noble, MS 725-5A

Hughes Aircraft Company
Centinella Ave. & Teale St.
Culver City CA 90230
Attn: John B. Singletary, MS [illegible]

Intelcom Rad Tech
P.O. Box 81087
San Diego CA 92138
Attn: Ralph H. Stahl
Attn: MDC
Attn: Technical Library
Attn: James A. Naber
Attn: Eric P. Wenaas

Johns Hopkins University
Applied Physics Laboratory
Johns Hopkins Road
Laurel MD 20810
Attn: Peter E. Partridge

Kaman Sciences Corp.
P.O. Box 7463
Colorado Springs CO 80933
Attn: W. Foster Rich
Attn: Dr. Frank H. Shelton

Lockheed Missiles and Space Co.
3251 Hanover St.
Palo Alto CA 94304
Attn: Clarence F. Kooi, 52-11

Maxwell Labs., Inc.
9244 Balboa Ave.
San Diego CA 92123
Attn: V. Fargo

MITRE Corp., The
Route 62 & Middlesex Turnpike
P.O. Box 208
Bedford MA 01730
Attn: M. E. Fitzgerald

Mission Research Corp.
735 State St.
Santa Barbara CA 93101
Attn: Technical Library

Northrop Corporation
Northrop Res & Tech Center
3401 West Boradway
Hawthorne CA 90250
Attn: David N. Pocock
Attn: James P. Raymond
Attn: Library

Physics International Co.
2700 Merced St.
San Leandro CA 94577
Attn: Doc Con for John H. Huntington
Attn: Doc Con for Charles H. Stallings
Attn: Doc Con for Philip W. Spence
Attn: Doc Con for Technical Library

Pulsar Associates, Inc.
7911 Herschel Ave.
LaJolla CA 92037
Attn: Carleton H. Jones Jr.

R&D Associates
P.O. Box 3580
Santa Monica CA 90403
Attn: Richard R. Schaefer
Attn: Robert A. Poll
Attn: S. Clay Rogers

Science Applications, Inc.
1651 Old Meadow Rd.
McLean VA 22101
Attn: William L. Chadsey

Science Applications, Inc.
P.O. Box 2351
LaJolla CA 92038
Attn: Dr. Charles Stevens

Simulation Physics, Inc.
41 "B" St.
Burlington MA 01803
Attn: Roger G. Little

Stanford Research Institute
333 Ravenswood Ave.
Menlo Park CA 94025
Attn: Robert A. Armistead

Systems, Science & Software, Inc.
P.O. Box 4803
Hayward CA 94540
Attn: Alan F. Klein

Systems, Science & Software, Inc.
P.O. Box 1620
LaJolla CA 92038
Attn: Andrew R. Wilson
Attn: Technical Library

Texas Instruments, Inc.
P.O. Box 6015
Dallas TX 75222
Attn: Sanders B. Cox, Jr., MS 909

TRW Systems Group
One Space Park
Redondo Beach CA 90278
Attn: A. Anderman, R1-2036
Attn: R. D. Loveland, R1-2036
Attn: Lillian G. Singletary, R1-1070
Attn: Paul Molmud

Dr. Victor A.J. Van Lint
7650 Convoy Court
San Diego CA 92111

Westinghouse Electric Corp.
R & D Center
1310 Beulah Rd, Churchill Borough
Pittsburgh, PA 15235
Attn: William E. Newell

Oak Ridge National Laboratory
Health Physics Division
P.O. Box X
Oak Ridge, TN 37830
Attn: Dr. J. C. Ashley (20 cys)

METRIC SYSTEM

BASE UNITS:

Quantity	Unit	SI Symbol	Formula
length	metre	m	...
mass	kilogram	kg	...
time	second	s	...
electric current	ampere	A	...
thermodynamic temperature	kelvin	K	...
amount of substance	mole	mol	...
luminous intensity	candela	cd	...

SUPPLEMENTARY UNITS:

plane angle	radian	rad	...
solid angle	steradian	sr	...

DERIVED UNITS:

Acceleration	metre per second squared	...	m/s
activity (of a radioactive source)	disintegration per second	...	(disintegration)/s
angular acceleration	radian per second squared	...	rad/s
angular velocity	radian per second	...	rad/s
area	square metre	...	m
density	kilogram per cubic metre	...	kg/m
electric capacitance	farad	F	A·s/V
electrical conductance	siemens	S	A/V
electric field strength	volt per metre	...	V/m
electric inductance	henry	H	V·s/A
electric potential difference	volt	V	W/A
electric resistance	ohm		V/A
electromotive force	volt	V	W/A
energy	joule	J	N·m
entropy	joule per kelvin	...	J/K
force	newton	N	kg·m/s
frequency	hertz	Hz	(cycle)/s
illuminance	lux	lx	lm/m
luminance	candela per square metre	...	cd/m
luminous flux	lumen	lm	cd·sr
magnetic field strength	ampere per metre	...	A/m
magnetic flux	weber	Wb	V·s
magnetic flux density	tesla	T	Wb/m
magnetomotive force	ampere	A	...
power	watt	W	J/s
pressure	pascal	Pa	N/m
quantity of electricity	coulomb	C	A·s
quantity of heat	joule	J	N·m
radiant intensity	watt per steradian	...	W/sr
specific heat	joule per kilogram-kelvin	...	J/kg·K
stress	pascal	Pa	N/m
thermal conductivity	watt per metre-kelvin	...	W/m·K
velocity	metre per second	...	m/s
viscosity, dynamic	pascal-second	...	Pa·s
viscosity, kinematic	square metre per second	...	m/s
voltage	volt	V	W/A
volume	cubic metre	...	m
wavenumber	reciprocal metre	...	(wave)/m
work	joule	J	N·m

SI PREFIXES:

Multiplication Factors	Prefix	SI Symbol
1 000 000 000 000 = 10^{12}	tera	T
1 000 000 000 = 10^{9}	giga	G
1 000 000 = 10^{6}	mega	M
1 000 = 10^{3}	kilo	k
100 = 10^{2}	hecto*	h
10 = 10^{1}	deka*	da
0.1 = 10^{-1}	deci*	d
0.01 = 10^{-2}	centi*	c
0.001 = 10^{-3}	milli	m
0.000 001 = 10^{-6}	micro	μ
0.000 000 001 = 10^{-9}	nano	n
0.000 000 000 001 = 10^{-12}	pico	p
0.000 000 000 000 001 = 10^{-15}	femto	f
0.000 000 000 000 000 001 = 10^{-18}	atto	a

* To be avoided where possible

MISSION
of
Rome Air Development Center

RADC plans and conducts research, exploratory and advanced development programs in command, control, and communications (C^3) activities, and in the C^3 areas of information sciences and intelligence. The principal technical mission areas are communications, electromagnetic guidance and control, surveillance of ground and aerospace objects, intelligence data collection and handling, information system technology, ionospheric propagation, solid state sciences, microwave physics and electronic reliability, maintainability and compatibility.



Printed by
United States Air Force
Hanscom AFB, Mass. 01731